**National Technical University of Athens**

School of Civil Engineering

MSc in Analysis and Design of Earthquake Resistant Structures


# Influence of Modeling on the Seismic Performance Assessment of an Existing Three Storey RC Building


A Study of

**Alexandros Tolis**


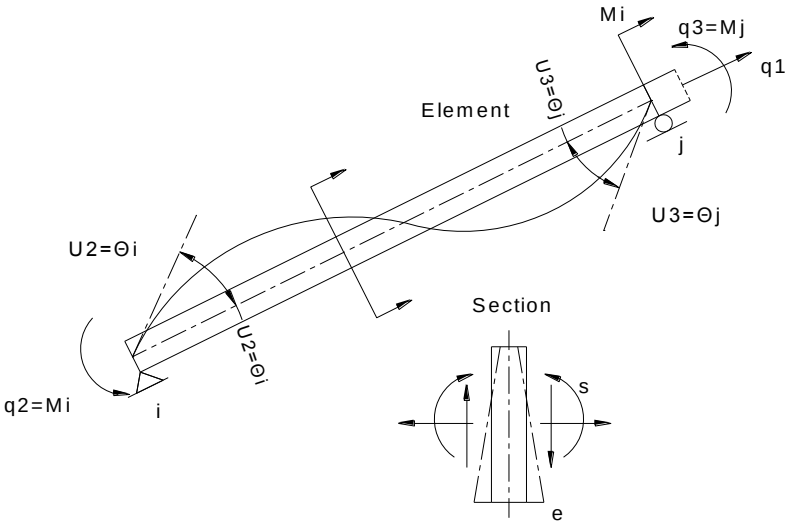



Supervisor Professors

**Dr. Michalis Fragiadakis**

**Dr. Vissarion Papadopoulos**

# ABSTRACT

The paper focuses on the study of typical reinforced concrete structures build between the years 1950 and 1970 in Southern Europe. These structures have been designed only for gravity loads and, apart from the lack of seismic design, the structural morphology of the majority promotes torsional response. Both experimental and analytical results are presented for a three-storey building that was tested on the shake table of TREES laboratory at EUCENTRE in Pavia, Italy. The building was dynamically tested using the Montenegro 1979 ground motion record (Herceg-Novi station), scaled to different levels of PGA to observe its progressive damage mode and overall capacity deterioration. In this paper the experimental data is compared with numerically obtained results using three different kind of non linear, force-based, fiber beam-column elements. Response parameters, such as damage distribution and drift capacity, are analyzed to identify the limitations of numerical modeling, of each specific element, with respect to the investigated engineering demand parameters.

# CONTENTS

## 1. Introduction

In a highly seismic area, such as the wider region of Southeast Europe, the main concern of civil engineering is to reduce the vulnerability of structures on seismic actions. Unfortunately, although the modern earthquake resistance codes of practice have reached a very good level of reliability, these old buildings are not designed to perform on seismic actions in a manner similar to that current earthquake science and practice is demanding.

The problem of seismic hazard assessment, of buildings under consideration, is on a great concern in today's practice because many of them designed before the introduction of early earthquake resistance codes of practice comprise a large percentage of the total existing structures.

Buildings with non-standard morphology are those whose structural system contains various static geometric unevenness, which adversely affects its behaviour. Such disparities could be the unbalanced distribution of either stiffness or mass, or both, in plan and elevation. Also unbalanced distribution can be caused by the lack in forming structural frames in one or both of the main directions of the building. The provisions of earlier codes of practice, coupled with some empirical techniques, determined some seismic protection in structures, but still the attitude was that structures should mainly transfer vertical loads. It is very frequent in such buildings to encounter structural systems consisting mainly of one way slabs supported on beams spanning in the other way only (transverse that of slab load direction), thereby leading to a one direction frame while in the other columns are left to act almost as vertical cantilevers. Often also the architectural aesthetic influenced the structural system, promoting the creation of indirect supports on beams and by that reducing the function of a full frame action. Finally, due to the lack of computing resources, the consulting practice wasn't able to estimate a more accurate distribution of seismic shear.

In this study, a building of this type will be modelled with finite element members with a beam-column non linear response. The model of the building may be formed by one of the following three different basic element models: the fiber element, the lumped element and the fiber lumped element. The aim is to highlight the advantages and disadvantages of each element modelling to the accuracy of the final result and the computational cost, as reference to the experimental data derived from a three storey building, on a scale of 1:2 in relation to the original.

# 2. Description of the reference Structure and of the Experimental Programme

## 2.1. Geometric Characteristics of Structure

The three-story building of the Experiment was designed by M.N Fardis and P. Negro, under the frame of the European research project SPEAR (Seismic Performance Assessment and Rehabilitation of Existing Buildings), and was built on a scale of 1:2 in relation to the original. The scale applies to the length of members, the dimensions of cross sections and the diameters of the longitudinal and shear reinforcement.


Figure 2–1: The building of the experiment NEARB

The design philosophy of the building was such that to represent the older structures often encountered in the southern European countries seismic areas. These buildings are characterized by the lack of seismic design and unfavorable characteristics that affect the seismic behavior, such as eccentricities and indirect support of beams. The building was designed for vertical loads only, is asymmetrical promoting torsional response, includes two beams that are not directly supported by columns (with eccentricities 0.25m and 0.5m respectively) and a beam-column joint (at column C2) with high eccentricity (fig.2-2). Condition of low ductility requirements was conducted by small splicing lengths of longitudinal rebar in columns, detailing and absence of stirrups in joints.

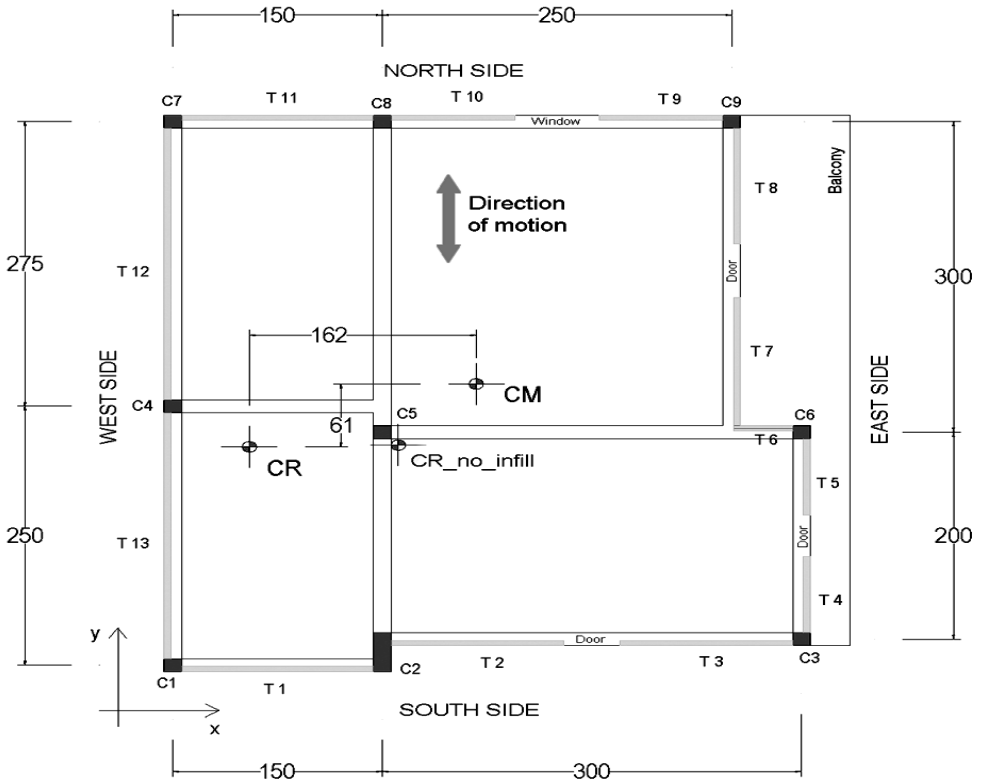


Figure 2–2: Typical building floor plan

In the experiment the storey height of the building is 1.5m, the slabs are 12cm thick, the beams have dimensions 12.5×25 cm and all columns are square 12.5×12.5 cm with the exception of column C2 (fig. 2-2) that has dimensions 12.5×37.5 cm. The beams are typically reinforced with 4 or 6R6 bars (R stands for round mild steel bars, dia in mm) on the bottom side and 2R6 bars on the topside. The columns are symmetrically reinforced with 4R6 bars for the square columns and 10R6 (see appendix) for column C2 and the slabs with R6-100 (symbol stands for round 6mm Ø bars at 100mm centers). The concrete cover is equal to 1cm for all RC members of the building, while the stirrups are R3-55 for the beams and R3-70 for the columns, resulting to rather pure passive confinement. There is lack of stirrups in the beam-column joints, resulting to a small rotational capacity. Moreover, beam B7 is not directly supported by a column, a design practice typically adopted to accommodate architectural requirements forming beam to-beam joints.

The building is regular in elevation with total height 4.5m, while it is irregular in plan and also torsionally sensitive, since the center of mass and the center of rigidity do not coincide. The average plan dimensions are 4×5 m. In order to have correct mass conservation in respect to the real structure, concrete blocks of 25cm thickness as additional masses are placed and anchored on top of the slabs (fig. 2-7). In the perimeter of every storey, infill walls with thick-

ness 5cm are placed (Fig 2-3). Another structural detail, that is expected to influence the response under seismic loading, is that the beam reinforcement is bent upwards at the supports where the sign of bending moments is reversed when only gravity loads are present. However, severe seismic loading may inverse the sign of bending moments, thus the rotational ductility capacity may not be sufficient. More details about the properties of the tested structure and the experimental set up can be found in appendix, at the end of this paper.

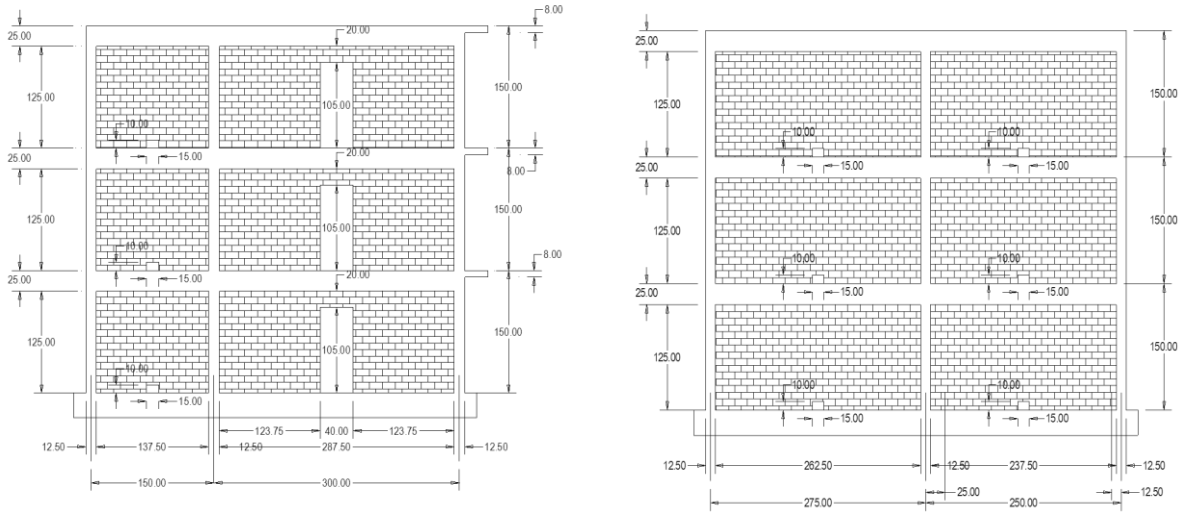


(a) (b)

Figure 2–3: Side frame elevations: (a) view A-A, (b) view B-B (see notation of Fig. 2 -2)

### 2.2. Material Properties

To determine the exact material properties of the scaled structure, additional laboratory tests have been carried out. The average tensile strength of the reinforcing steel was approximately equal to 293MPa after tensile tests on smooth rebars with diameters equal to Ø3, Ø6 and Ø10. The compressive strength of the concrete was obtained from four samples for every storey. Therefore, the average compressive strength was found equal to 37.7, 38.4, 31.5MPa for the columns of the first, second and third storey, respectively, and 50.6, 50.9 and 42.5MPa for the slabs and the beams.

(a) (b)

Figure 2–4: compressive strength (a) vertical $f_m$ = 2.2 MPa (b) horizontal $f_h$ = 1.8 MPa

Finally, the masonry was found to have 2.2MPa vertical compressive strength, 1.8MPa horizontal compressive strength and 0.24MPa shear strength. The modulus of elasticity $E_m$ of the masonry was equal to 1600MPa and the corresponding mass density is 484 kg/m$^3$.

| | Max Compressive Strength (Kg) | Area(mm$^2$) | Rcm (MPa) | avg (MPa) |
|---|---|---|---|---|
| Foundation | 84000 | 22500 | 37.33 | 38.0 |
| | 87000 | 22500 | 38.67 | |
| Column 1st floor | 88000 | 22500 | 39.11 | 38.44 |
| | 85000 | 22500 | 37.78 | |
| Slabs & beams 1st floor | 117000 | 22500 | 52.00 | 50.89 |
| | 112000 | 22500 | 49.78 | |
| Column 2nd floor | 78000 | 22500 | 34.67 | 39.67 |
| | 94000 | 22500 | 41.78 | |
| | 93000 | 22500 | 41.33 | |
| | 92000 | 22500 | 40.89 | |
| Slabs & beams 1st floor | 108000 | 22500 | 48.00 | 48.44 |
| | 110000 | 22500 | 48.89 | |
| Column 3rd floor | 75000 | 22500 | 33.33 | 32.11 |
| | 70000 | 22500 | 31.11 | |
| | 74000 | 22500 | 32.89 | |
| | 70000 | 22500 | 31.11 | |
| Slabs & beams 3rd floor | 88000 | 22500 | 39.11 | 39.56 |
| | 90000 | 22500 | 40.00 | |

Figure 2–5: Results of Experiment concrete samples

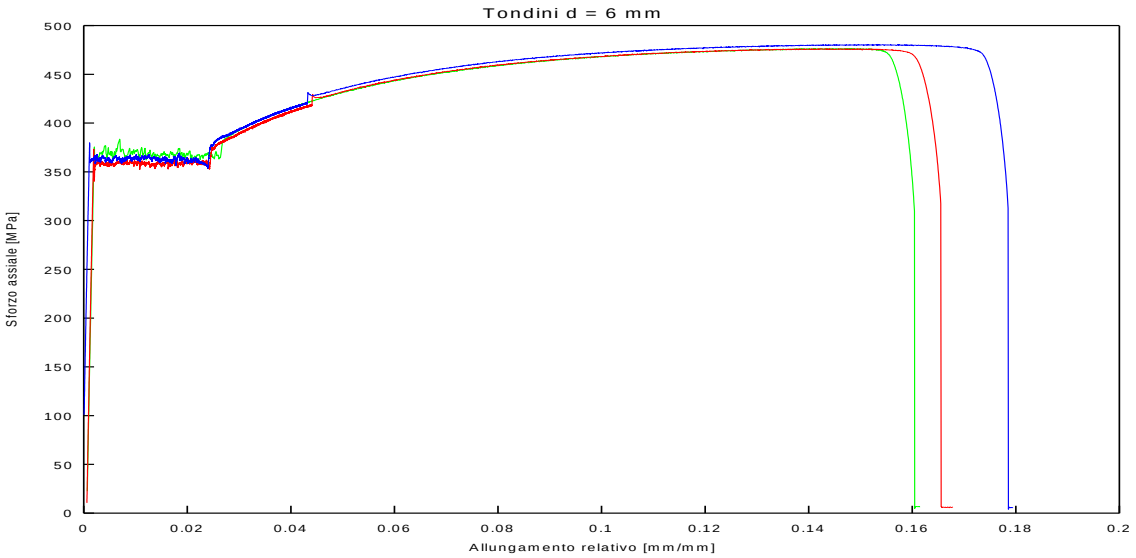


(a)

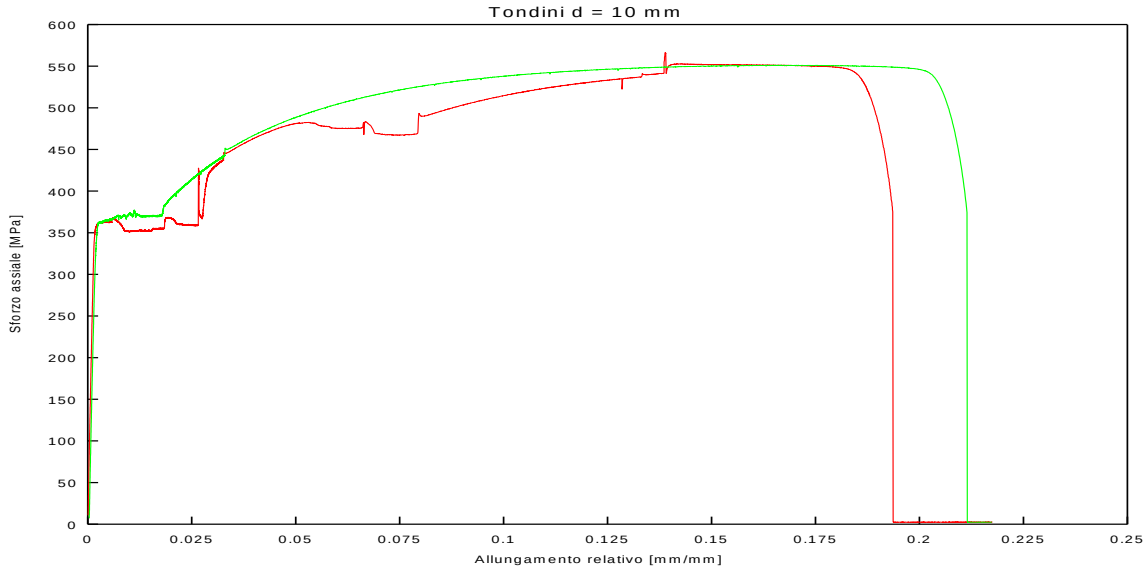


(b)

Figure 2–6: Stress - strain diagram of experiment steel samples (a) d = 6mm (b) d = 10mm

### 2.3. Building mass

As already mentioned before, in order to achieve a realistic mass conservation in respect to the real structure, masses of unreinforced concrete castings, 25 cm thick, were placed and anchored on the floors of each storey, with a total mass of 27 tons (9 per storey).

Figure 2–7: Additional mass for the simulation of storey superimposed dead and live loads

| Storey | Mass (tons) |
|---|---|
| 1st | 18636 |
| 2nd | 18636 |
| 3rd | 18307 |
| Total mass | 55579 |

Figure 2–8: Model storey additional mass placement

### 2.4. Experimental Program

In the frame of SPEAR project similar buildings have been built in several research programs, under which were investigated various software modeling issues. The experimental, and computational results extracted from these experiments, based on SPEAR buildings, are very important for studying the simulation of existing reinforced concrete structures.

Figure 2–9: The building of the seismic experiment NEARB on the shake table

One such experiment took place on May 20, 2008, where a three-story building (fig. 2-9) tested dynamically at the Laboratory for Training and Research in Earthquake Engineering and Seismology (TREES Lab), of EUCENTRE (the European Research Center for Earthquake Engineering) in Pavia, Italy. This experiment was also used for the evaluation of the Italian Rules ("Numerical and Experimental Assessment of Recommendations for existing RC Buildings (NEARB) included in OPCM") developed in the frame of the "Computational and experimental suggestions assessment of concrete structures in accordance with Directive OPCM 3274». The purpose of this research is to verify the effectiveness and accuracy of the Directive through computer simulations and experimental tests of buildings typical of earlier decades. The accelerograms which have been used in order to take place the experiment were the earthquake of 1979 in Montenegro (Herceg-Novi station). The accelerograms escalated to levels of maximum ground acceleration 0.30g and 0.54g, in order to assess the structural vulnerability of the large-scale seismic intensity. The purpose of exciting the building with accelerograms in medium and high intensity (peak ground acceleration 0.30g and 0.54g, respectively) is the evaluation of inelastic response, as plastic yielding was expected in materials, steel and concrete, as well as the possibility of formation of plastic hinges at some members.

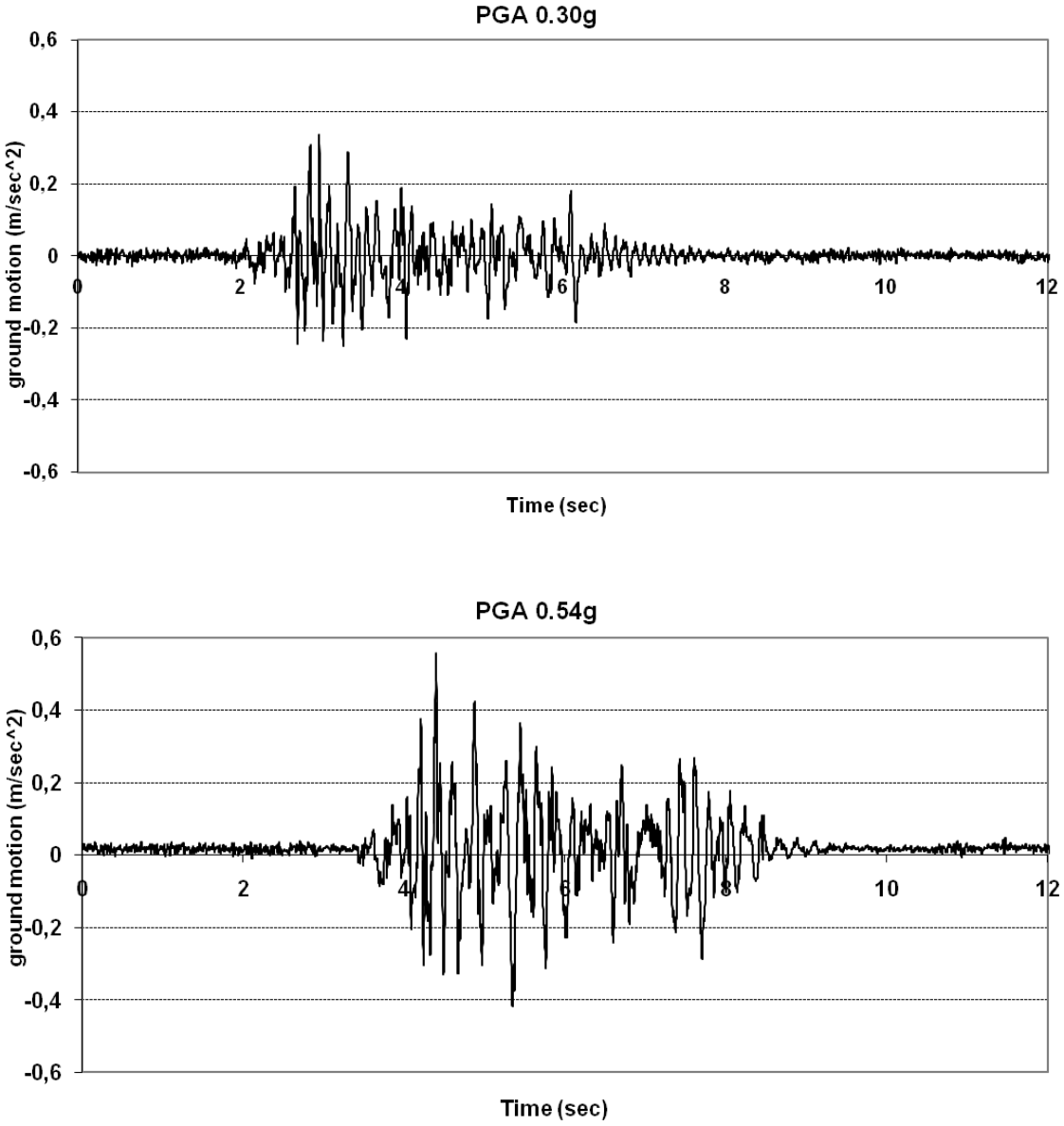


Figure 2–10: Montenegro earthquake accelerograms

Finally because the building was constructed in 1:2 scale compared to normal, a factor equal to √2 was applied on the time of axis of the record.

# 3. Modelling and Analysis of Structures Under Seismic Actions

## 3.1. General

To determine the level of damage, it was used a nonlinear static method, also known as pushover analysis, as well as non-linear dynamic analysis. In the second method, the response is determined by time integration of the equation of motion by the application of seismic recordings to structure.

Non-linear analysis methods allow the use of higher-level controls. These controls are usually referred to plastic rotations or relative movements, with the possibility to use controls even for the deformations, depending on the material. Concerning the stability of structure, where non-linear analysis takes into account the deformed geometry, the second order effects are taken into account directly.

## 3.2. Push over analysis

According to the static non-linear mathematical model of the method, the structure is "pushed" by a distribution of horizontal lateral loads. These horizontal loads are applied together with the vertical gravity loads defined by the seismic load combination according to the relevant design code. That horizontal loading is increased in steps so that the displacement of the attribute node to be equal to the target displacement. As an attribute node is usually considered a characteristic one of the roof of the modelled structure.

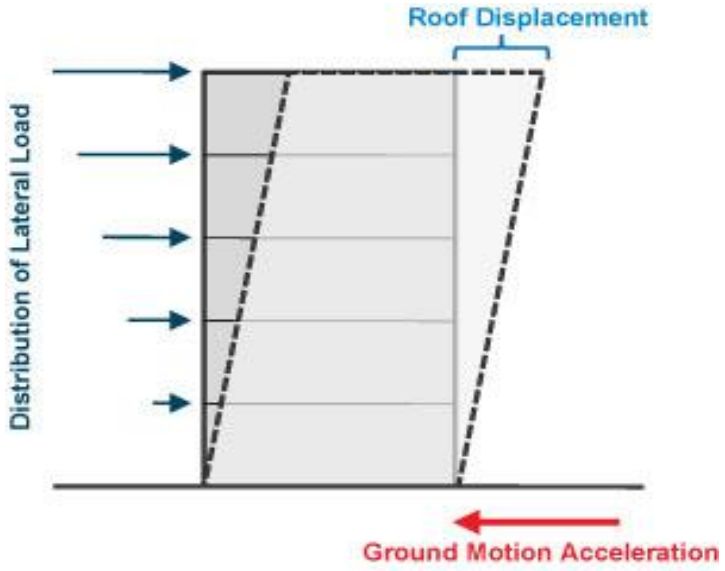


Figure 3–1: Schematic representation of the static non linear analysis

In this method, the seismic action is applied by an equivalent static horizontal force which is distributed over the height of the structure model based on following:

- In an one degree oscillator the maximum force $F_{max}$ is developed at the state of the maximum relative displacement $x_{max}$, and corresponds to the maximum stress on the body.
- From the design response spectrum the maximum relative displacement can be derived by the maximum spectral acceleration *Sa* that corresponds to the fundamental period of the oscillator.
- The acting spring force is proportional to the maximum relative displacement.

Concluding the foregoing, the applied force should be proportional to the maximum relative displacement that represents the fundamental mode of oscillation under the condition that higher modes can be omitted.

In a structure fully fixed at the base, the basic transport eigenmode can have the following shape:

a. parabolic if the flexural deformation is dominant (wall systems) and the system is fully fixed at the base,
b. linear (or approximately linear) if the shear deformation is dominant (frame systems).

In the case of dominant bending deformation and rotationally deformable foundation the shape lies somewhere in between.

Therefore, the distribution of equivalent loading shall be, according to conditions, parabolic or triangular. For practical reasons under constant distribution of the masses in elevation a triangular distribution of loading is preferred. The triangular loading distribution can be expressed mathematically as follows:

$$P_i = \frac{m_i h_i}{\sum_{i=1}^{n} m_i h_i} W_{tot} \quad (1)$$

$P_i$ : equivalent total force of floor

$m_i$ : floor mass

$h_i$ : floor elevation (from the base of the building)

$w_{tot}$ : total weight of the building

The incremental static analysis method, known as pushover analysis, is the most widely used non-linear method of calculation of seismic demand. The method is approximate, due to the fact that earthquake is a dynamic phenomenon, but since it is a non-linear method of analysis, it takes into account directly the non-linearity of the material and geometry.

The advantages of this method are as follows:

- Realistic estimate of potentially brittle states, such as axial demand in columns, moment demand of a beam to column joint or shear forces in walls and short columns.
- Assessment of the displacement requirement in elements forming plastic joints in order to absorb the seismic energy, direct calculation of the relative displacements, allowing damage control to non-structural elements.
- Possibility to take into account the contribution of non structural elements in capacity of structure.
- Evaluation of the influence of the resistance of particular members to the ultimate resistance of the structure.
- Identification of critical areas, where the inelastic deformations are expected to be high.

Apart from these advantages pushover analysis has a number of disadvantages which in many cases require attention to prevent its use, in cases where not appropriate. These disadvantages can be summarized as follows:

- The theoretical background of the method is incomplete and in many cases difficult to support. The main hypothesis that the response of a system of many degrees of freedom can be associated with the response of a Single Degree of Freedom is not correct due to the fact that the first eigenmode is not constant and changes depending on the inelastic deformation. Thus, where the involvement of higher modes is important, the method can give misleading results.
- There is difficulty in applying the method to space structures without structural regularity. Generally there is no agreement within the research community on how to apply the equivalent static lateral loads in space structure models.
- The distribution of equivalent static lateral load ignores the reduction of structure stiffness and thereby the change on the fundamental eigenmode as increases the intensity of the load.
- During load increments it is considered that energy is absorbed through inelastic deformations and it is ignored the part of energy absorption due hysteretic behaviour of the material. It also ignores the influence of the duration of the earthquake and the number of loading cycles.

### 3.3. Dynamic analysis with time histories

For the non-linear calculation with the time integration, as seismic activity is used the artificially generated diagram of ground acceleration versus time that is compatible with the design response spectrum. In comparison with a recorded activity, during an earthquake, the artificial compatible has the advantage that all frequencies of the structure are excited exactly as the design response spectrum.

The differential equations of motion of all degrees of freedom of the structure can be written in matrix form as follows:

$$Ma + Cv + r(d) = p(t) \tag{2}$$

Where M and C is the matrix of mass and damping, respectively, v and a is the nodal velocity and acceleration, first and second derivative of displacement d respectively, r is the stiffness matrix which produces the internal forces that depend non-linearly with d, and p is the external load. The above equation can easily be solved step by step with numerical integration and calculate the response of d for any external load p. At each step, the calculated displacements d are applied to structure. The internal forces that are developed and recorded at the end of each step are used to calculate the displacements of the next step, according to matrices of the mass and damping and external load p. This is repeated until the time recording of ground motion is concluded.

It should be noted that the method of time integration requires a large amount of calculation effort as well as numerical models suitable to model the nonlinear behaviour of materials under cyclic loading.

### 3.4. Development of mathematical model

The columns were introduced as linear elements with a single member per storey. For beams separate data are used for their ends, and in accordance with the construction practices of past decades, a percentage of longitudinal reinforcement bars of the bottom reinforcement bent upward at the supports. Also, at floor levels high rigidity linear elements imported and properly arranged in order to describe the operation of the diaphragm plates.

The boundary conditions at the bases of the columns were considered as fixed to the ground floor, representing thus a non deformable strong foundation, which is the case of the experiment that is based on the seismic table using appropriate anchors through holes in order to avoid slipping or twisting of the building during the application of ground motion (fig. A-5).

In forming of the structural system model, all data entered on the basis of axial dimensions without the use of rigid ends (rigid offsets) at beam to column nodes. This assumption was made to take into account the deformation of the node, which may be important, especially in old buildings. Reasons for the deformation may be, inadequate anchorage of longitudinal reinforcement within the nodes, producing slip on seismic response of the structure and not maintaining stirrups within nodes. Exception In this practice was the largest column C2, dimensions 0.125 x 0.375m, as connecting beams are associated with this column with high eccentricity.

Stirrup construction techniques, typical of structures without increased ductility requirements, lead to consideration of non-confined concrete core sections of the members of the building.

The vertical loads, permanent and live, as well as self weight of the structure were summarized and considered as point masses at the nodes.

In the dynamic non-linear analysis, in all cases, dumping was calculated by the Rayleigh form $C = a_0M + a_1K$, with material dumping factor $\zeta = 5\%$, based on the first two eigenfrequencies $\omega_1$ and $\omega_2$, where:

$$\alpha_0 = \zeta \ (2\ \omega_1\ \omega_2) / (\omega_1 + \omega_2) \quad (3)$$

$$\alpha_1 = 2\ \zeta / (\omega_1 + \omega_2) \quad (4)$$

### 3.4.1. OpenSees software

The software used for analysis is the open source program OpenSees of the University of Berkley. Based on the logic of object-oriented programming, enables user to combine existing libraries with new components through appropriate parameters, in order to describe the mathematical model, without changing the original code.

Analyses are based on the finite element method, taking into account the nonlinearity of the material (Linear Transformation), as well as geometric non-linearity and the influence of second-order phenomena (Corotational). Specifically, the local stress-strain relationship for all sub elements with which the member has been divided, is calculated by integration of non-linear material behaviour, for every finite element separately. These discretizations form exactly a distributed plasticity along the member, result of which, is a smoother transition from elastic to inelastic area.

The solution of equilibrium equations was obtained using the method of successive approximations Newton-Raphson. In cases where the Newton-Raphson method had difficulties in convergence, the method of the survey line is used, or the method of Broyden.

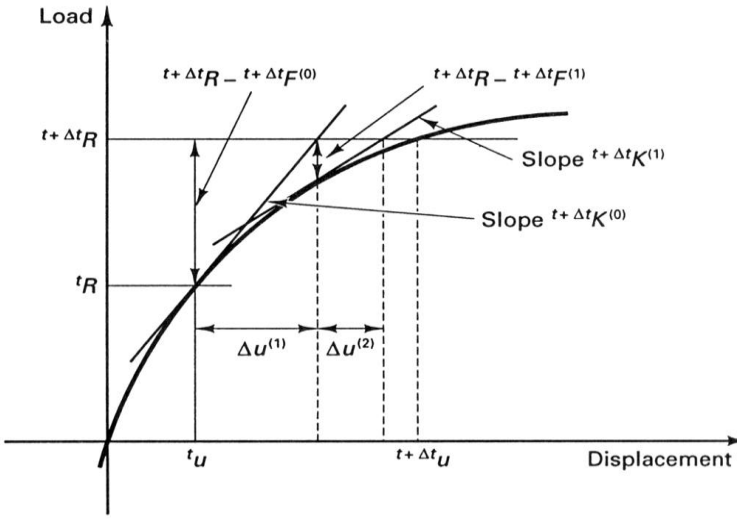


Figure 3–2 Schematic illustration of the method of Newton-Raphson

The time integration was done by the method of Newmark, on the basis of approximate formulas for the displacement and velocity (i +1) of time step Dt:

$$\dot{u}_{i+1} = \dot{u}_i + [(1-\gamma)\Delta t]\ddot{u}_i + (\gamma\Delta t)\ddot{u}_{i+1} \quad (5)$$

$$u_{i+1} = u_i + (\Delta t)\dot{u}_i + [(0.5-\beta)\Delta t^2]\ddot{u}_i + [\beta(\Delta t)^2]\ddot{u}_{i+1} \quad (6)$$

Where the coefficients c and b are given values γ= 0.5 and β = 0. 25

### 3.4.2. Non-linear models

In the non-linear analysis of RC structures which are under monotonically increasing non-seismic forces is commonly used the modelling at the material (steel and concrete), and point by point. It is used a large number of finite element for the analysis for two or three dimensions, with different figures for the two materials and often for their interaction. In the analytical models it is able to be reproduced the geometry in great detail and to follow the evolution of stress and displacement point-to-point. The computational requirements of such tests, however, limit their application to seismic activities in the form of accelerograms to individual members (wall) or a combination of a few members (a beam and a column in the node). At the present it is prohibitive to implement for real structures. The non-linear analysis of such structures is generally simulated coarser, in which individual members (beams, columns, wall portion between adjacent floors) are represented by an element of the simulation. One such simulation is able to capture and reproduce the main features of seismic response and behaviour, including the distribution of rigid between members and along the member. The requirements of the time and computer memory, also for preparation of data and interpreting and using the results are so little that allow its use for the analysis of real structures with hundreds of members, including the resumption of the analysis for a large number of ground motions. Thus the simulation of RC structures in members level are currently the main, if not exclusive, tool for non-linear dynamic analysis in practice and is likely to retain this role for the foreseeable future. So this paper is restricted to this type of simulation.

This building has been simulated with three force-based beam-column different models which are elements with distributed plasticity (fiber elements) and concentrated plasticity (lumped & fiber-lumped elements). The first method is more accurate and the method of concentrated plasticity is more stable and has a lower computational cost. These simulations are presented below analytically.

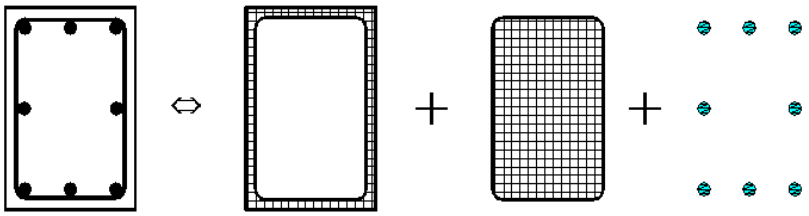

Figure 3–3 Simulation of the reinforcement concrete section with force-based elements

### 3.4.2.1. Force-Based Element Formulation

Force-based beam-column elements are formulated in a basic system without rigid-body displacement nodes. The element deformations, in the vector ***v***, are assumed small compared to the element length. There are three element deformations for two-dimensional elements, as shown in Fig.3-4 for a simply supported basic system, and six for three-dimensional elements.

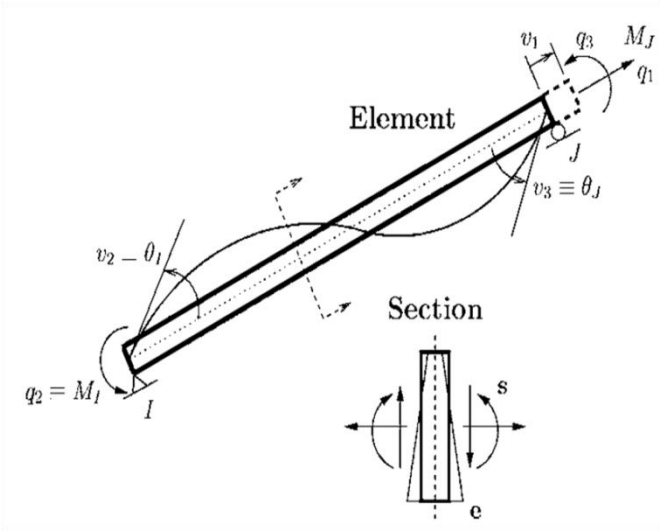


Figure 3–4 Simply supported basic system for two-dimensional beam-column elements and cross section of element

The vector of forces in the basic system, $q = q(v)$, is a function of the element deformations. The section behaviour is expressed in terms of the section deformations, ***e***, and the corresponding section forces, $s = s(e)$. The element kinematic relationship is assumed linear in this paper, but it can be extended to large displacements.

Equilibrium between the basic and section forces is expressed in strong form as

$$s = bq \tag{7}$$

Where the matrix **b** contains interpolation functions relating section forces to basic forces from equilibrium of the basic system. The axial force and bending moment at location *x* along the element for a two-dimensional simply supported basic system is given by the following equilibrium interpolation matrix:

$$b = \begin{bmatrix} 1 & 0 & 0 \\ 0 & x/L - 1 & x/L \end{bmatrix} \tag{8}$$

Eqs. (7) and (8) can be extended to include member loads section shear. From the principle of virtual forces, the compatibility relationship between the section and element deformation is

$$v = \int_0^L b^T e dx \tag{9}$$

The linearization of Eq. (9) with respect to the basic forces gives the element flexibility matrix

$$f = \frac{\partial v}{\partial q} = \int_0^L b^T f_s b dx \tag{10}$$

The section stiffness matrix is $k_s = \partial s / \partial e$, and its inverse gives the section flexibility matrix, $f_s = k_s^{-1}$. The element stiffness matrix, k, in the basic system is the inverse of the element flexibility matrix, $k = f^{-1}$, as given in Eq. (10). Details of the implementation of the force-based beam-column element for use in a general finite element analysis framework using the direct stiffness method are given by Neuenhofer and Filippou (1997).

The compatibility relationship in Eq. (9) is evaluated by numerical quadrature

$$v = \sum_{i=1}^{N_p} (b^T e \mid_{x=\xi_i}) \omega_i \tag{11}$$

Where ξ and ω=locations and associated weights, respectively, of the $N_p$ integration points over the element length [0,L]. In a similar manner, the element flexibility matrix in Eq. (10) is evaluated numerically

$$f = \sum_{i=1}^{N_p} (b^T f_s b \mid_{x=\xi_i}) \omega_i \tag{12}$$

Gauss-Lobatto quadrature is used in force-based elements because it places integration points at the element ends, where the bending moments are largest in the absence of member loads. A graphical representation of the four-point ($N_p = 4$) Gauss-Lobatto quadrature rule applied to Eq. (11) is shown in fig. 3-5, where the integrand, $b^T e$, is evaluated at the *i*th location $\xi_i$, and treated as constant over the length $\omega_i$. The highest order polynomial integrated exactly by the Gauss-Lobatto quadrature rule is $2N_p - 3$, which is two orders lower than Gauss-Legendre quadrature (Hildebrand 1984).

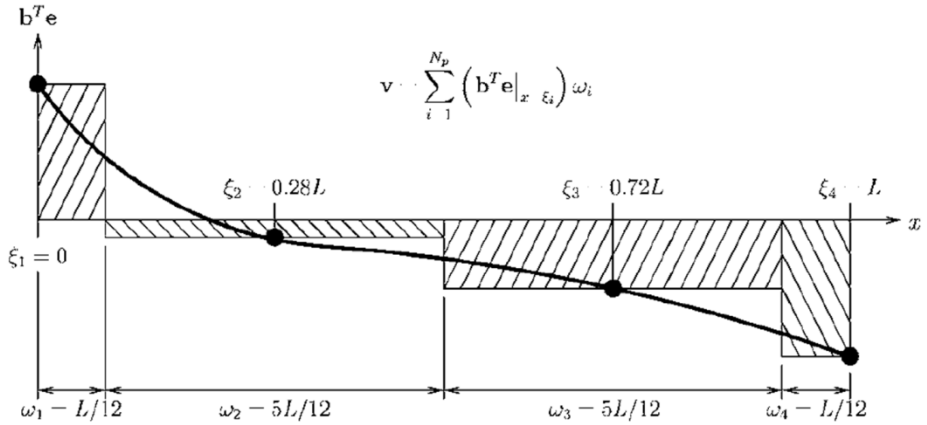


Figure 3–5 Application of four-point Gauss-Lobatto quadrature rule to evaluate force-based element compatibility relationship

For a linear-elastic, prismatic beam-column element without member loads, quadratic polynomials appear in the integrand of Eq.(9) due to the product of the linear curvature distribution in the vector ***e*** with the linear interpolation functions for the bending moment in the matrix **b**. Therefore, at least three Gauss-Lobatto integration points are required to represent exactly a linear curvature distribution along the element. To represent accurately the nonlinear material response of a force-based beam-column element, four to six Gauss-Lobatto integration points are typically used.

The primary advantage of Gauss-Lobatto integration rule is it permits the spread of plasticity along the element length. For hardening section behaviour, the computed element response will converge to a unique solution as the number of integration points increases. On the other hand, for softening section behaviour where deformations localize at a single integration point, a unique solution does not exist and the computed response depends on the characteristic length implied by the integration weights of the Gauss-Lobatto quadrature rule. This leads to a loss of objectivity, where the element response will change as a function of $N_p$ .

To address the loss of objectivity in force-based beam-column elements, Coleman and Spacone (2001) developed a regularization technique that modifies the material stress-strain behaviour to maintain a constant energy release after strain-softening initiates. Coleman and Spacone applied this method to the Kent-Park concrete model (Kent and Park 1971) showing fig. 3-6, where the shaded area is equal to the energy released after the onset of strain softening.

$$\frac{G_f^c}{l_p} = 0.6\, f_c^{'}(\varepsilon_{20} - \varepsilon_c + \frac{0.8\, f_c^{'}}{E_c}) \tag{13}$$

The parameters for the Kent-Park concrete model are $f_c^{'}$ = concrete compressive strength; $\varepsilon_c$ = peak compressive strain; $E_c$ = elastic modulus; and $\varepsilon_{20}$ = strain corresponding to 20% of the compressive strength. The parameter $G_f^c$ = concrete fracture energy in compression, and $l_p$ = plastic hinge length, which acts as the characteristic length for the purpose of providing objective response.

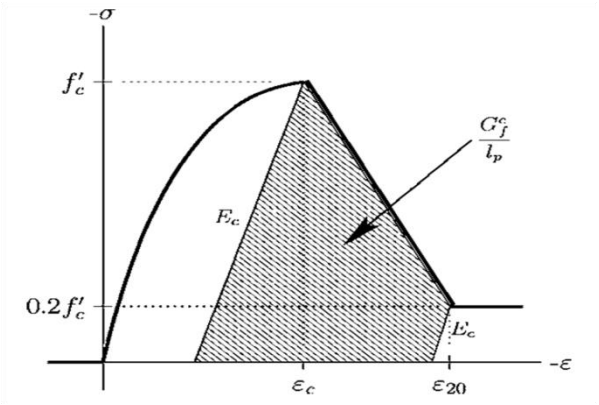


Figure 3–6 Kent-Park concrete stress-strain model with fracture energy in compression as shaded area

As discussed in the previous section, the plastic hinge length in the model is directly related to the element integration rule for the force-based elements. For the $l_p$ implied by the number of Gauss-Lombatto integration points, $\varepsilon_{20}$ must be modified according to Eq.(13) in order to maintain a constant energy release.

$$\varepsilon_{20} = \frac{G_f^c}{0.6\, f_c^{'} l_p} - \frac{0.8\, f_c^{'}}{E_c} + \varepsilon_c \tag{14}$$

Although this approach maintains objective response at the global level, it affects the local section response through an unnatural coupling of the concrete material properties to the element integration rule. A second regularization is required to correct for the loss of objectivity in the section response that result from this approach.

For the plastic hinge integration methods presented in this work, $l_p$ is a specified part of the element integration rule and it becomes a free parameter. Therefore, it is possible to determine a plastic hinge length that will maintain a constant energy release without modification to the concrete stress-strain relationship, alleviating the need for a subsequent regularization of the section response. For example, using the approach of Coleman and Spacone, the plastic hinge length can be determined from the concrete properties using Eq. (13)

$$l_p = \frac{G_f^c}{0.6 f_c^{'}(\varepsilon_{20} - \varepsilon_c + 0.8 f_c^{'} / E_c)} \tag{15}$$

The introduction of a plastic hinge length, such as that computed by Eq. (15), to the element integration rule maintains the logical separation of the material properties from the element integration rule.

Alternatively, the plastic hinge length can be specified using an empirically validated relationship, such as the Paulay and Priestley (1992) equation for reinforced concrete members

$$l_p = 0.08L + 0.022 f_y d_b (kN, mm) \tag{16}$$

Where $L =$ length of the member; $f_y$ and $d_b =$ yield strength and diameter, respectively, of the longitudinal reinforcing bars. The advantage of this approach is that the plastic hinge length includes the effect of strain softening and localization as determined by experiments.

### 3.4.2.2. Distributed plasticity elements

The advent of performance-based earthquake engineering has placed an emphasis on simulating the nonlinear response of a structural system to seismic excitations. Severe earthquake ground motions are expected to deform a structure into the inelastic range of behavior through multiple excursions. The design of a structural system subjected to earthquake ground motion recognizes that plastic hinges will form in frame members. One of the most accurate methods of inelastic analysis with linear elements is when the structure is composed of elements with distributed plasticity known as fiber elements. These elements are divided along their fibers as shown in Figure 3-7. The response of the fiber depends on the law of material from which it is formed. So with integration it can be specified the response of the total cross section.

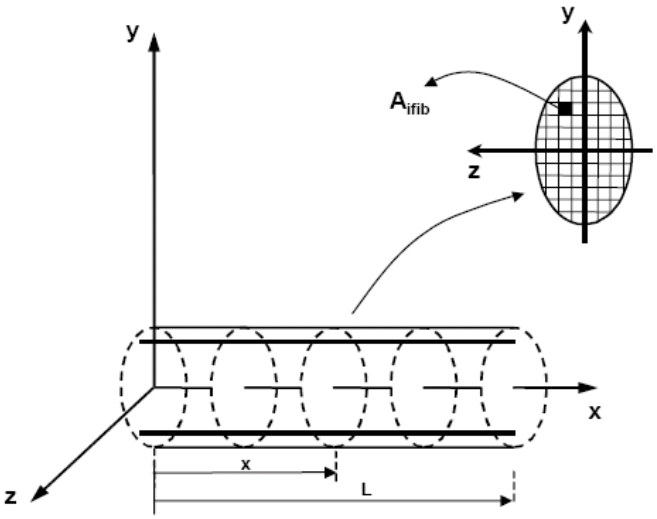


Figure 3–7 Beam element in the local system: sub-section of fiber

Taucer et al. (1991) presented a methodology for the inelastic analysis of a fiber beam element. The non-linear behavior of the member is due to the non-linear stress-strain of the material fibers.

The accuracy of the results is affected by the discretization of the element, such as the number of sections on each element and the number of fibers of each section. Greater number of fibers achieving better simulation, but it also increases the computational cost.

The fibers of the figure above are divided by a specific number of sections where there are the numerical integration points. The figure (3-8) below shows an element with 5 points of integration. These points separate the element and with numerical integration the properties of the element can be calculated. The response of each of the five sections will result with the numerical integration of stress and stiffness. The response of

the element is calculated by the superposition of the responses of each section taking into account certain weight factors.

The main problem in fiber modeling is how the internal forces are distributed within the element. For this purpose, the following equation is used:

$$D(x) = b(x) \cdot Q \tag{17}$$

Where D(x) is the matrix of forces of the section, Q is the matrix of the external forces of the element nodes and b (x) is the matrix containing the interpolation functions of forces.

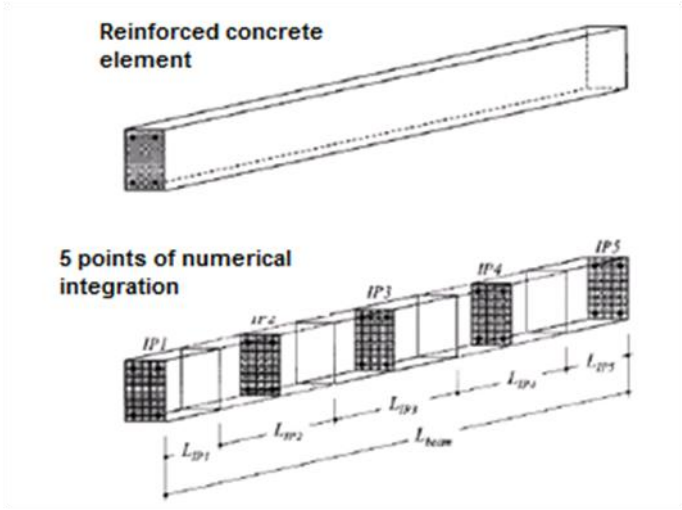


Figure 3–8 Beam element with five-point numerical integration

The forces of the section are determined by the forces of the element and then the resulting stresses in every fiber from the kinematic relations of the section. The definition of fiber stresses by the forces at a section is a statically indeterminate problem for a section with more than one fiber. This is because these stresses cannot be calculated from the axial force and bending moment of the section because there are only two equilibrium equations in uniaxial bending and three or more unknown factors.

The solution to the above problem is the linearization of the constituent relations of section and the calculation of deformation of the section by the emerging forces.

### 3.4.2.3. Concentrate Plasticity Elements

### 3.4.2.4. Lumped elements

The inelastic behavior of reinforced concrete frames when subjected to seismic loading is usually more intensive at the ends of beams and columns. So the first models used were based on elements with zero-length plastic hinges in the form of non-linear rotational springs at the ends of the members. The first element presented by Clough and Johnston (1967) [2], consisted of two elements in parallel, a bilinear elastic - plastic representing the yield and a perfectly elastic representing the material hardening (Fig. 3-9). The overall stiffness of the element is the sum of the stiffness of the two members.

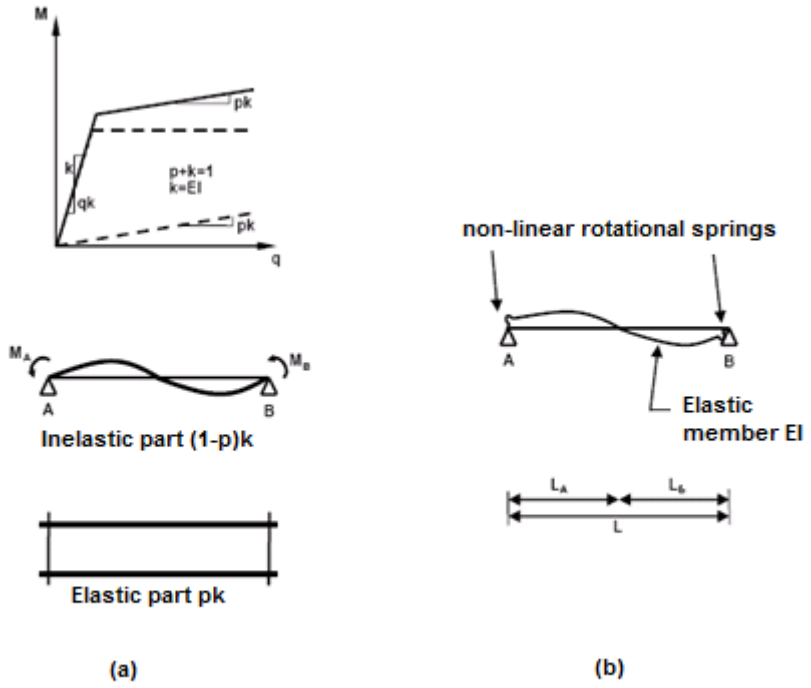


Figure 3–9: Simplified item with concentrated plasticity (a) Model of Clough-Johnston (b) Model of Giberson

A slightly different format is that two elements are connected in series (Giberson, 1966). This element consists of a linear elastic element with two equivalent non-linear rotational springs at each end (Figure 3-9b). In this way the non-linear deformations occur in these two springs. This model is more flexible than that of Clough, since it is able to describe more complex hysteretic behavior with the appropriate selection of moment-curvature relations in springs. This ability makes it suitable for describing the behavior of reinforced concrete members.

The assumption of the concentrated plasticity is a simplification of the actual behavior which does not include the gradual plasticization of the member which actually happens. This is the main drawback of the assumption of concentrated non-linearity. On the other hand, the main advantage is the simplicity that reduces significantly the computational

effort. Unfortunately, many of concentrated plasticity models fail to describe the behavior hysteretic members of reinforced concrete.

To overcome some of the constraints on the functioning of the members with concentrated plasticity, Lai et al. (1984) suggested an element consisting of an elastic section throughout its length which has a non linear section at each end (Figure 3-10). Each end part is comprised with a non-linear spring at every side of the section, representing the longitudinal reinforcing steel, and a central spring receiving only compressive stress representing the concrete. With five springs is possible to have a better simulation of the interaction of axial force and biaxial bending moment. The stiffness of these springs is related to the moment-curvature relations of each section.

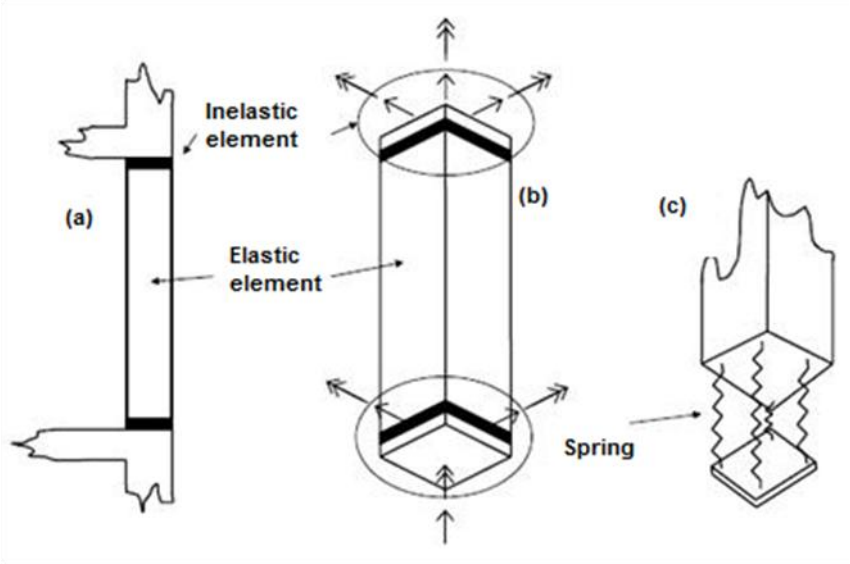


Figure 3–10:Model of Lai: rigid beam element of reinforced concrete under biaxial bending and axial load (a) point in construction (b) the model of (c) rigid element

For the determination of these relations was used the software Response 2000. This is an easy to use program that calculates the strength and ductility of a reinforced concrete cross-section subjected to shear, bending and axial forces. All three actions are considered to act simultaneously in order to find the deformation using modern research based on the modified compression field theory. In order to create these curves is required the specification of the type and the dimensions of each section (fig.3-11b), the material properties (concrete, steel) (fig.3-11c).

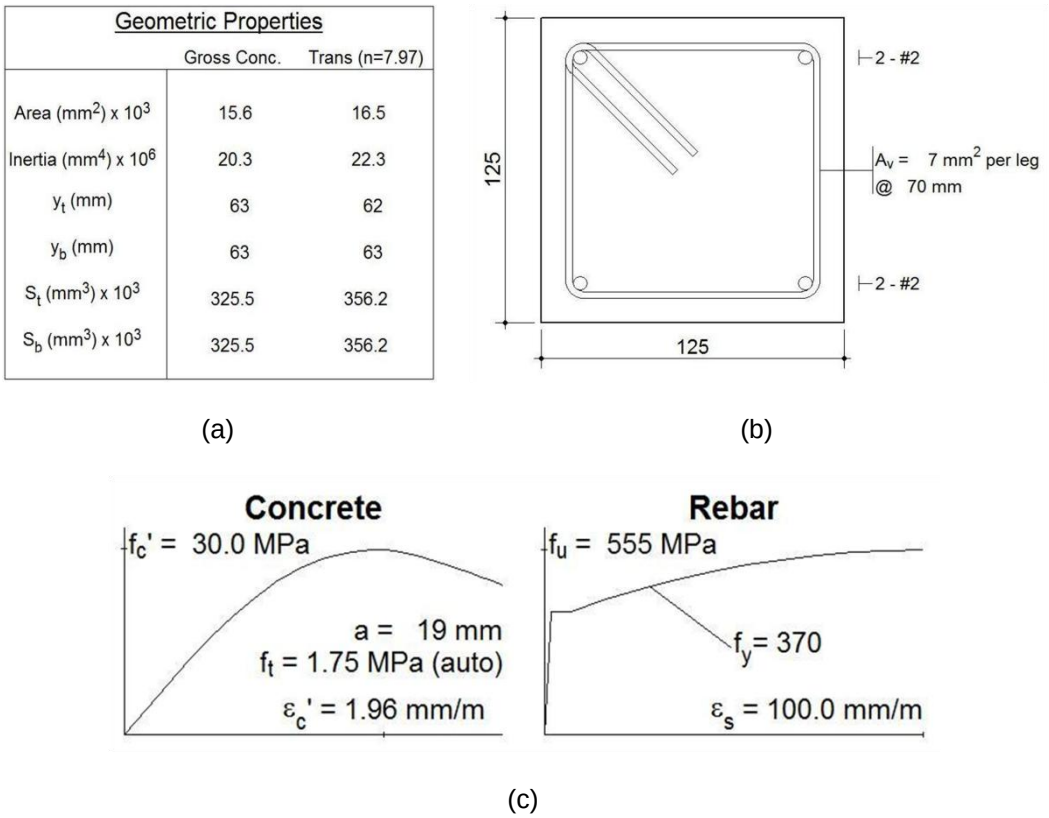


Figure 3–11: (a) Geometric properties of (b) square section and (c) material properties

It is also needed the order of the longitudinal and transverse bars, and finally the forces which subject to the cross-sections. It was chosen nine representative values of axial force for the square sections and three for rectangular. So there are defined twelve different lumped elements each with the following moment curvature relations (fig. 3-12, 3-13). The software developed at the University of Toronto by Evan Bentz and P. Collins.

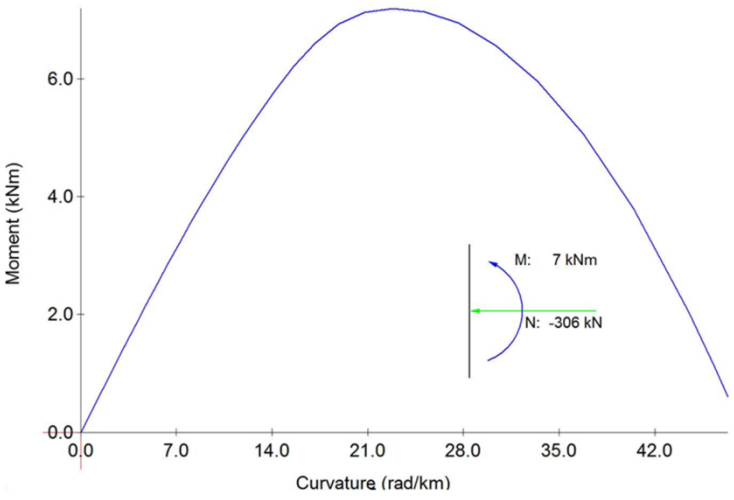


Figure 3–12 Bending curve for axial load N=306kN

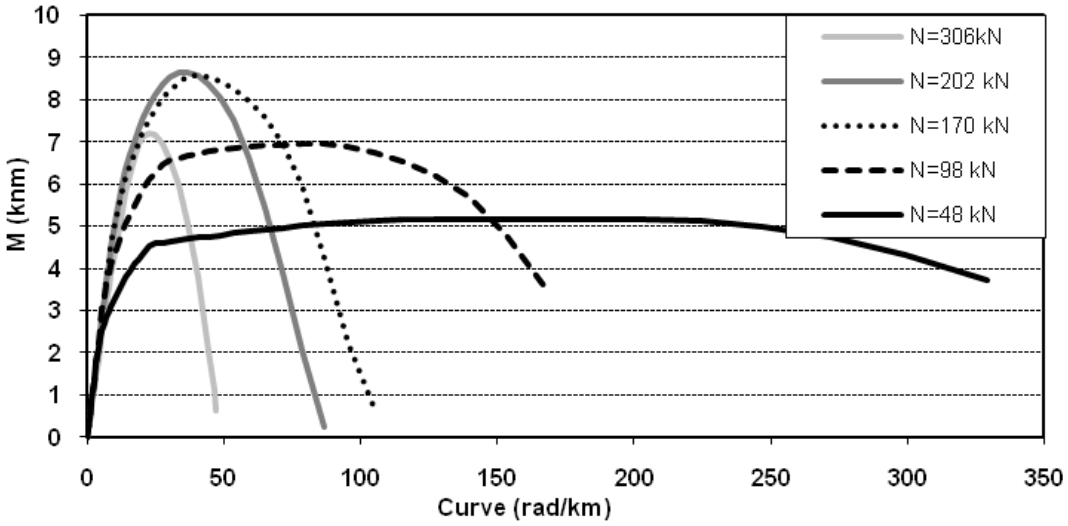


Figure 3–13 Bending curves for various values of curvature and axial load

#### 3.4.2.5. Fiber Lumped

Elements of concentrated plasticity of fiber (fiber-lumped) are a synthesis of these two previous elements. These elements are consisted of an elastic part and two inelastic at the edges of the element exactly as lumped elements. The inelastic part, however, does not consist of a nonlinear spring, but consisted of fibers as happens with the fiber elements. So these new elements have the advantage of low computational effort and a greater accuracy in comparison with the lumped elements.

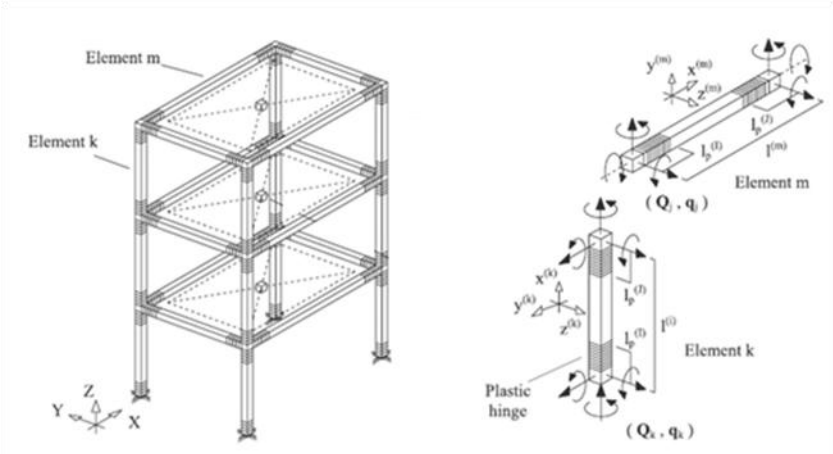


Figure 3–14 General building model and element used

#### 3.4.2.6. Modelling of the infills

A simplified model is adopted in order to include in the analysis the influence of the masonry infills. A masonry infill panel can be modeled by replacing the panel with two diagonal compressive-only struts. By ignoring the tensile strength of the infill, the combination of the two struts provides a lateral load-resisting mechanism for the opposite lateral direction of loading. The nonlinear force-deformation relationship of the struts is based on a simplified peak-oriented model that is able to include most of the sources of deterioration and also to account for a residual strength after deterioration. Thus, the relationship adopted is a quadrilinear model that consists of four controlling branches (Figure 3-15): a lineal elastic branch with slope $a_{el}$, a post-elastic branch with slope $a_h/a_{el}$, a post-capping branch with negative slope $-a_c/a_{el}$ and a final horizontal branch.

Such modeling is able to provide the capacity degradation through a series of rules for stiffness and strength deterioration as well as pinching. A thorough discussion of the cyclic rules, their implementation and their calibration can be found in references [12,13].

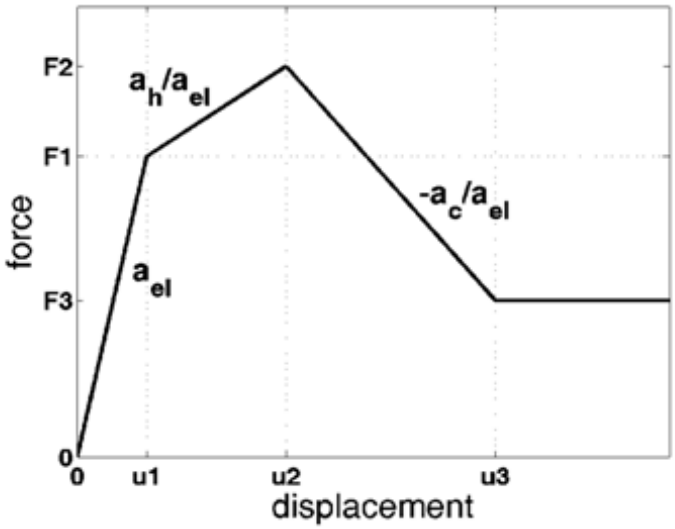


Figure 3–15 Quadrilinear peak-oriented model used for modelling the masonry infills

A number of studies that suggest approaches to calculate the monotonic envelope of Figure 3-15 can be found in the literature [14-17]. In this study it is adopted the expression proposed by Zarnic and Gostic [18] in order to calculate the maximum strength of the infill, thus:

$$F_2 = 0.818 \frac{L_{net} t_w f_{tp}}{C_1} \left(1 + \sqrt{C_1^2 + 1}\right) \quad (18)$$

$$C_1 = 1.925 \frac{L_{net}}{H_{net}} \quad (19)$$

where $L_{net}$,$H_{net}$ are the net dimensions of the infill, $t_w$ is the wall thickness and $f_{tp}$ is the cracking strength of the infill. The displacement at the maximum lateral force can be estimated using the equation [19]:

$$u_2 = \frac{\varepsilon_m \sqrt{L_{net}^2 + H_{net}^2}}{\cos\theta} \tag{20}$$

where $\varepsilon_m$ is the masonry compression strain at the maximum compression stress, here taken equal to 0.001. The initial stiffness $a_{el}$ is obtained using the formula [19]:

$$a_{el} = 2\left(\frac{F_2}{u_2}\right) \tag{21}$$

Previous experience has shown that the slopes $a_h$ and $a_c$ can be assumed equal to 3% and -10% of $a_{el}$. Finally the area of the struts can be approximated using the effective width of the diagonal $W_{eff}$ [17, 20]:

$$W_{eff} = 0.175(\lambda_h H)^{-0.4}\sqrt{H^2 + L^2}, \quad \lambda_h = \sqrt[4]{\frac{E_w t_w \sin(2\theta)}{4E_c t_c H_{net}}} \tag{22}$$

where *H, L* are the storey height and the bay length, respectively. Finally the area of the equivalent diagonal struts will be $A_m = W_{eff} t_w$. In the equations above $E_w$, $G_w$ are the Young and the shear modulus of the wall and $E_c$, $I_c$ are the Young modulus and the moment of inertia of the columns of the surrounding frame. $\theta$ is the inclination of the diagonal obtained as $\theta = arc\tan\left(\frac{H}{L}\right)$. Regarding the cyclic behavior model, following the notation of reference [13], it is assumed that the model has moderate pinching and no damage due to ductility.

### 3.4.3. Simulation of construction materials

#### 3.4.3.1. Concrete

During the analysis with the software OpenSees the material model used for the concrete was ''*Concrete01*'' (unidirectional behaviour Kent-Scott-Park) with linear branches loading / unloading cycles under cyclic loading by Karsan-Jirsa, and zero tensile strength. Two materials were used, one for columns and one of the beams. Their compressive strength was taken as the average of tests taken during the construction of the building and the strength obtained was that of 36.7MPa to 46.3MPa.

The parameters that determined the behaviour of the material were as follows:

$f_{pc}$ = 36.7-46.3 Mpa : compressive strength of concrete 28 days

$\varepsilon_{psc0}$ = 0.002 : maximum deformation resistance of concrete

$f_{pcu}$ = 0.85 $f_{pc}$ Mpa : compressive strength of concrete fracture

$\varepsilon_{pcU}$ = 0.004 : deformation of concrete fracture

The following stress-strain diagram for short-term load shows the meaning of these parameters:

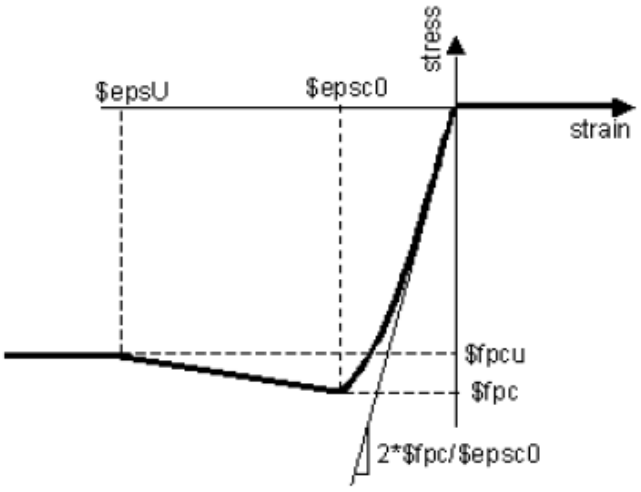


Figure 3–16 Trend Chart model "*Concrete01*" deformation under monotonic loading

The initial slope of the graph, which specifies the concrete modulus $E_c$, calculated from the equation: $2 \cdot f_{pc} / \varepsilon_{psc0}$ . The behaviour of the material in cyclic charge is shown by the following typical hysterical stress-strain loop.

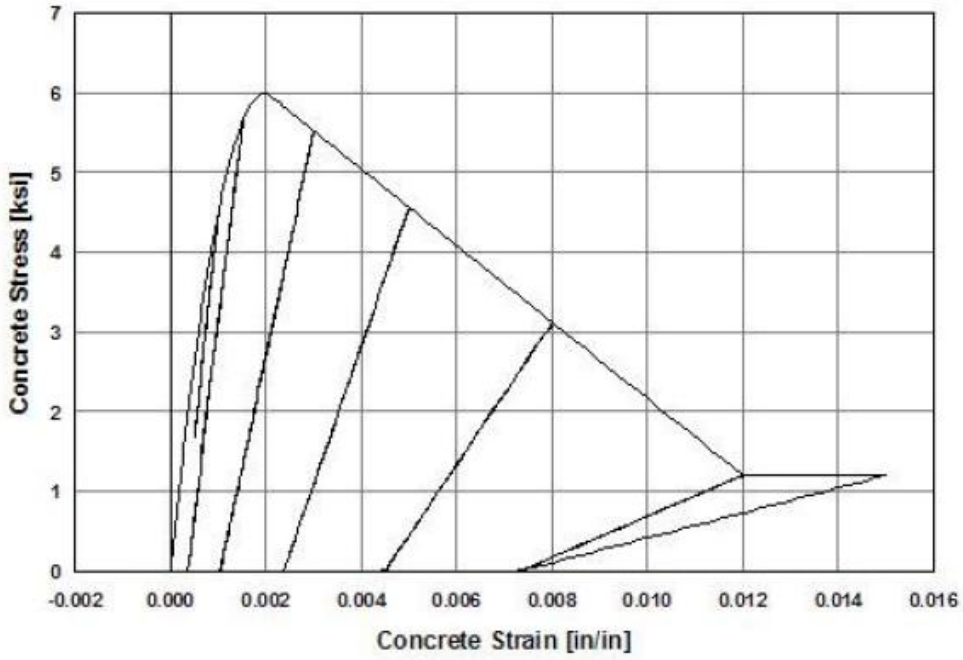


Figure 3–17 Trend Chart model "*Concrete01*" deformation under cyclic loading

### 3.4.4. Steel reinforcement

For steel, the material model used was "*Steel01*", which has unidirectional behaviour with bilinear stress-strain diagram to simulate material hardening. The mechanical behaviour is described by the following parameters:

fy= 371 Mpa : yield stress.

$E_s$=200 Gpa : Modulus of Elasticity of steel.

b= 0.004 : rate of material hardening.

The following simplified elasto-plastic stress-strain diagram under monotonic loading set the following parameters:

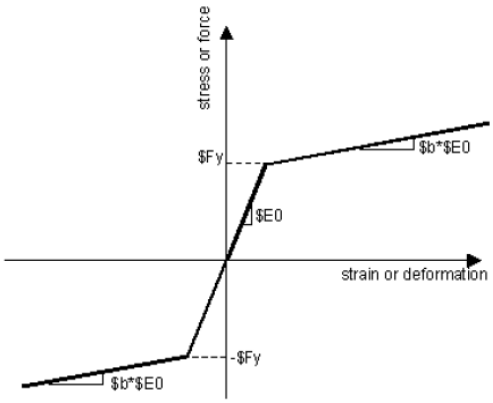


Figure 3–18 Trend Chart model "*Steel 01*" strain under monotonic loading

The behavior of material under cyclic loading is shown in the following typical hysteric loop:

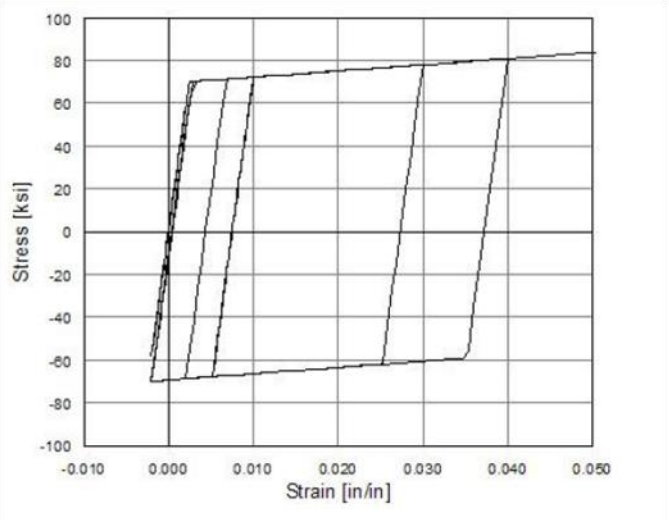


Figure 3–19 Trend Chart model "*Steel01*" deformation under cyclic loading

## 4. Modal Analysis

Below are listed the eigenperiod of the experimental building, which resulted from the solution of singular problems $(K-\omega^2 M)\cdot\varphi=0$, where the K is the stiffness matrix and M the mass record.

The solution of the above system of linear equations results the eigenperiods. The numerical results of the analysis are listed below. From the shapes of the first eigenmodes (fig. 4-4 and 4-5) it is concluded that are coupled, containing rotational component to a greater or lesser degree, which is expected due to the asymmetries and the static eccentricity that has the structural system of the building.

| T (sec) | Lumped | | Fiber-lumped | | Fiber | | Experimental | |
|---|---|---|---|---|---|---|---|---|
| | infills | bare | infills | bare | infills | bare | infills | bare |
| 1st | 0.33 | 0.40 | 0.26 | 0.29 | 0.33 | 0.40 | 0.20 | 0.43 |
| 2nd | 0.24 | 0.28 | 0.23 | 0.26 | 0.27 | 0.30 | 0.15 | 0.37 |
| 3rd | 0.19 | 0.22 | 0.17 | 0.19 | 0.21 | 0.25 | 0.13 | 0.28 |
| 4th | 0.12 | 0.14 | 0.10 | 0.10 | 0.12 | 0.14 | 0.09 | 0.15 |
| 5th | 0.08 | 0.09 | 0.07 | 0.08 | 0.09 | 0.10 | 0.07 | 0.12 |

Figure 4–1: Comparative values of eigenperiods

From the above results it is assumed that the simulations, which do not include the influence of the masonry, proved to be a very good approximation especially for the fiber and lumped elements (maximum deviations of 1$^{st}$ eigenperiod: 7%, 2$^{nd}$: 22% and 3$^{rd}$: 17%) but good enough for the fiber-lumped (maximum deviations of 1$^{st}$: 32% 2$^{nd}$: 30% 3$^{rd}$: 32%). All analytical results have, however, lower values of eigenperiod than those of the experiment.

The simulations that include the influence of the masonry have significantly greater deviation from the experimental results with the additional characteristic that eigenperiods are above than those of the experiment. It seems that the experiment is stiffer than the analytical models. Again the fiber and lumped elements are very close but eigenperiods are now higher than the experimental results (maximum deviations of 1$^{st}$: 65%, 2$^{nd}$: 66% 3$^{rd}$: 53%) compared with the corresponding results for fiber-lumped elements (maximum differences 1$^{st}$: 30% 2$^{nd}$: 53% 3$^{rd}$: 30%). These deviations are calculated as the absolute difference from the ratio of unit size analysis by experiment.

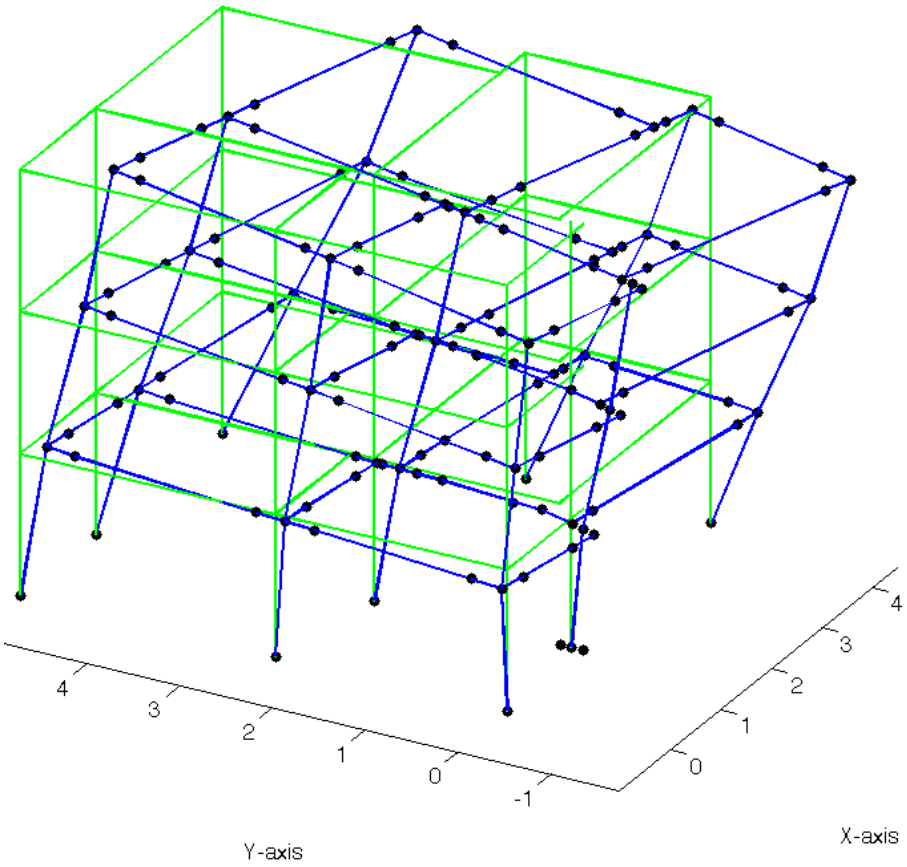


Figure 4–2 Display of 1st Eigenperiod

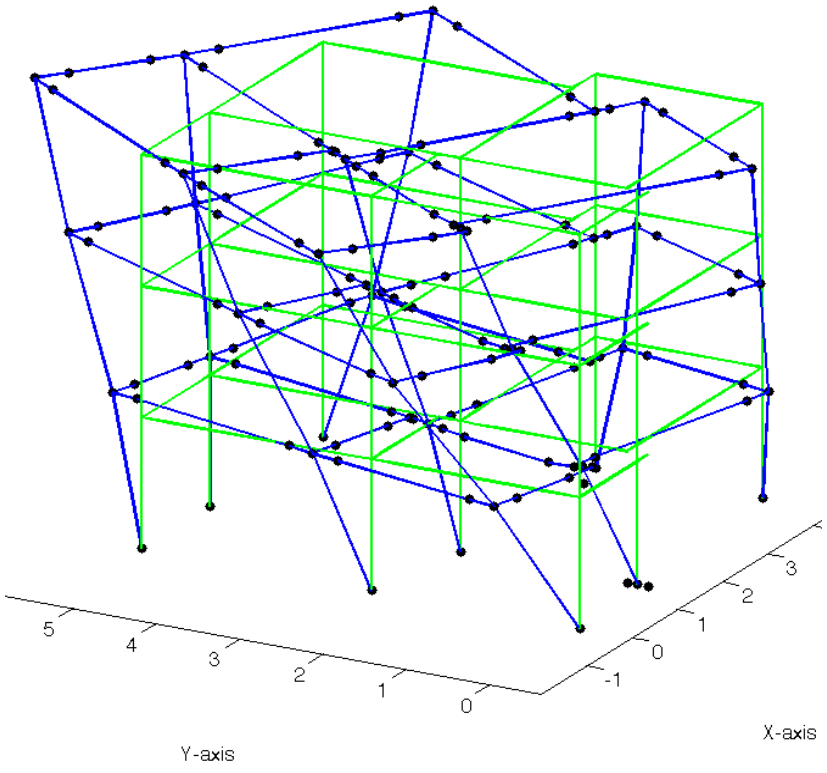


Figure 4–3 Display of 2nd Eigenperiod

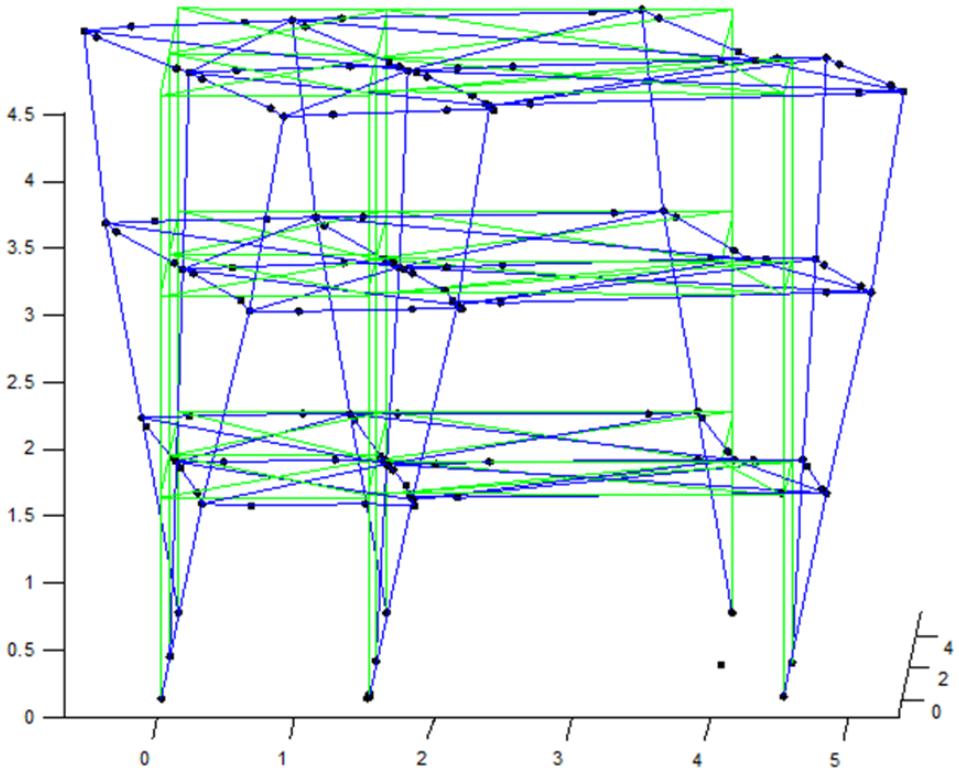


Figure 4–4 Display of 3rd Eigenperiod

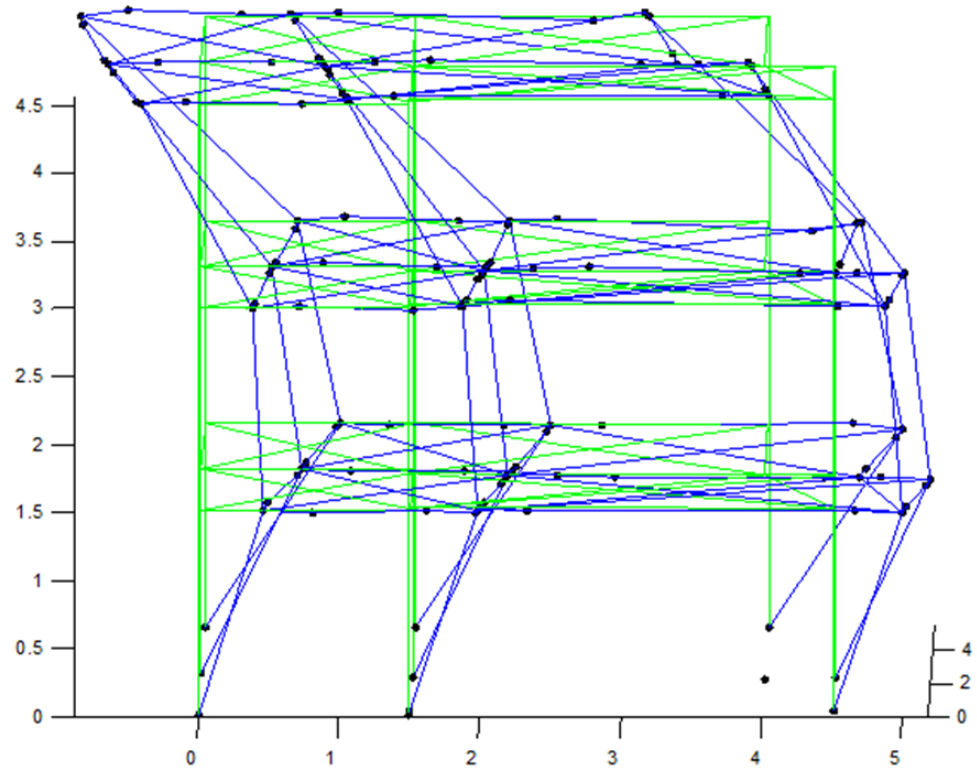


Figure 4–5 Display of 4th Eigenperiod

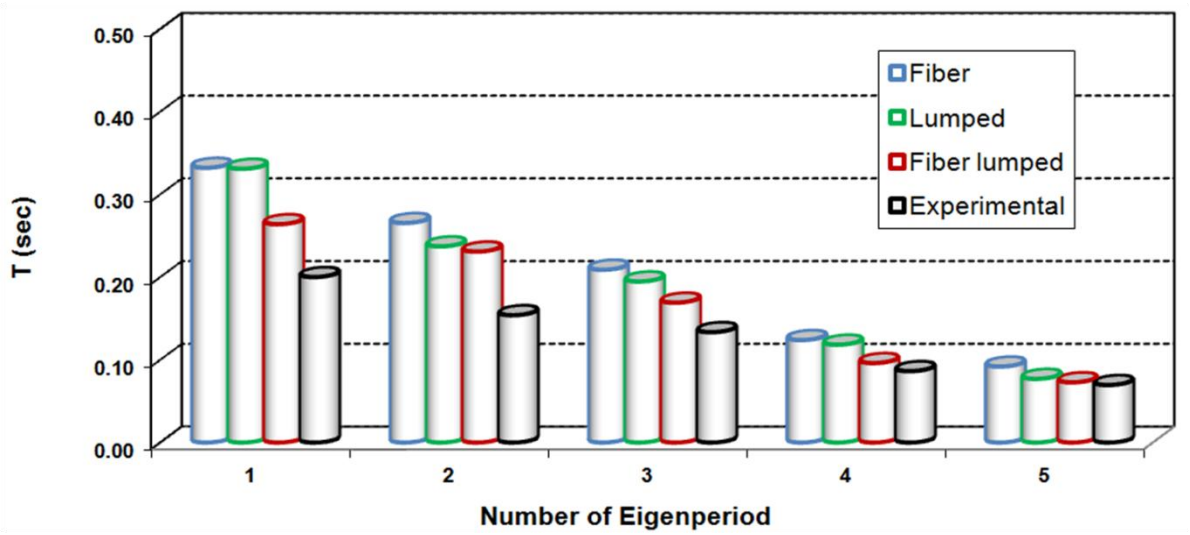


Figure 4–6: Comparison between the eigenperiods of the infilled building versus the experimental data

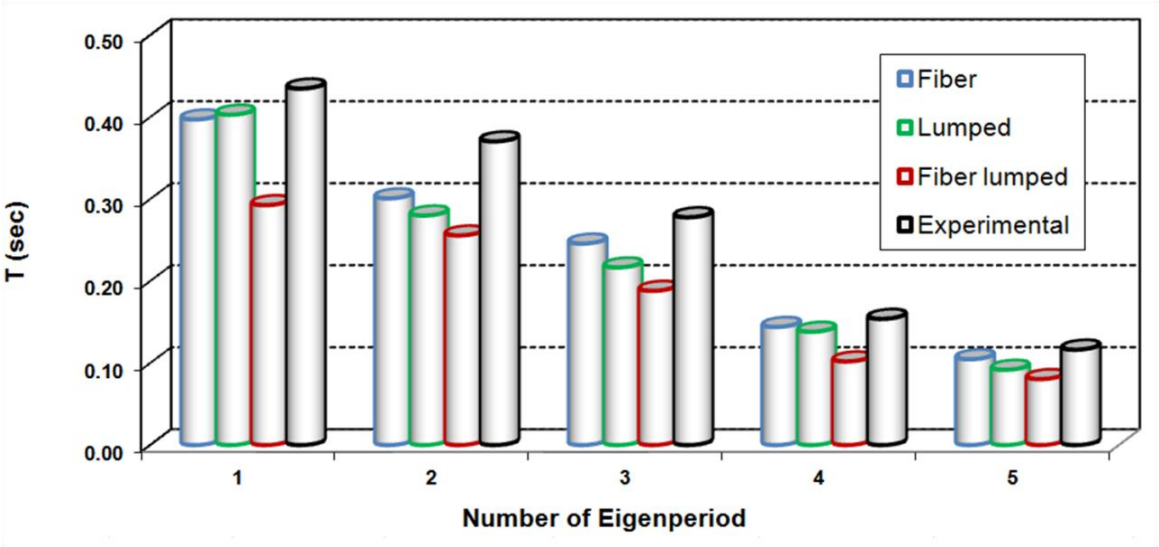


Figure 4–7: Comparison between the eigenperiods of the bare building versus the experimental data

# 5. Numerical results

This chapter presents the analyses results of the modelled structure with the elements as described in chapter 3. The simulation of fiber elements is considered as the most accurate, so initially, these detailed results will be presented and then will be compared with the experimental, obtained from the shake table, so as to come in useful conclusions regarding practice. Afterwards the simulation of lumped and fiber-lumped elements will be presented and compared with the experimental data. Also a comparison will be made between the fiber elements in order to make clear which is the most accurate simulation.

## 5.1. Distributed plasticity elements

Results relate the roof displacement response to the base shear for static analysis and comprise both positive and negative direction of X axis (± X) and Y axis respectively (± Y). In dynamic analysis time related displacements were extracted at every level and maximum displacements in the elevation of certain columns.

### 5.1.1. Static Analysis

For the analysis under consideration, at each direction, a compare is made between with a reference response and those emerging from changes in modeling. The aim of this is to examine the influence of various factors in solution such as that of infill walls, P- Delta effects, storey slab stiffness and direction's influence.

As reference response is considered the one at positive axis, at each direction under consideration, with the influence of the infill walls and slabs in the model. This reference analysis takes also into account non-linearity of materials and geometry (P-Delta).

The resulting response curves relate the base shear with the roof displacement or the interstorey drift. In the following, solutions with changes to the aforementioned factors will be presented, at first those for excitation of the structure to X axis and then those to Y axis.

**Infill walls influence**: The presence of the wall infills increases the base shear capacity of the building. The maximum base shear capacity of the bare frame is 55kN while the one with masonry is up to 80kN (fig. 5-1). Furthermore, if the non-linearity of geometry is not taken into account then the resistance of the structure is underestimated, mostly the residual resistance (fig. 5-2).

**Slab stiffness influence**: The base shear capacity is slightly reduced when slab stiffness is not taken into account (fig. 5-3).

**Loading direction influence**: In addition the structure has a similar reaction in both directions and the main difference is in the negative direction where the maximum strength is slightly larger than in the positive one. The same happens with the stiffness of the structure (fig. 5-4). Below are presented the corresponding charts.

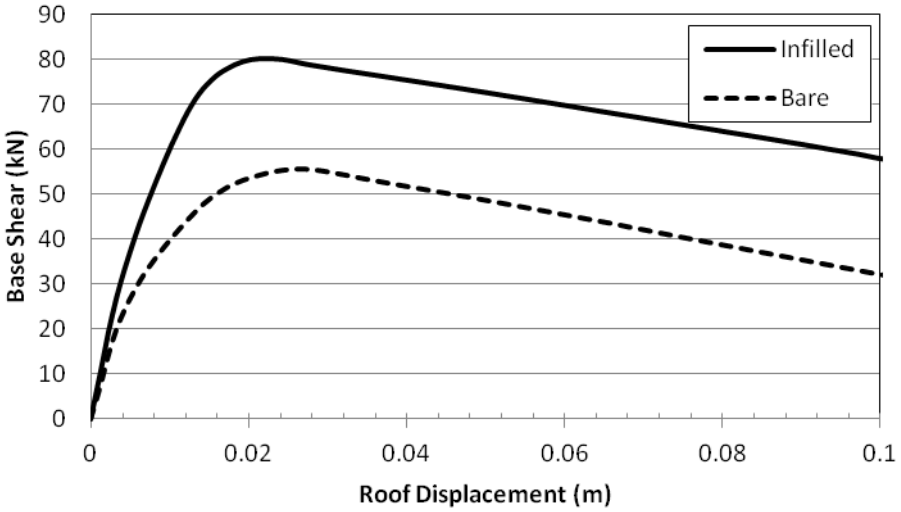


Figure 5–1: Bare versus infilled frame

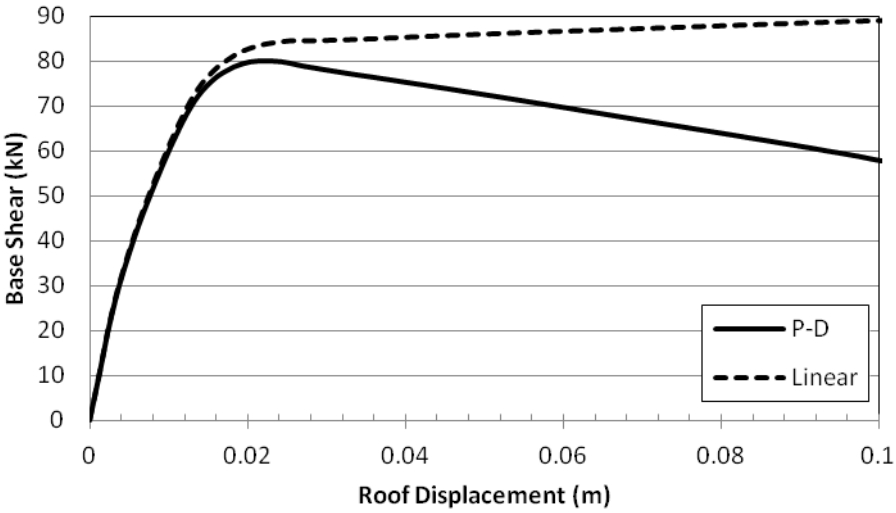


Figure 5–2: Influence of P-Delta effects in (X-direction)

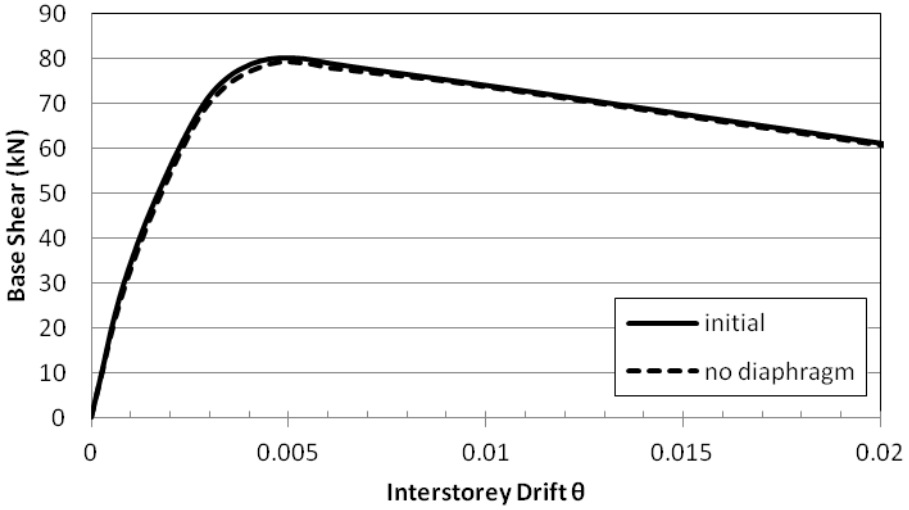


Figure 5–3: Influence of rigid diaphragm (X direction)

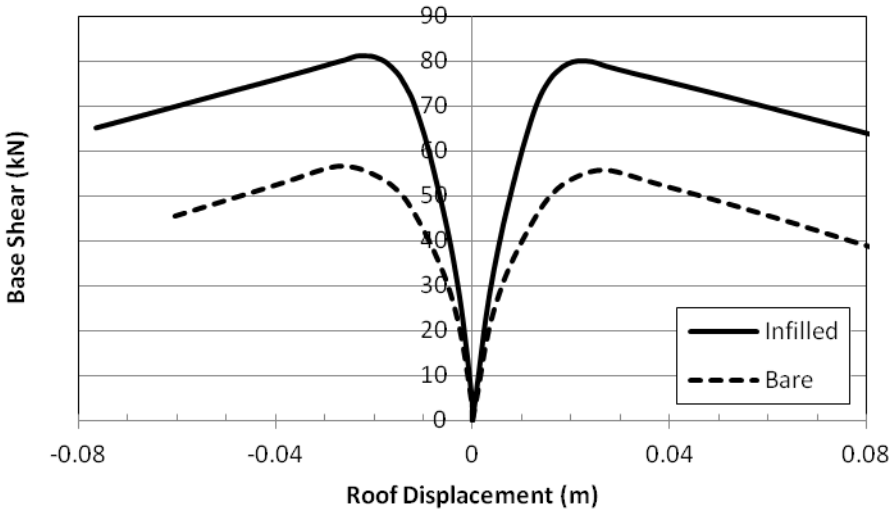


Figure 5–4: Response on the X axis in both directions

**Y direction**: As in the case of X direction, already examined, the presence of the infill walls clearly increases the overall stiffness in the direction Y axis also. Furthermore, it is observed that the building in the direction Y is more stiff than in X direction, mainly due to the presence of column C2 (0.375 x 0.125) (fig. 5-5). Again the infill walls increase about 25% the building's shear capacity (fig. 5-6) while the second order effects in the Y direction are less severe than in X direction, due to column C2 favourable action (figure 5-8). Finally the absence of the slabs in the simulation reduces the structure capacity at a higher percentage than the X's direction due to the strongest moment of inertia in Y direction (fig. 5-7).

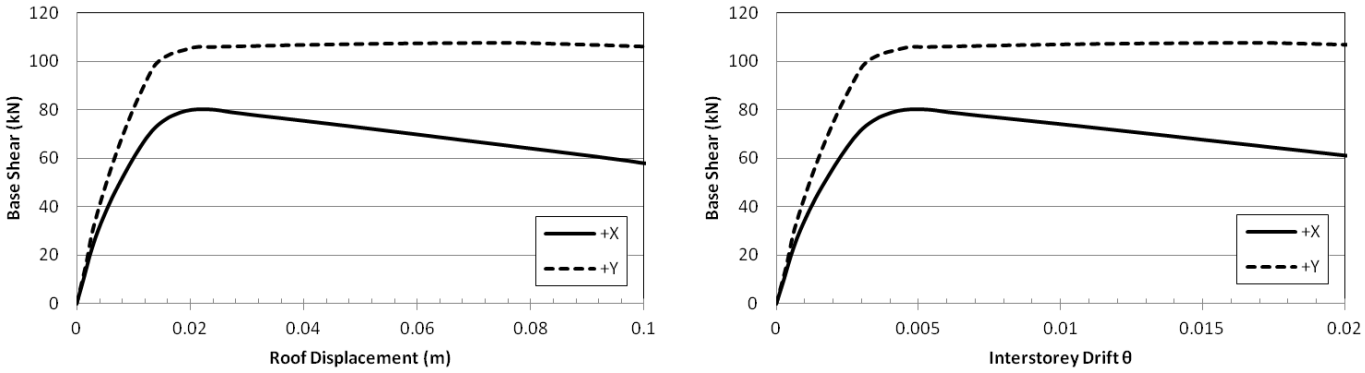


(a) (b)

Figure 5–5: Comparison of response between X and Y axis: (a) Drift (b) roof displacement

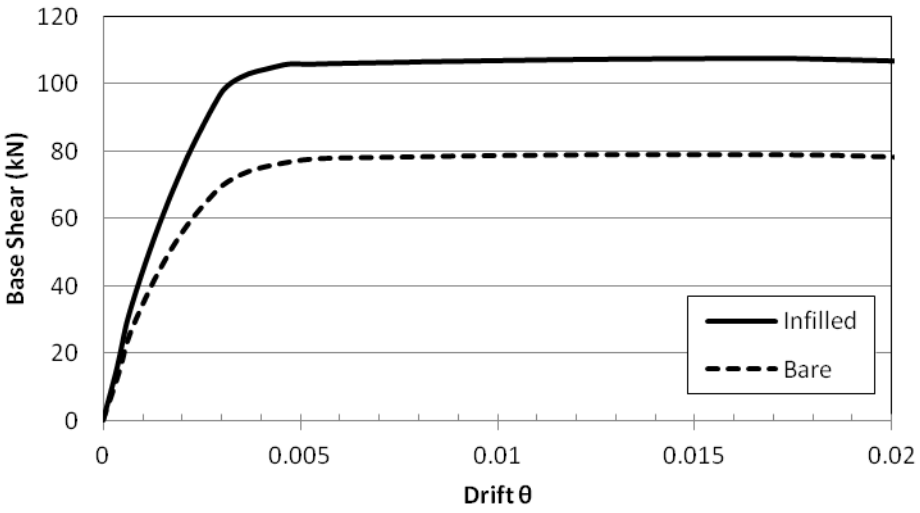


Figure 5–6: Infill walls influence at Y axis

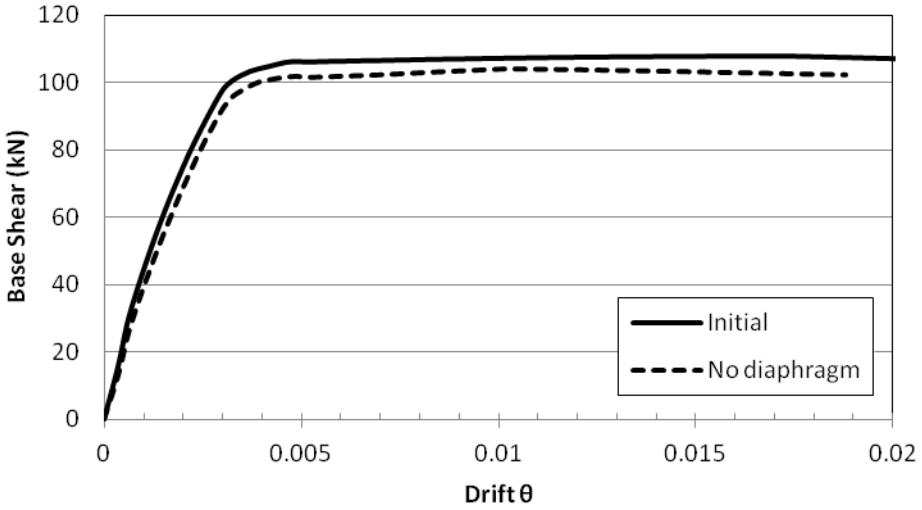


Figure 5–7: Slab stiffness influence at Y axis

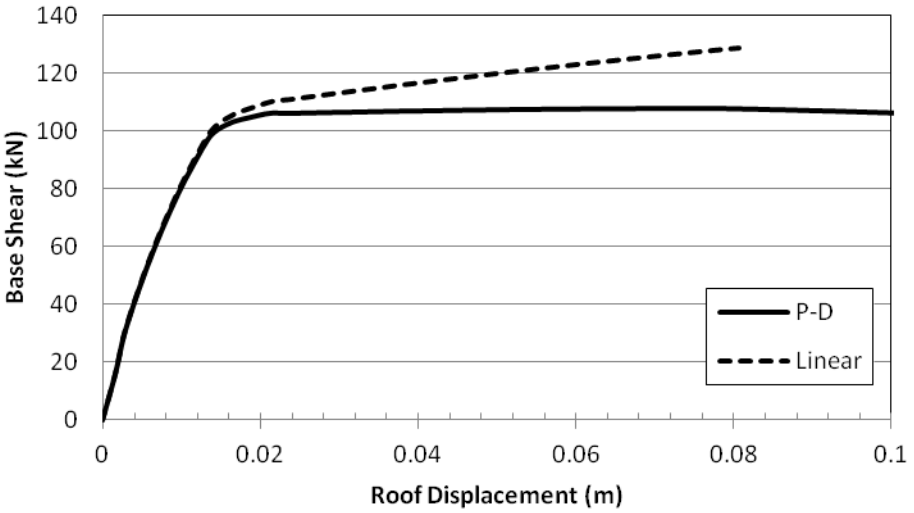


Figure 5–8: P-Delta effects influence at Y axis

### 5.1.2. Non Linear Response History Analysis

The simulation with fiber elements underwent two ground excitations with ground accelerations 0.30g and 0.54g respectably following the accelerograms of the earthquake of Montenegro. At the figures below are listed the relevant envelops of horizontal displacements as a percentage of the height of each floor (drift) in the direction of ground motion.

Figure 5–9: Displacement gauges of column C6

In this case also the reference time history simulation is the one that takes into account the presence of the infill walls and the second order phenomena (P-Delta) for ground acceleration 0,54g. The other simulations are compared with this.

As an overall conclusion the relevant displacements of the first two floors seem to be similar, while on the third are much smaller (fig. 5-10) and have the shape of the first eigenmode (fig. 4-4). The influence of non-linearity of geometry at the displacements is relatively small compared with the overall, while the absence of the masonry increases the movement (fig. 5-11). Finally the displacements of the more intense ground motion (0.54g) are three times higher than the less (0.30g) (fig. 5-12).

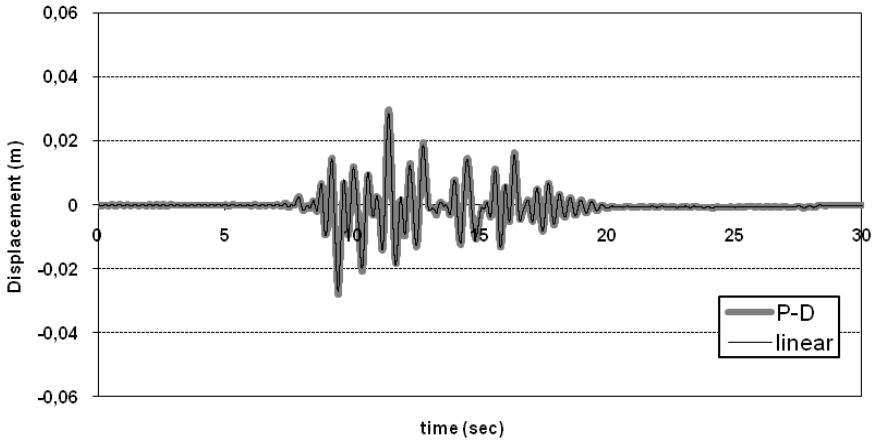


(a)

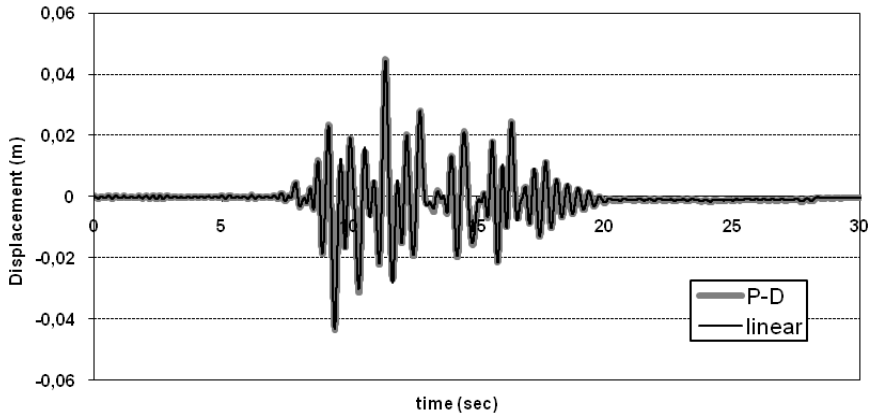


(b)

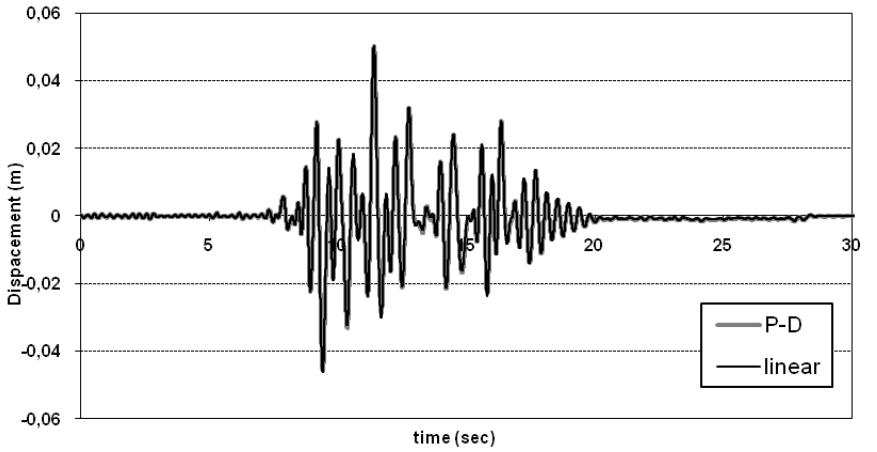


(c)

Figure 5–10:Displacement time history, with and without P-Delta effects, (a) 1st floor, (b) 2nd floor, (c) 3rd floor

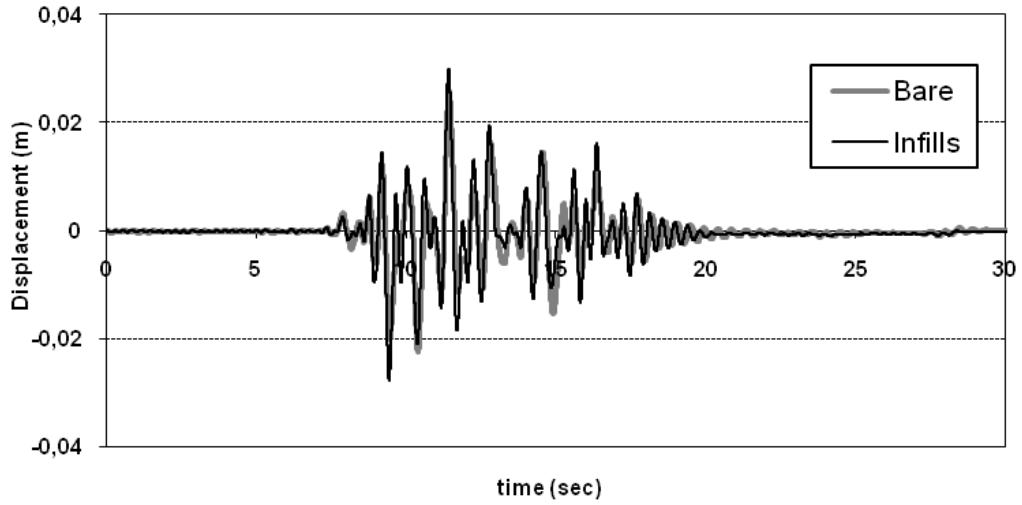


Figure 5–11:Displacement time history of the first floor, with and without infill walls, taking into account the non-linearity of material

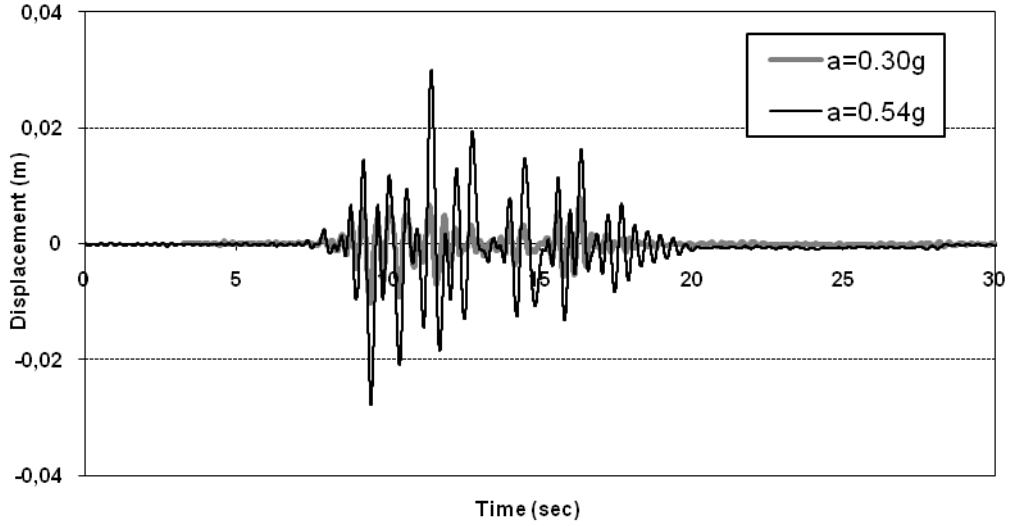


Figure 5–12:Displacement time history of the first floor, with infill walls for ground accelerations 0.3g & 0.54g, taking into account the non-linearity of material

In figures 5-11 and 5-12 the displacement time history of the first floor of the structure was presented but looking the displacements in elevation the distribution of damages over the height of the building can also be estimated. These next two charts show the displacements over height, with and without infill walls. Disregarding the first floor it is evident that the presence of the infill walls helps to reduce deformation of the building.

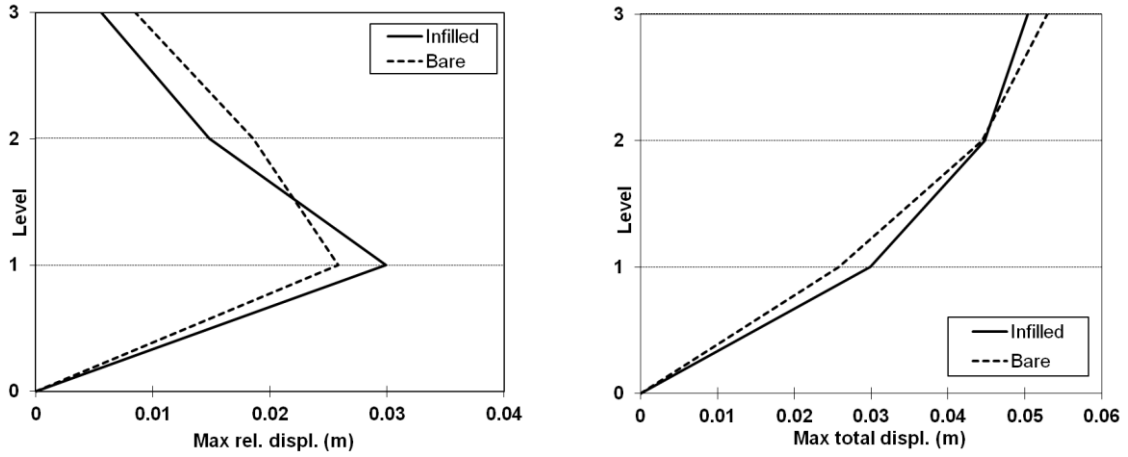


(a) (b)

Figure 5–13: Influence of infill walls: (a) Maximum relative displacements (b) Peak shifts

On the previous charts the nonlinearity of the material was taken into account. On the next is presented the maximum and relative displacements of structure depending on whether or not there is linearity in geometry. As revealed by the displacement time history of the first floor the P-Delta effect does not play an important role as a reference for the displacements.

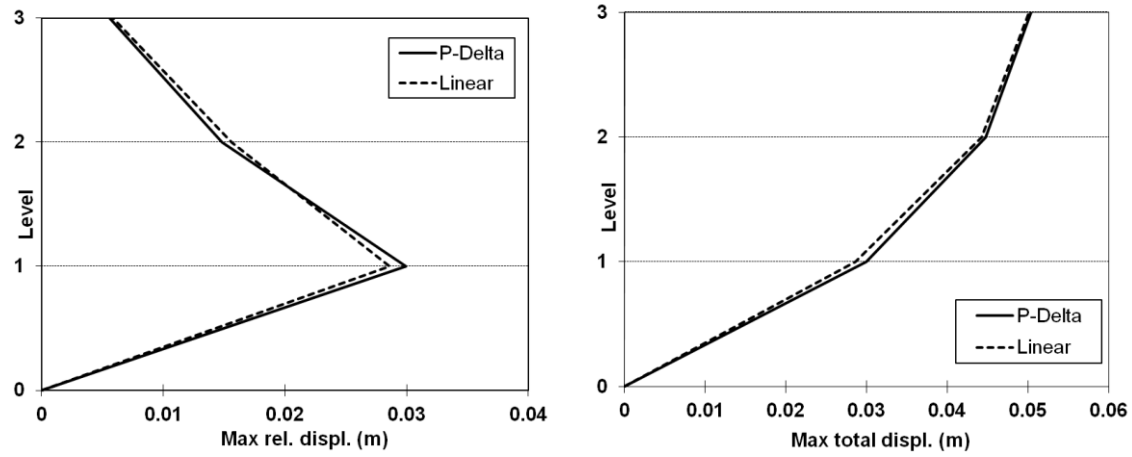


(a) (b)

Figure 5–14:Geometry nonlinearity (P-Delta effect) (a) Comparison of maximum relative displacements (b) Comparison of maximum displacements

Finally the structure maximum and relative displacements are compared for ground accelerations 0.54g and 0.30g, respectively. It is worth to notice the non analogous response, as displacements concern, to ground motion intensity.

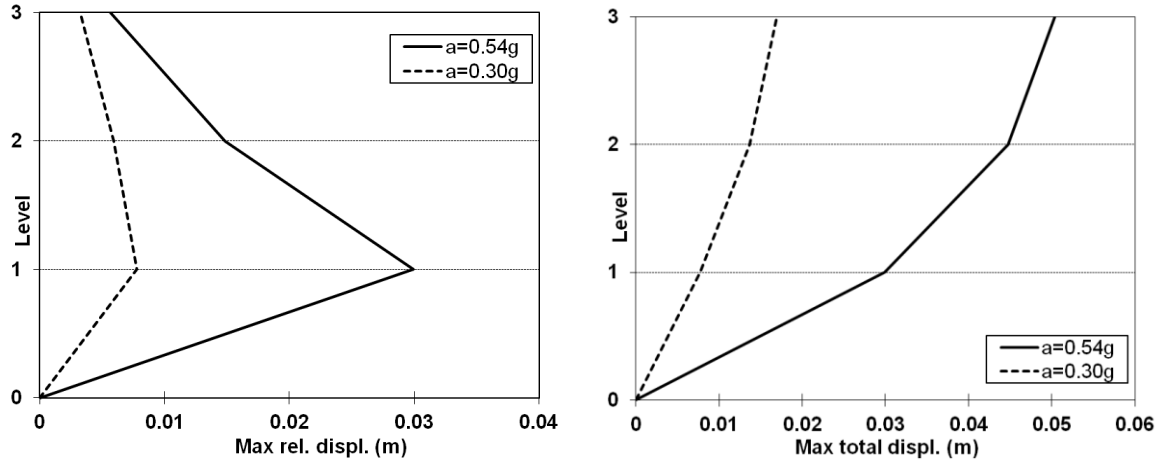


(a) (b)

Figure 5–15:Ground excitation intensity for ground acceleration 0.54g and 0.30g: (a)Maximum relative displacements (b)Maximum displacements

### 5.1.3. Comparison of experimental results with analytical results

In order to compare simulation with experimental results the most reliable model (i.e. fiber elements) was selected. This simulation takes into account non-linearities of the materials, geometry and structure infill walls.

In the following figures is compared the time history of displacements and drift (maximum relative displacement to storey height) and also the maximum relative displacements of one column (C6 was selected) for ground accelerations 0.54g and 0.30g.

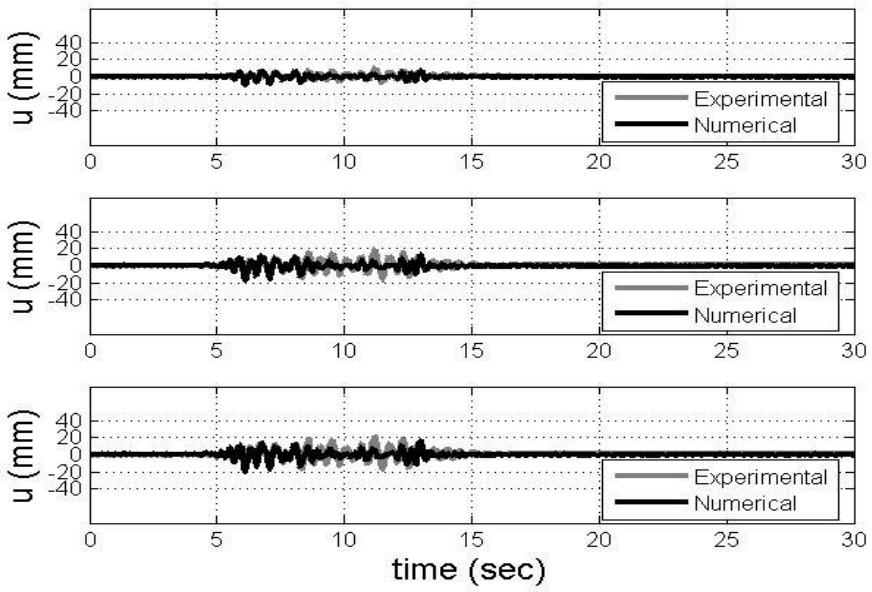


(a)

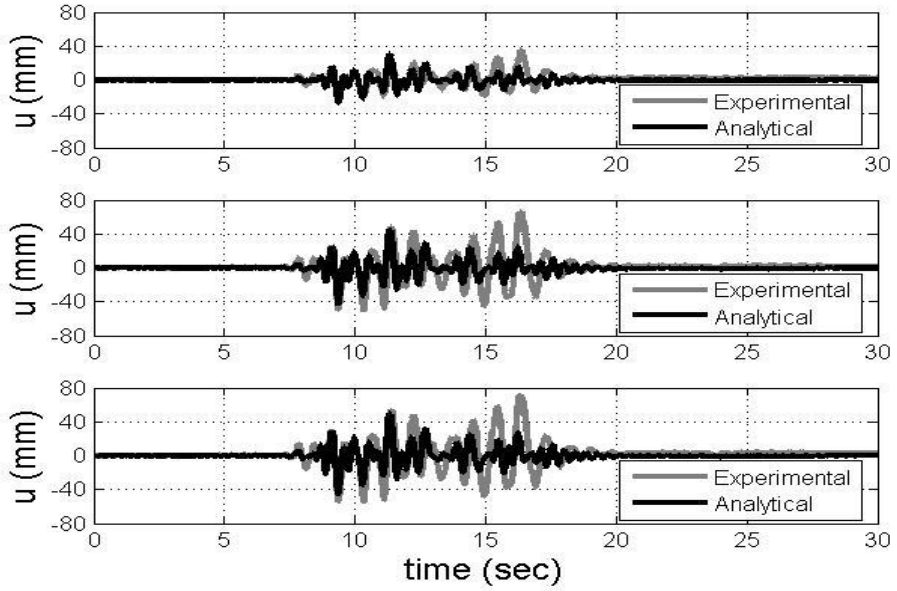


(b)

Figure 5–16: Displacement time history for the three floors of building for ground acceleration (a) 0.30g, (b) 0.54g

**Displacements time history:** In the above figure 5-16 the three floors displacements time history of the column C6 (fig. 2-2) for ground accelerations 0.30g and 0.54g, are compared. For ground acceleration 0.30g simulation follows successfully the format of the curve especially in the area on the eighth second. During the 11th to 12th seconds, there was a little difference, but all the peaks are registered. For the ground motion of 0.54g, experimental results show two main pulses at the 9th and 16th seconds. The results of the analysis describe satisfactory the time history until the 14th second, and after that point a mistake is apparent on the period and range. The inability of the simulation to describe the difference is probably due to a lack of evaluation of the behaviour of the infill walls; it is also possible that the underestimation of the largest ground acceleration it is due to the persistent failures of the experimental structure of prior test with ground acceleration 0.3g.

**Drift time history:** Figure 5-17 shows the relative movement of the first floor divided by the height of the floor (drift) for both ground accelerations. The maximum drift difference for ground acceleration 0.54g is approximately equal to 2.4% but for the first seconds. Then the situation described above is clearly displayed, i.e. deviation from the 14th second and then.

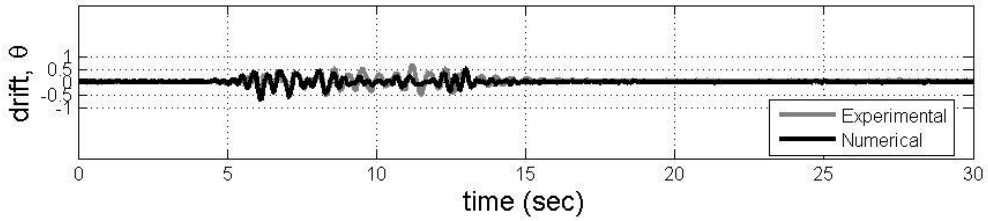


(a)

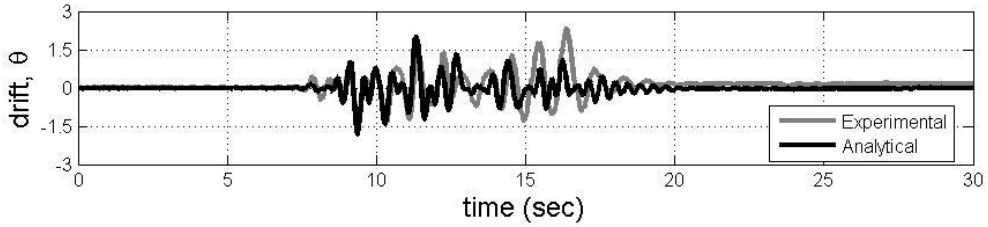


(b)

Figure 5–17:Drift for the 1st floor of building for PGA (a) 0.30g, (b) 0.54g of fiber elements

**Column C6 maximum relative displacements:** The aim is to present (figure 5-18) the ability to estimate damage distribution over height as well as column rotation demand. The maximum relative displacement is located on the level of the first floor, for both time histories, while on the level of the second is somehow the same. The deviation of analysis from experiment results is small in both cases. Actually the first time history (a=0.30g, fig. 5-18a) analysis overestimates displacements while the second (a=0.54g, fig. 5-20b) underestimates them. In both cases 3rd floor displacement is exact. It is probable that underestimation of displacements of the second case to be depended on residual cracks due to the first excitation of the experimental structure.

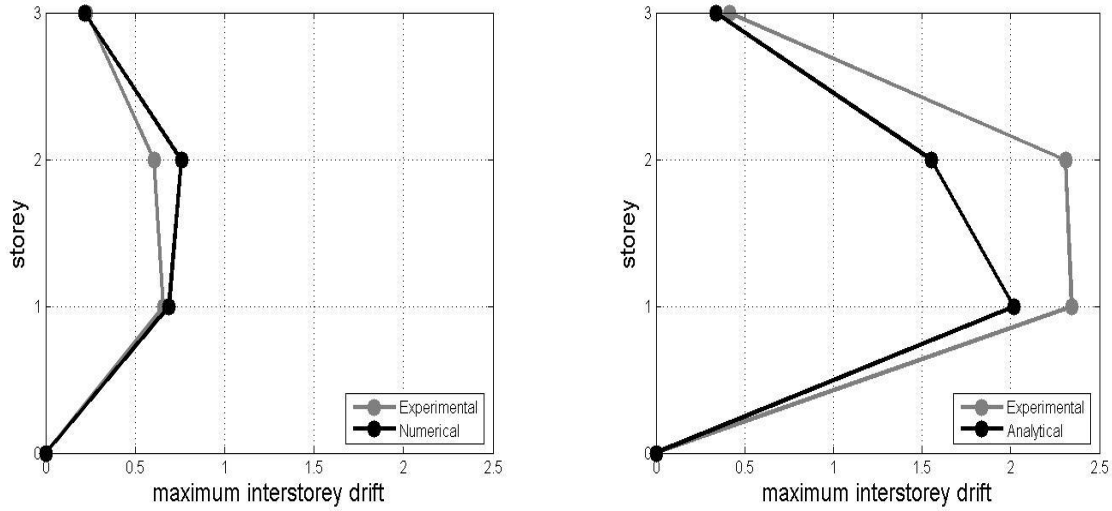


(a) (b)

Figure 5–18:Maximum relative displacement of structure C6 column for ground acceleration (a) 0.30g, (b) 0.54g

## *NUMERICAL RESULTS WITH DISTRIBUTED PLASTICITY ELEMENTS*

Below are presented few typical failures after the end of the 0.30g and 0.54g ground motion. The failures which occur after the small motion are mainly cracks at the infill walls, except of a local collapse on the second floor, but not at the R.C. frame of building (fig. 5-19). In the opposite side, failures at beams and columns mainly, occur after the second ground motion. More specifically in fig 5-20 are presented the damages at column C1, C5 and the damage in elevation of column C2. These of C2 are spalling of concrete cover and destabilization of the longitudinal bars (fig.5-21).

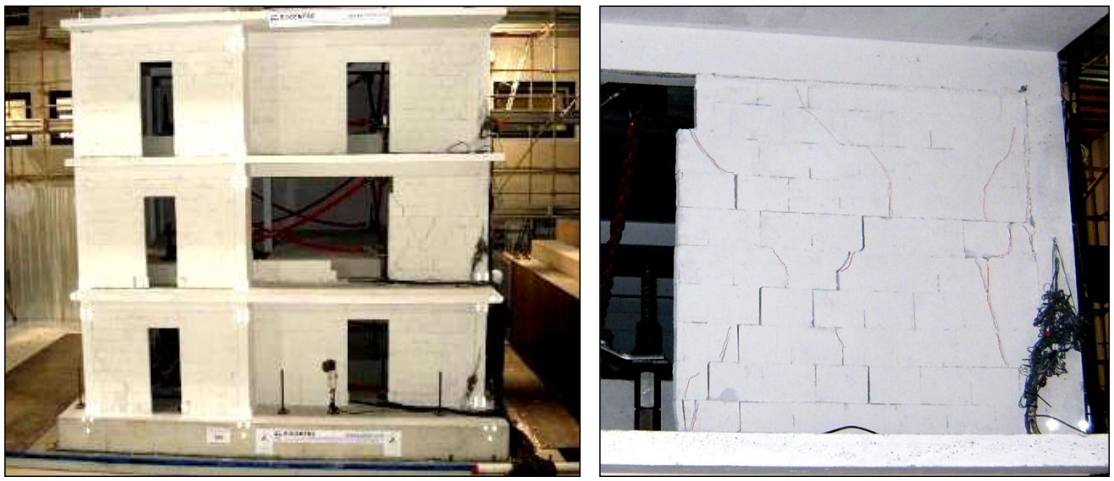

(a) (b)

Figure 5–19: (a)East side view of the structure, after the first ground motion PGA = 0.30g, and (b)Detailed picture of the cracks developed in the infill walls of the second floor

(a) (b) (c)

Figure 5–20:Horizontal cracks at mid-height of column 1, (b) Damages at the top of column 5, Level 1, (c) Damage in elevation of column C2 after the second test at PGA = 0.54g

(a) (b)

Figure 5–21:Detail of damage of column C2, with spalling of concrete cover and destabilization of the longitudinal bars after the second ground acceleration (0.54g).

## 5.2. Concentrated plasticity elements

### 5.2.1. General

So far the response of the structure simulated with elements of distributed plasticity (fiber elements) was presented. In this work, however, the structure is simulated also with two other element types, lumped and fiber-lumped elements. In the following presentation, it is compared the response of the original simulation (i.e. distributed plasticity) with the other two, but also with the experimental results of the seismic table in order to see how realistic are the simulations of the structure, using these types of elements.

### 5.2.2. Static analysis

As previously, a reference response is used in order to examine the influence of various factors. As a reference, this time, are considered two responses, one for the lumped and one for the fiber-lumped elements, both at positive axis, at each direction under consideration, with the influence of the infill walls and slabs in the model. These references analyses take into account non-linearity of materials and geometry (P-Delta). The resulting response curves relate the base shear with the roof displacement or the interstorey drift.

In the following, solutions with changes to the aforementioned factors will be presented, at first those for excitation of the structure to X axis and then those to Y axis.

The form of the resistance curves for fiber model, either distributed or concentrated plasticity, are similar and very close to each other, in contrast to the curves of resistance from the simulation with concentrated plasticity (lumped elements), since it is less precise than the other two (fig. 5-22). At the simulation with lumped elements, the structure appears to have its maximum at 100kN while at the other two simulations the peak strength is 80kN. Nevertheless the structure with lumped elements has smaller residual strength in comparison with the fiber elements. So, for the case examined, approach with lumped element seems to be more conservative.

**Infill walls influence**: The presence of the wall infills increases the base shear capacity of the building. The maximum base shear capacity for the lumped and fiber-lumped elements of the bare frame is 74kN and 56kN respectively while the one with masonry influence is up to 100kN and 80kN (fig. 5-23). The percentage of the base shear increase is 26% and 30% respectively.

**Second order phenomena**: Furthermore, if the non-linearity of geometry is not taken into account then the resistance of the structure is overestimated, mostly the residual resistance (fig. 5-24). This happens for both elements.

**Slab stiffness influence**: The base shear capacity is slightly reduced when slab stiffness is not taken into account for both elements (fig. 5-26).

**Loading direction influence**: The difference in the form of resistance curves for lumped simulations on the X axis is not remarkable for the two models except for the increased structure stiffness at the negative direction (fig. 5-25). Below are presented the corresponding charts.

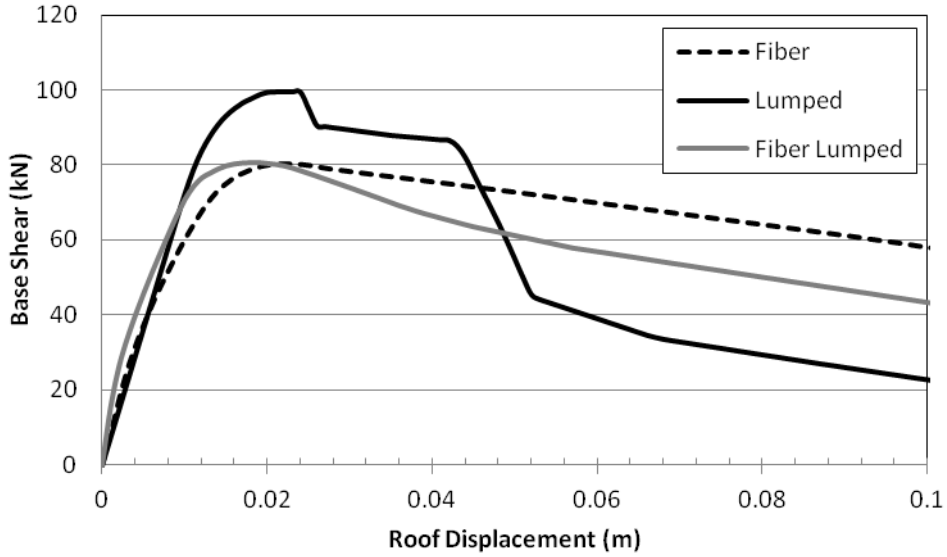


Figure 5–22:Comparison of three different simulations

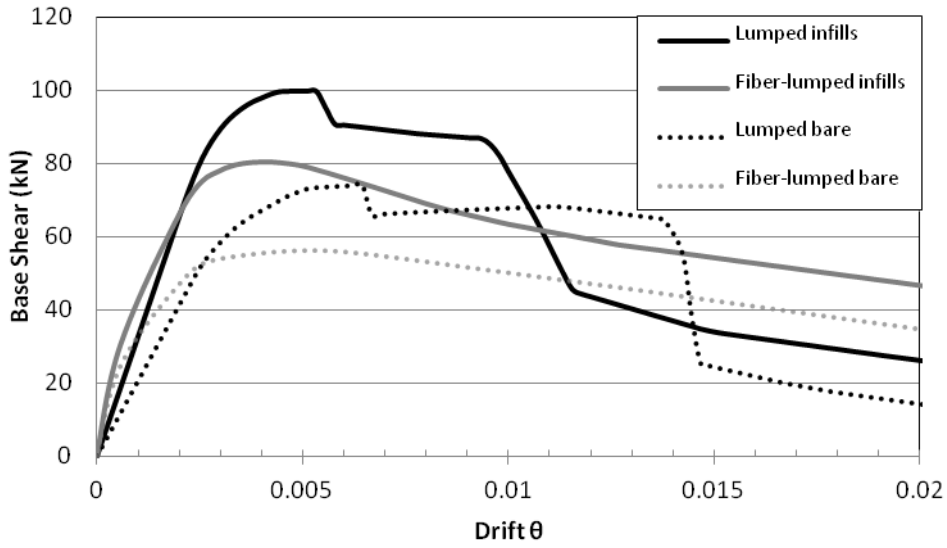


Figure 5–23:Comparison of simulations between lumped and fiber lumped elements with and without the presence of infill walls

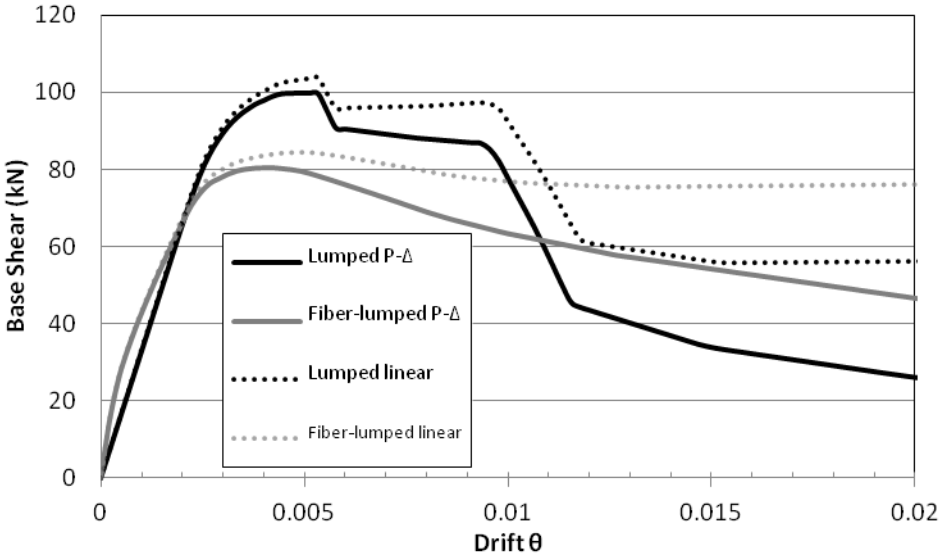


Figure 5–24:Comparison of simulations with or without P-Delta effects - lumped and fiber lumped elements

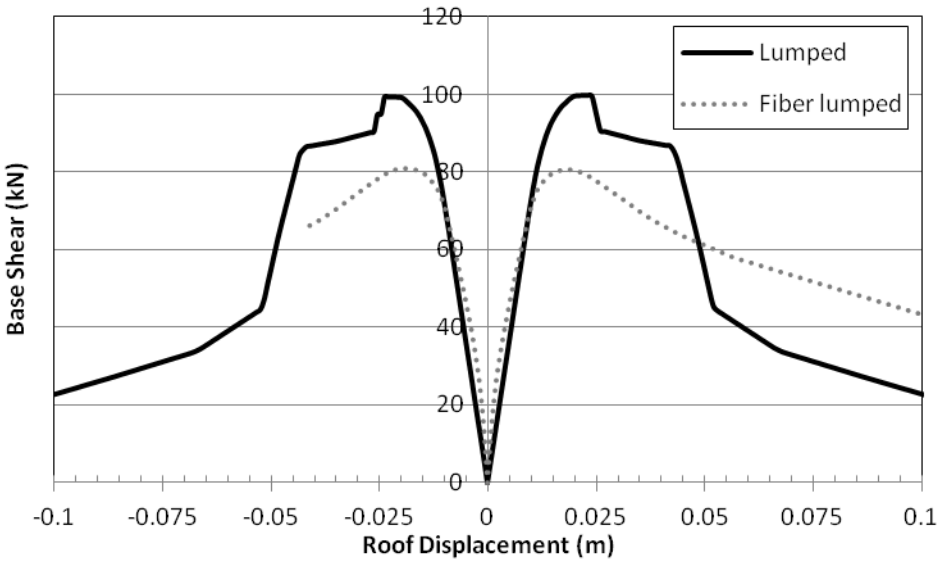


Figure 5–25:Comparison of simulation between lumped and fiber lumped elements on X axis

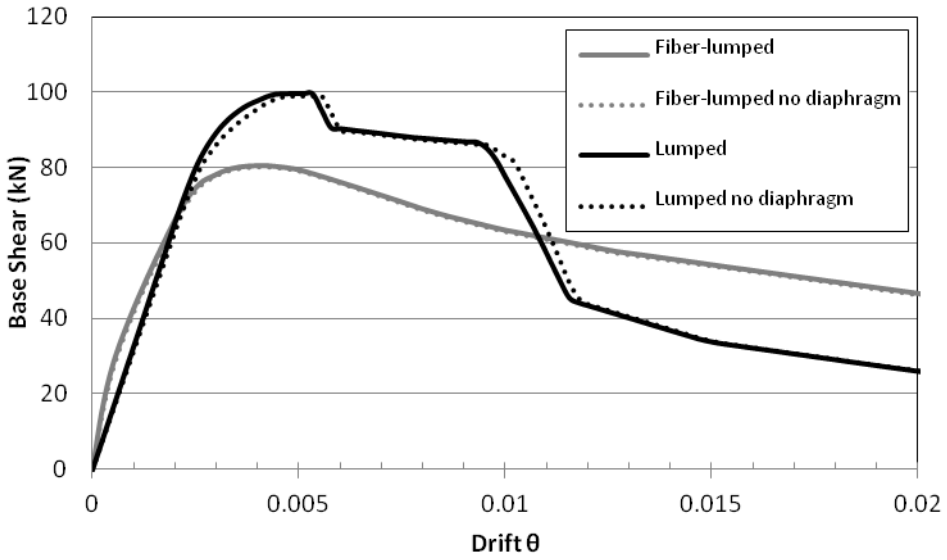


Figure 5–26:Comparison of simulations with and without the presence of slab stiffness - lumped and fiber lumped elements

It should be noted that the resistance curves in X and Y are almost identical with the difference that the Y direction shows a little more resistance due to the presence of column 2 which is the only with rectangular section and has the strongest moment of inertia in Y direction (fig. 5-27). Also, the presence of infill walls for fiber-lumped simulation in the direction Y increases the resistance about 30% (fig. 5-28), same percentage as in relevant of X.

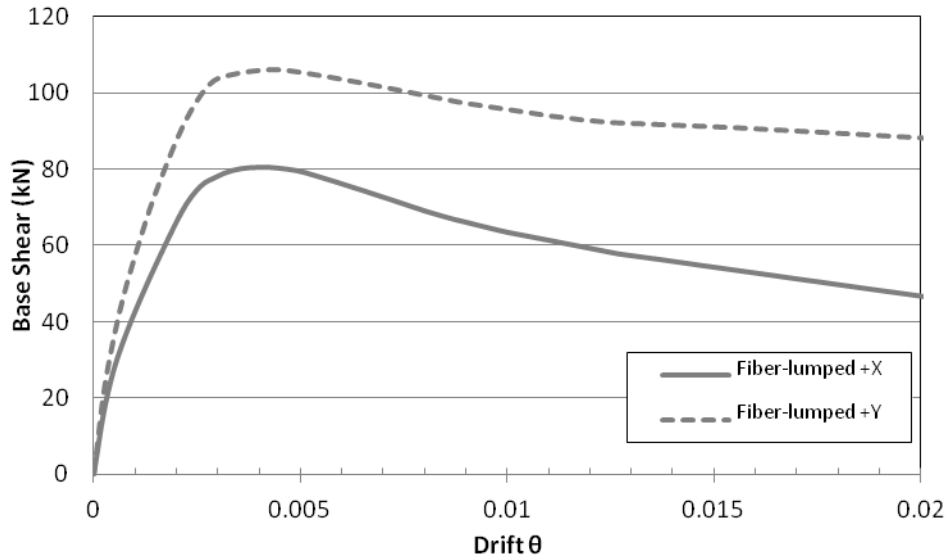


Figure 5–27:Comparison of fiber-lumped resistance curves between axis X and Y.

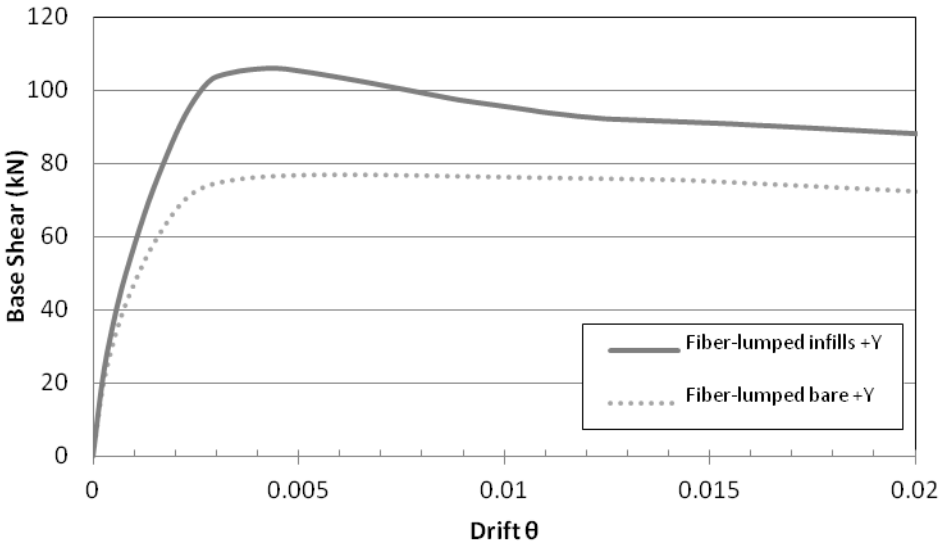


Figure 5–28:Comparing fiber-lumped simulation with and without the presence of infill walls to axis Y

In the following discussion, two more special characteristics of lumped elements will be presented. One is the influence of axial force variation, in columns, to the moment curvature diagram of plastic joint and the second is the influence of plastic joint length.

In lumped elements the moment curvature diagram is calculated based on static axial force of column and so the stiffness of the structure is affected, according to the preselected local moment-curvature diagram for each one point. Figure 5-29, however, presents the variation of axial forces applied to each member and clearly the axial force during the ground motion is far from being constant. Reasons for this phenomenon are the redistribution of stiffness and the non-linearity of geometry due to the local damages.

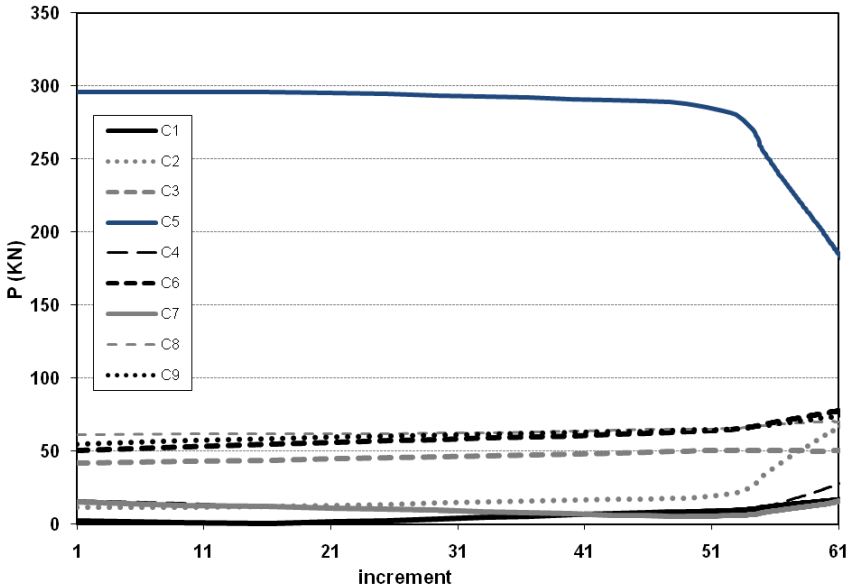


Figure 5–29: Variation of axial force in columns, during the ground motion, in the first floor (lumped elements)

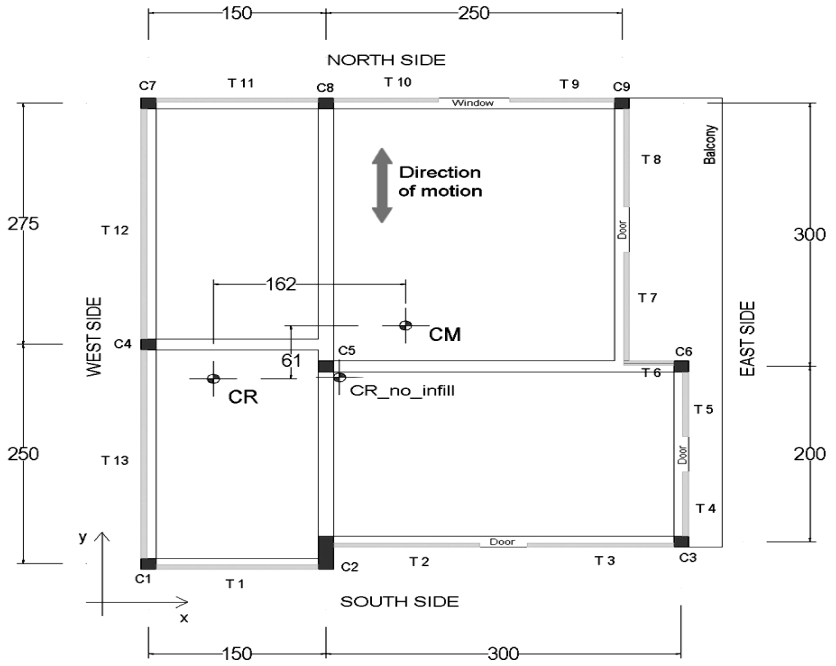


Figure 5–30:Typical floor plan

Figure 5-29 refers to the first floor of structure but still the format is compatible with the other two floors. The influence of the axial force in moment-curvature relations was introduced in the simulation with the lumped elements. The difference in the response of the structure appears in the figure below (fig. 5-31). The increase in strength may be explained due to the redistribution of axial force in the elements of the structure.

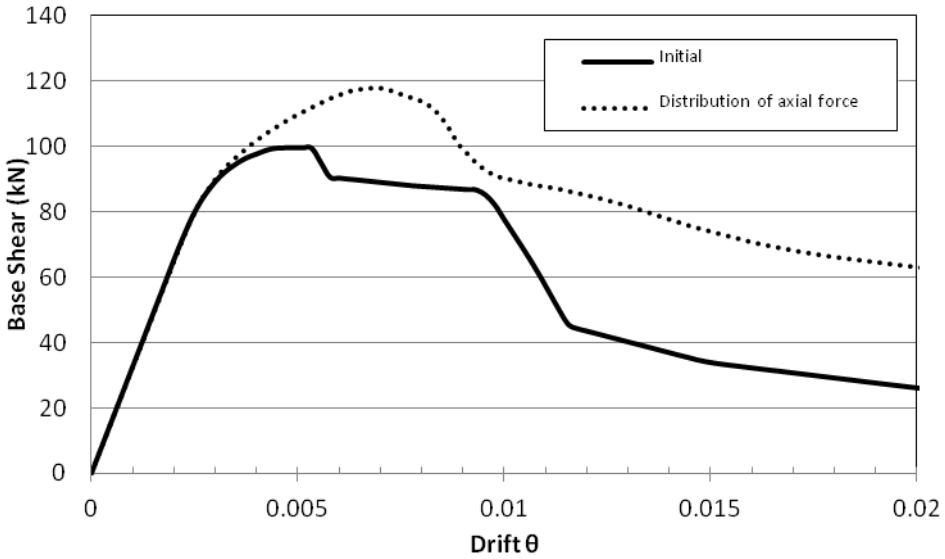


Figure 5–31:Comparison of response when taking into account the effect of the redistribution of the axial force

Concentrated plasticity elements have a very significant disadvantage in relation to distributed plasticity elements; a parameter which affecting the response of the structure is the theoretical length of plastic hinge. The length of the plastic joint has a variable length and depends on many

factors. In all previous analysis presented, the length is considered equal to the height of the cross section of the column (L = h). In order to estimate the influence of this length, the response of the structure was calculated with a range of lengths of plastic hinge. In these calculations the length of plastic hinge considered as 0.5h, 2.0h, $l_p$, and $l_p$*, where $l_p$ is the length proposed at the paper of Scott & Fenves [6] for plastic hinge length and $l_p$* is the length of plastic joint proposed in KAN.EPE (Greek code of practice for the strengthening and repairing of buildings). The values of $l_p$*, $l_p$ depend on the cross section of the element, yield of steel and the diameter of rebar.

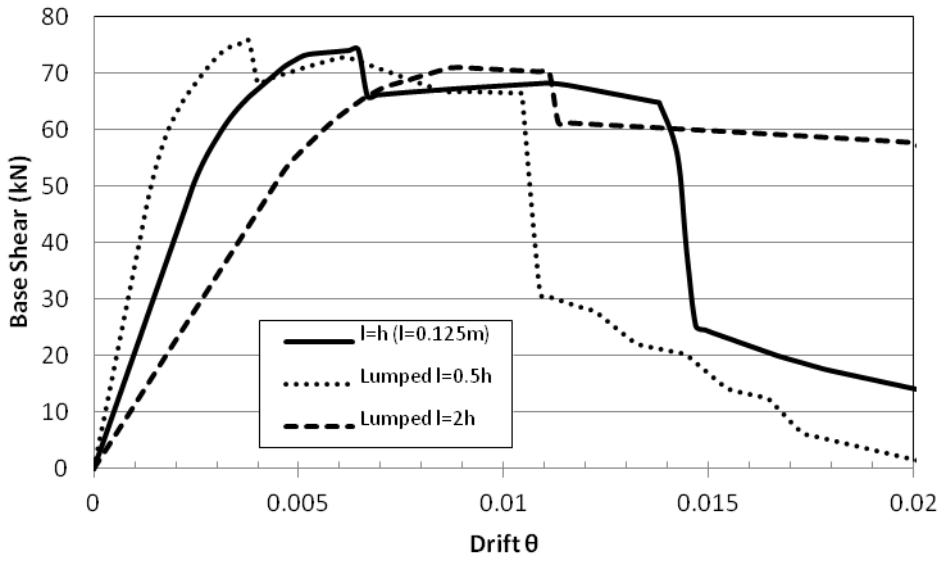


(a) Sensitivity analysis

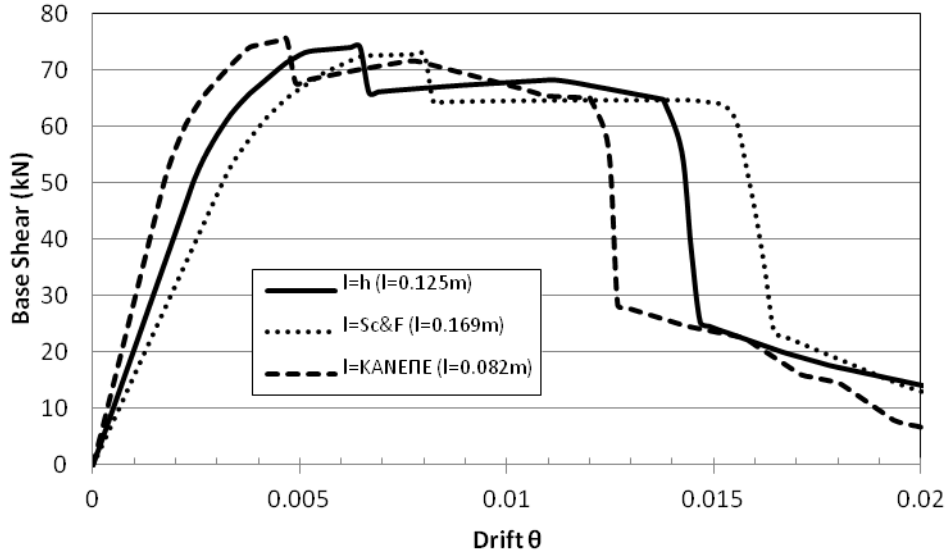


(b) Values from the literature

Figure 5–32 Curves of resistance in the direction of X axis for concentrated plasticity elements and various lengths of plastic hinge

## *NUMERICAL RESULTS WITH CONCENTRATED PLASTICITY ELEMENTS*

It is obvious that, increasing the length of plastic hinges, the stiffness of the structure in the elastic region is reduced but the overall strength of structure increased. The next figure describes the same procedure as above, with the difference that the simulation was with fiber-lumped elements.

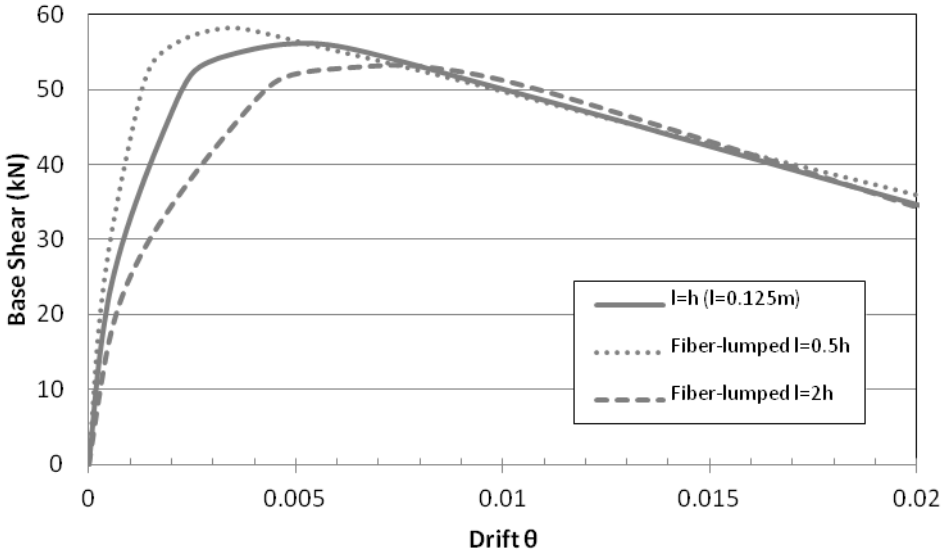


(a) Sensitivity analysis

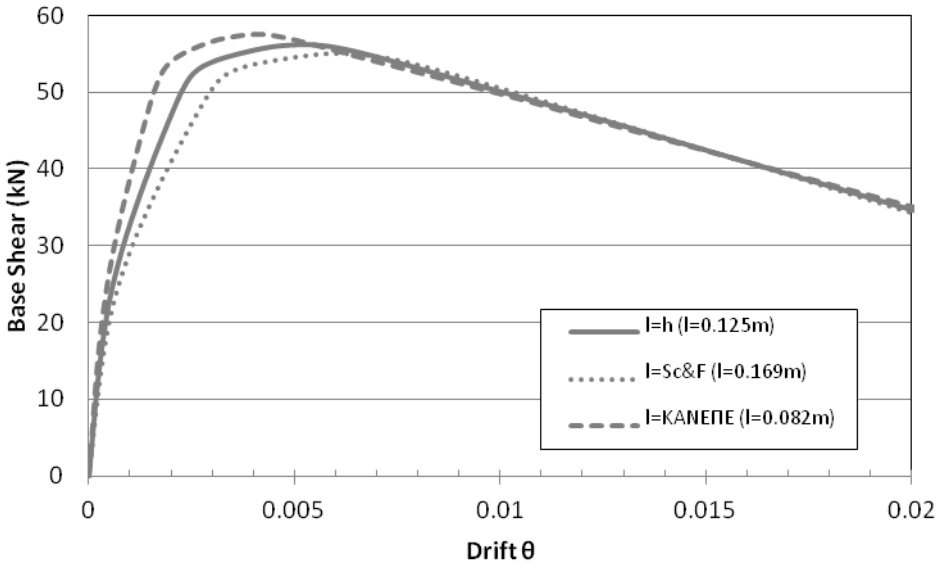


(b) Values from the literature

Figure 5–33: Curves of resistance in the direction of X axis for fiber concentrated plasticity elements and various lengths of plastic hinge

### 5.2.3. Non Linear Response History Analysis

In this chapter the maximum and relative displacements time histories of the structure are presented, for each of the different simulations. In order to evaluate better the three simulations, time history has been calculated without the presence of infill walls but takes in account the non-linearity of materials. The shape of the movements is quite the same for all elements but there are differences in the range of displacements. The biggest displacements occurred from the fiber elements followed by the fiber-lumped elements while the lumped elements result the smallest displacements (fig. 5-34).

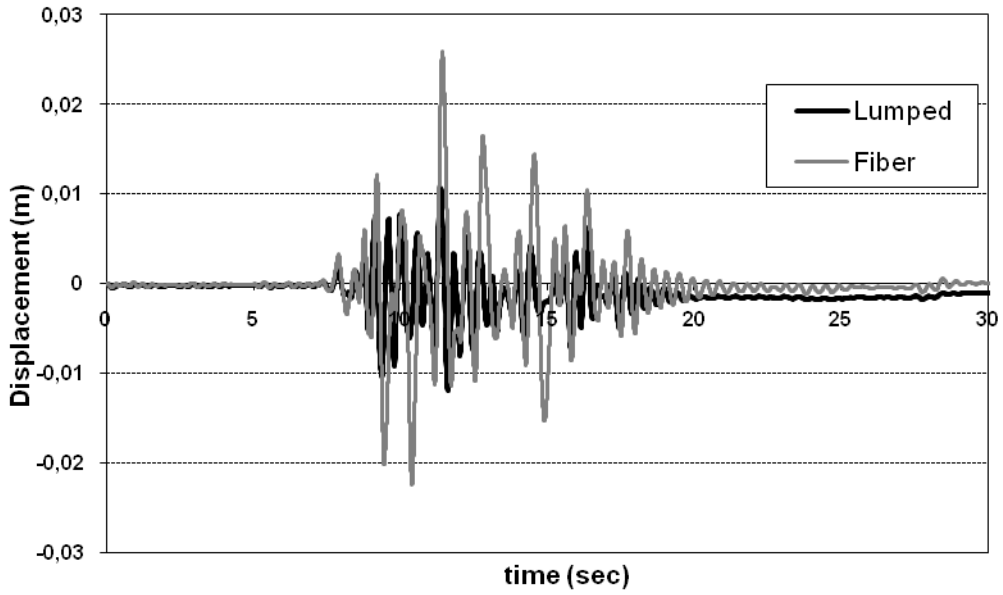


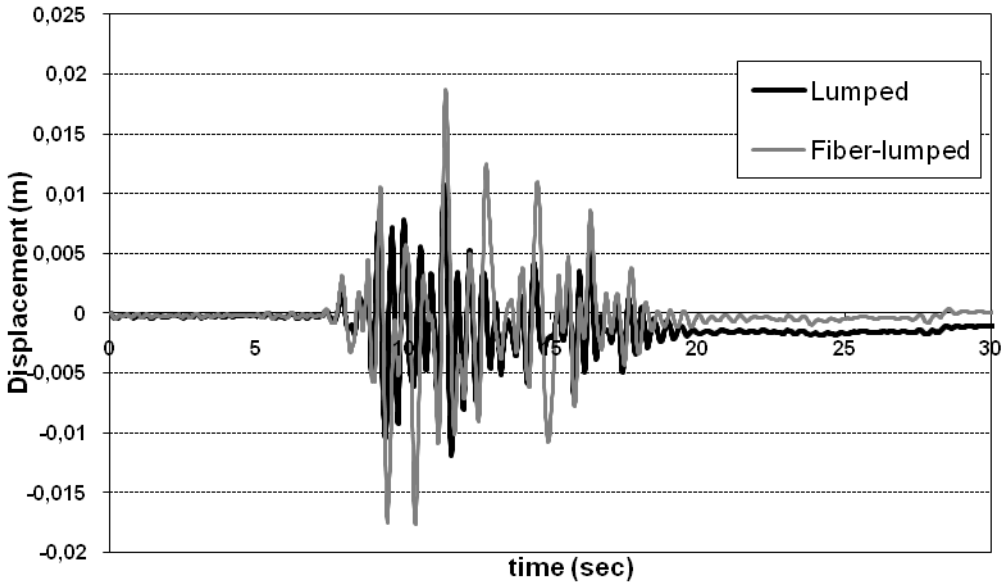

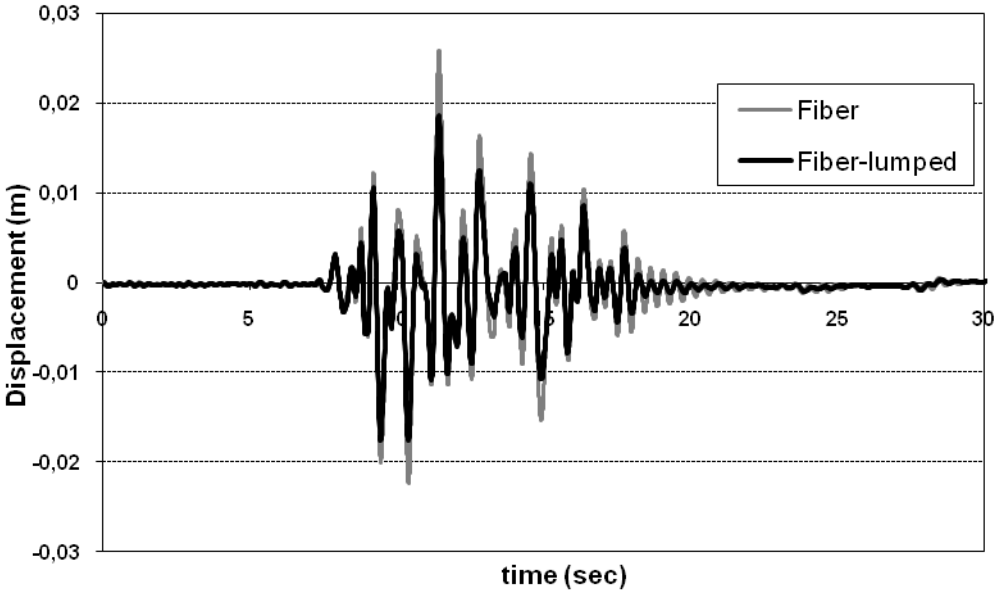


Figure 5–34:Comparison, in pairs, of 1st floor displacement time histories for the three different simulations

The form of time history of the other floors is similar to the first. The maximum and the maximum relative displacements of the other floors are presented in the following charts. As expected from the previous figure, the curve of the fiber-lumped elements is closer to that of the distributed plasticity elements more than the curve of lumped elements.

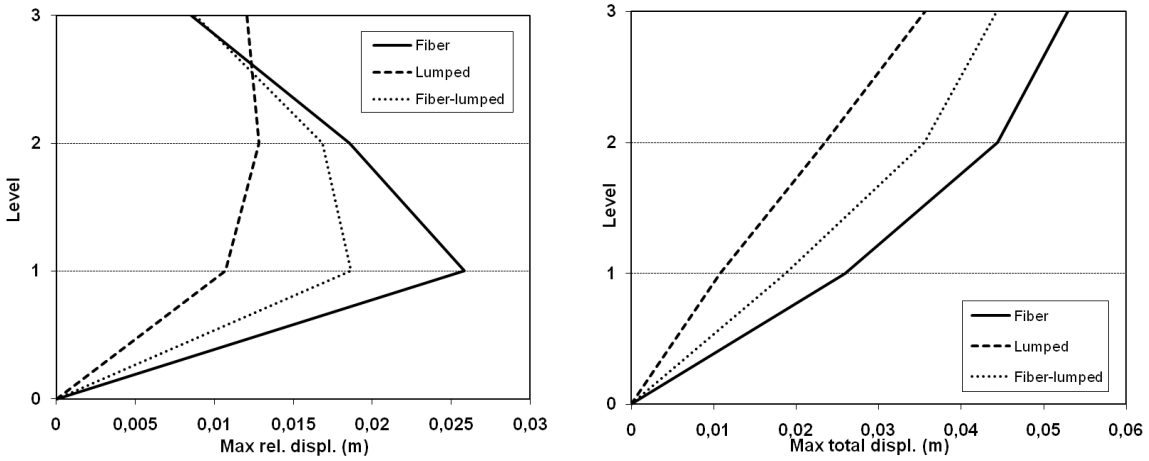


(a) (b)

Figure 5–35:(a) Maximum relative (b) Maximum displacements of the three floors for the three simulations

### 5.2.4. Comparison of analytical results with experimental

#### 5.2.4.1. Fiber Lumped elements

In the following a comparison is made between the simulation of fiber-lumped elements and the test results for ground acceleration 0.54g and 0.30g in order to examine the accuracy of the simulation. On those results effects of material non-linearitiy and infill walls are taken into account.

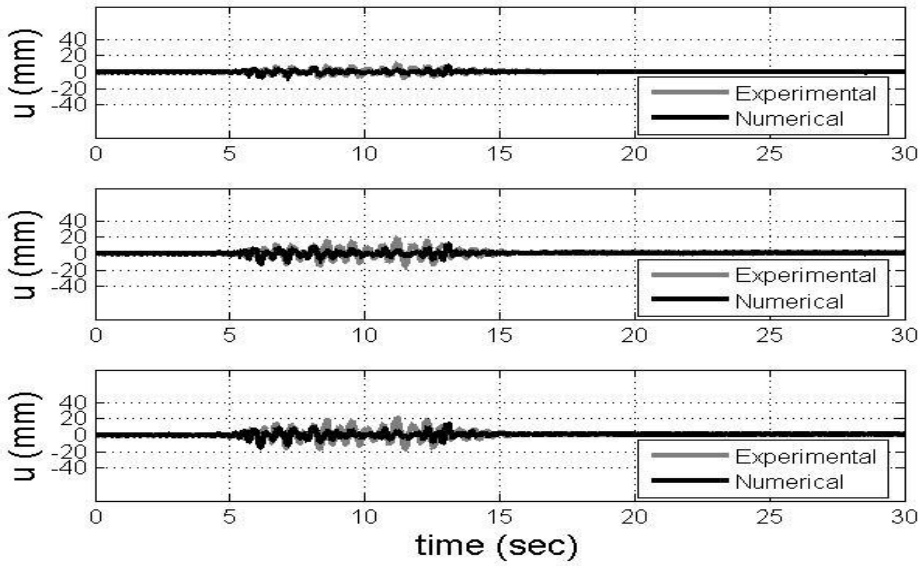


(a)

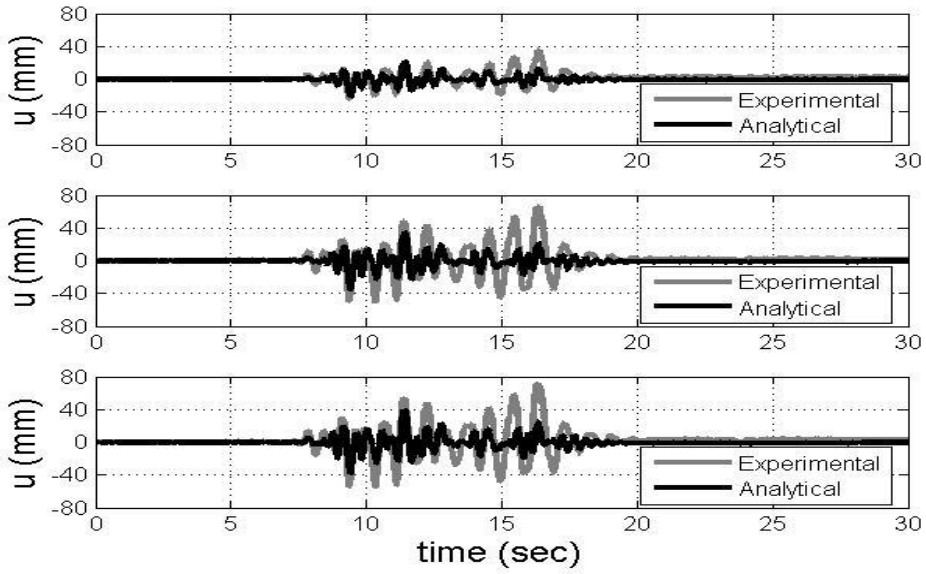


(b)

Figure 5–36:Displacements time histories of three floors with ground acceleration (a) 0.30g, (b) 0.54g of the simulation with concentrated fiber plasticity elements

More specifically figure 5-36 shows the displacement time histories of the column C6 (see Fig. 2-2) for the three floors and for ground accelerations 0.30g and 0.54g, respectively.

For the ground acceleration of 0.30g the simulation with fiber lumped elements follows successfully the format of the experiment, except during the period between the 11th and 12th seconds. The record, however, of the maximum movement of the simulation is quite accurate as shown in Figure 5-38.

For the ground acceleration of 0.54g experimental results show two main pulses at the 9th and 16th seconds. The results of the analysis describe well the time history until the 14th second, and after that a mistake is apparent on the period and range. On figure 5-37 this difference is more obvious, on figure 5-38 the relative displacement of the first two floors is significant while on the third floor analysis and experimental results coincide. The inability of the simulation to describe the difference, similar with to that of fiber elements (see 5.1.3.), is probably due to a lack of evaluation of the behaviour of the infill walls; it is also possible that the underestimation of the largest ground acceleration it is due to the persistent failures of the prior test with ground acceleration 0.3g. More generally, the simulation with fiber lumped elements are close enough with the simulation of fiber elements (distributed plasticity).

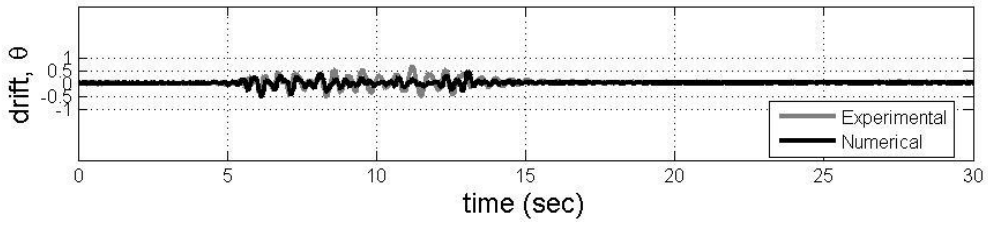


(a)

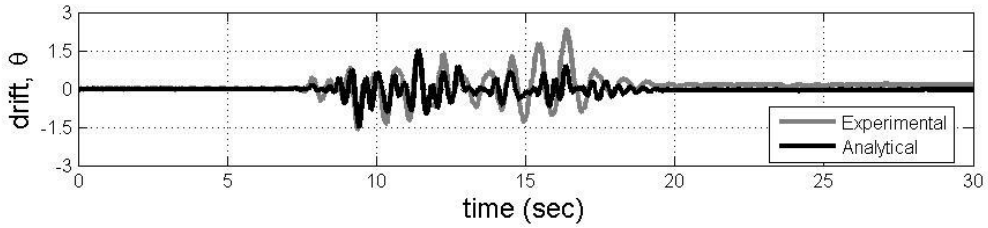


(b)

Figure 5–37:Drift time histories of the first floor for ground acceleration (a) 0.30g, (b) 0.54g - fiber lumped elements

The following figures show the maximum relative displacements of column 6 (C6). These graphs can provide an estimate for the distribution of damages over the height of the building and reflect the rotational demand.

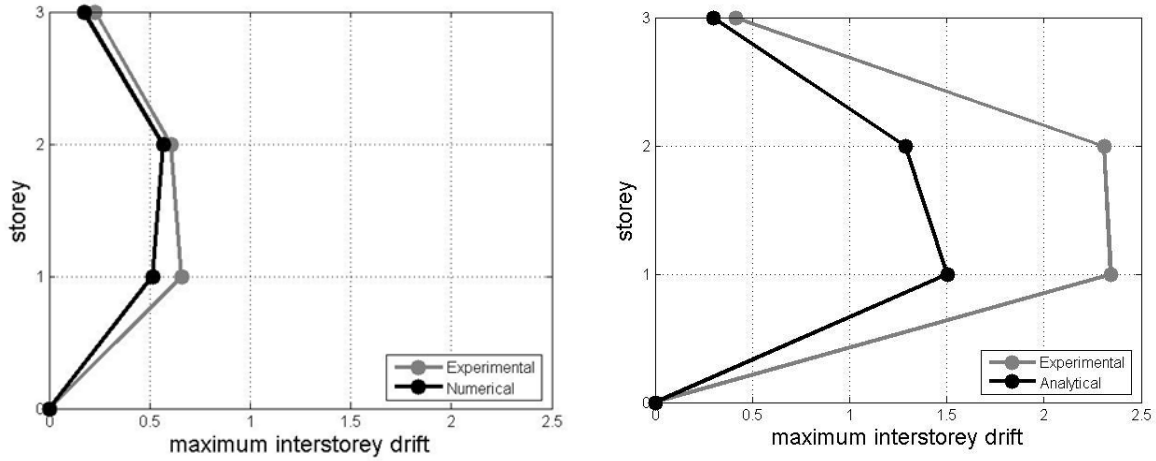


(a) (b)

Figure 5–38:Maximum relative displacement of C6 column for ground acceleration (a) 0.30g, (b) 0.54g

#### 5.2.4.2. Lumped Elements

Concluding elements simulation behavior the comparison of the case of lumped elements with the experimental results is presented.

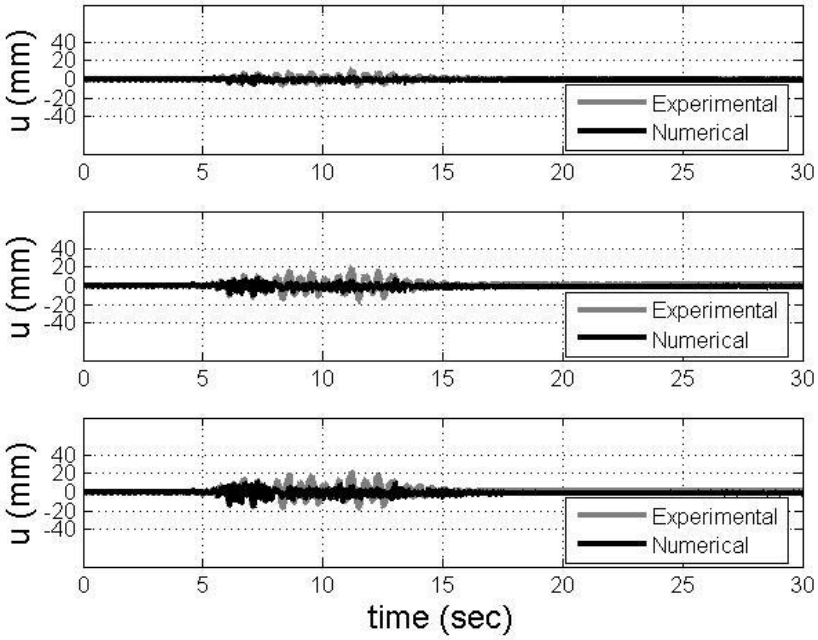


(a)

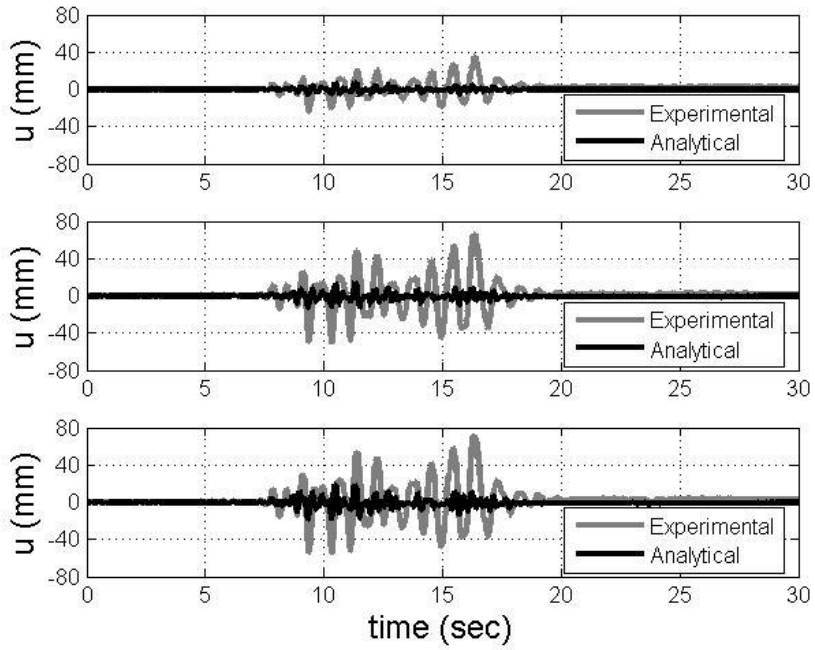


(b)

Figure 5–39: Displacement time histories of three floors for ground acceleration (a) 0.30g, (b) 0.54g - lumped elements

Figure 5-39 show the time histories of three floors of the C6 column for ground acceleration 0.30g and 0.54g, respectively. For the acceleration of 0.30g, the curve of the simulation (fig. 5-40) with lumped elements follows that of experiment with good accuracy in shape and data. The maximum relative displacements are shown in Figure 5-41. For the ground acceleration 0.54g results of the analysis don't match that of experimental simulation which shows much less movement than actual. This large difference appears clearly in Figure 5-41 showing the maximum relative movement of the floors.

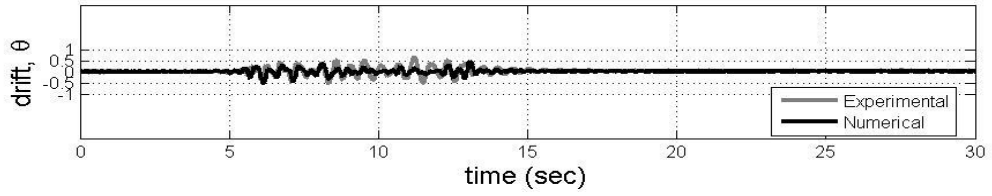


(a)

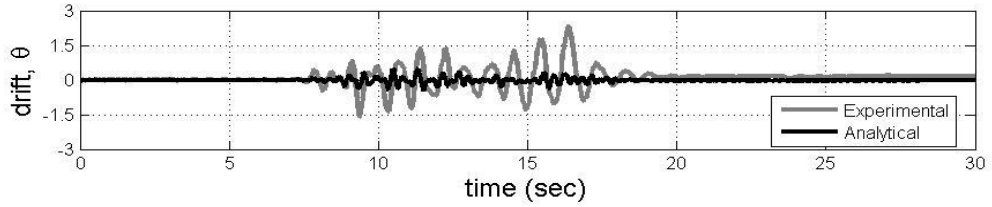


(b)

Figure 5–40:Drift time histories for the first floor of building with ground acceleration (a) 0.30g, (b) 0.54g - lumped elements

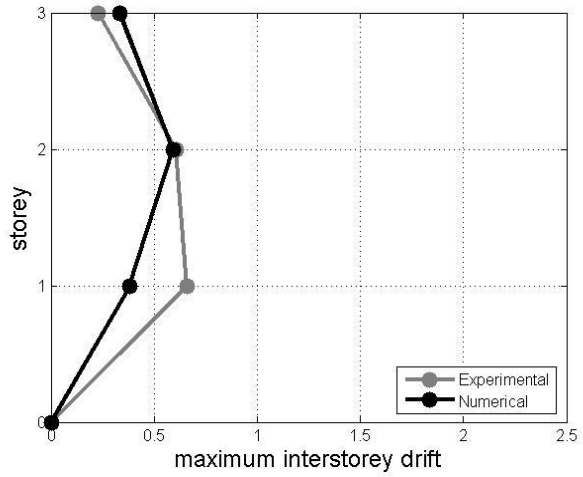


(a)

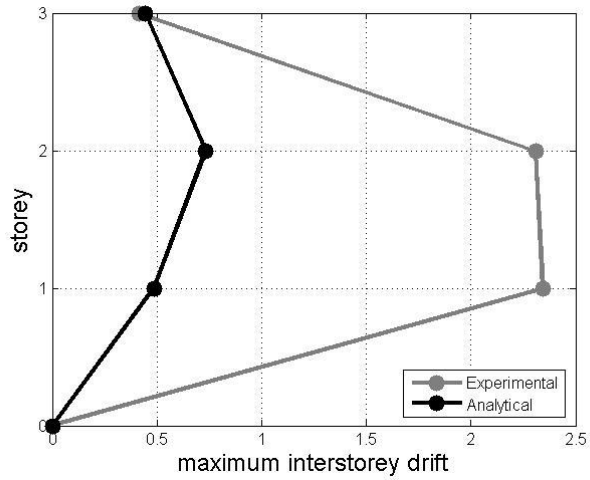


(b)

Figure 5–41 Maximum relative displacement of C6 column for ground acceleration (a) 0.30g, (b) 0.54g

## 6. Sensitivity Analysis of the Infill Wall Model

As we have seen in previous analysis, important roles in the response of the building have the infill walls. The effect in structural strength is an increase about 30%, also reduce the eigen-period making it susceptible to another part of the spectrum.

In this chapter there will be an effort to illustrate the sensitivity of each of the entry parameters that describe the infill wall model. More over three other simulated infills were used, slightly different to the original, in order to check the sensitivity of the response of the building in relation to the infill model.

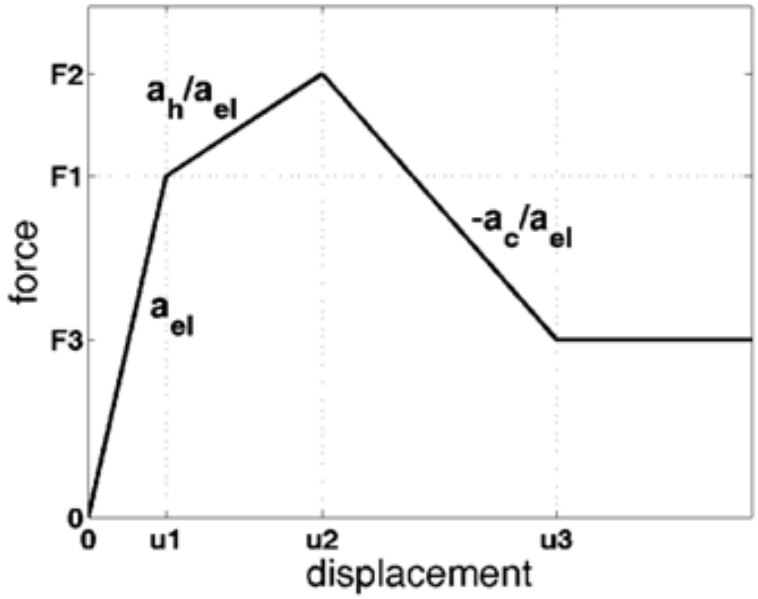


Figure 6–1: Quadrilinear peak-oriented model used for modeling the masonry infills

### 6.1. Sensitivity of the entry parameters

The following charts show the response of the building in relation to factors $F_1$, $F_2$, $F_3$. The $F_1$ factor determines the yield point on the force-displacement curve (see above), the $F_2$ factor is the maximum resistance achieved by the infill walls and the factor $F_3$ the residual strength of the masonry after the collapse. More specifically in the graphs are depicted the response of the structure, where each of the above factors is doubled or halved.

It is evident from the three diagrams, figure 6-2, that the response of the structure is more sensitive to doubling the $F_1$, $F_2$, $F_3$ factors rather than halve them. As expected the change in $F_1$ factor, the vertical movement of the yield point, varies the maximum base shear of the building and the residual strength after the failure of infill walls, but not particularly the modulus of elasticity. The ratio $F_2$, the vertical movement of maximum resistance, affects more than the $F_1$ factor the structure, because this increases the contribution of infill walls in the structure response.

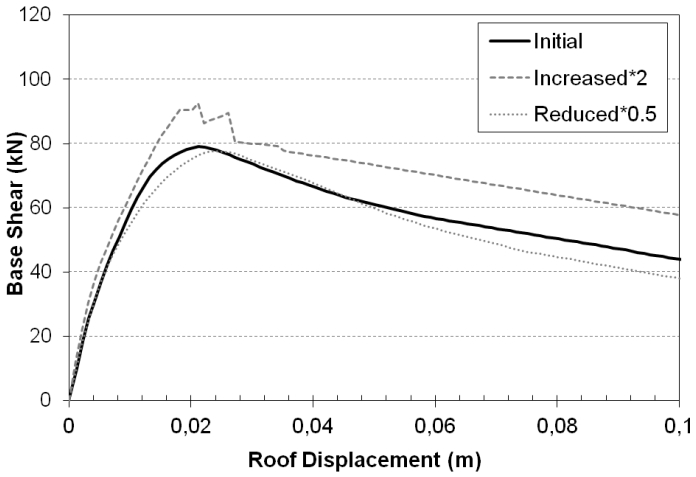


(a)

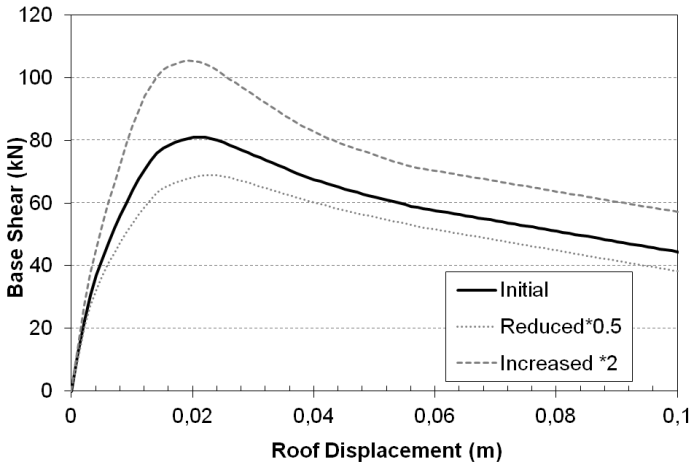


(b)

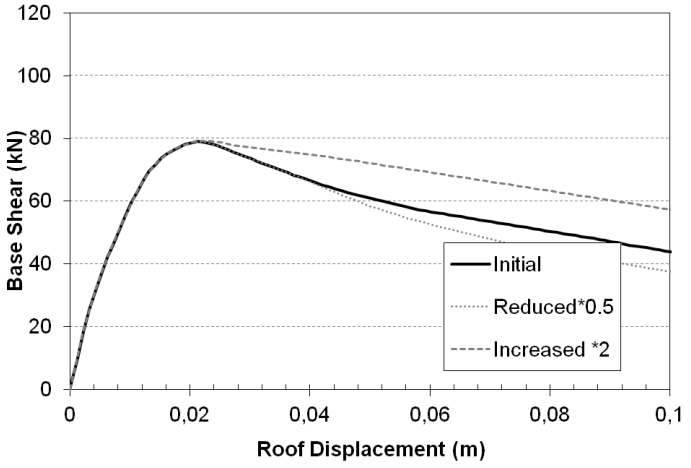


(c)

Figure 6–2 Response of the structure depending on the rate of variation in (a) $F_1$, (b) $F_2$, (c) $F_3$

Thus, the $F_2$ factor influences the peak and residual strength of the building and also the modulus of elasticity. Finally, as it was expected, the change in factor $F_3$, the vertical displacement of the residual strength of the walls, changes only the residual strength of the structure. This can be easily seen in the next two charts below, figure 6-3.

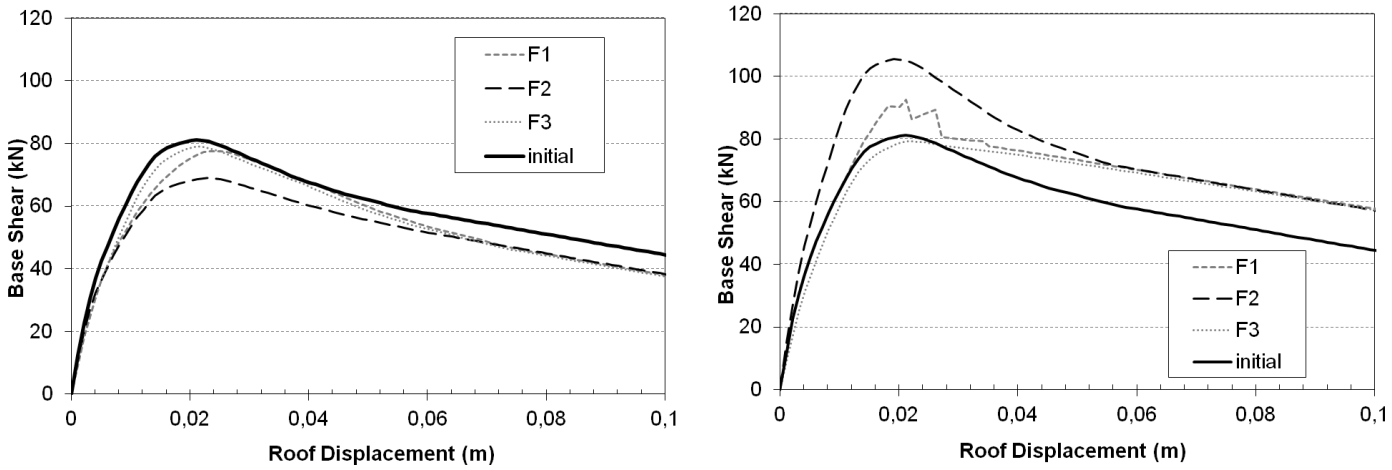


(a) (b)

Figure 6–3 Response of the structure depending on the rate of variation in (a) half (b) double of factors $F_1$, $F_2$, $F_3$

Figure 6–4 The specimen infill panels are made of cellular concrete Gasbeton RDB, thickness 50mm

## *INCREMENTAL DYNAMIC ANALYSIS*

The following charts show the sensitivity response of the building in relation to the rest factors of the model, ie $a_h$, $a_c$, $u_2$. The other three variables, $a_{el}$, $u_1$, $u_3$ are linearly dependent on the previous, so their vulnerability is not examined. The change of variable $a_h$ does not particularly affect the response of the structure because the length of second branch $u_1$- $u_2$ is relatively small. Conversely, the change in the $a_c$ factor affects the residual strength of structure because it addresses a bigger part of the model wall behaviour. Finally, the change in the factor $u_2$, the point of maximum reaction force, does not affect the maximum and residual strength of the building, but moves the response curve of the structure horizontal.

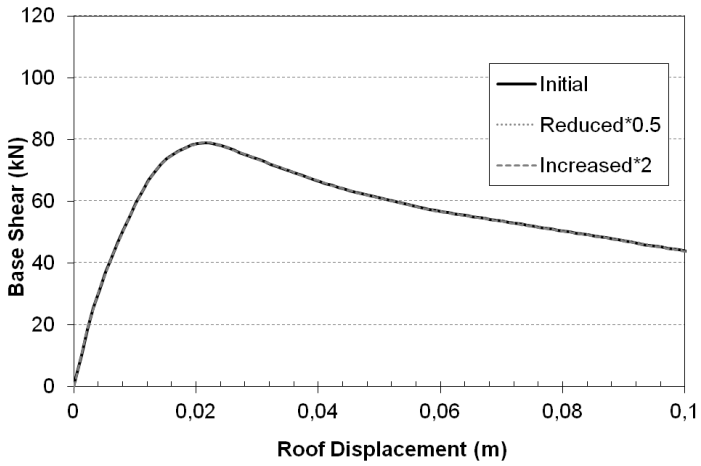


(a)

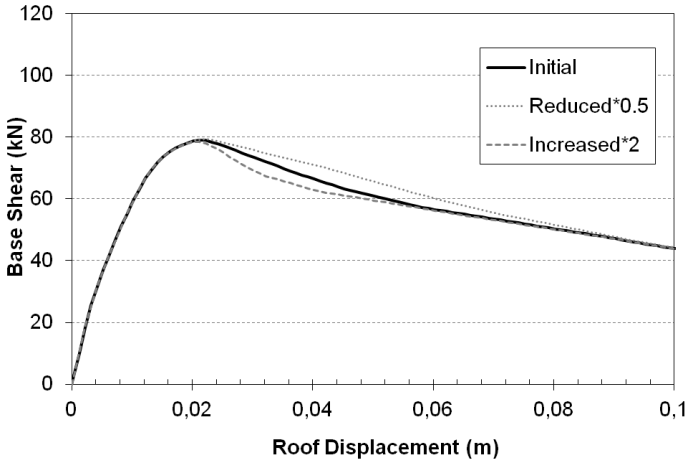


(b)

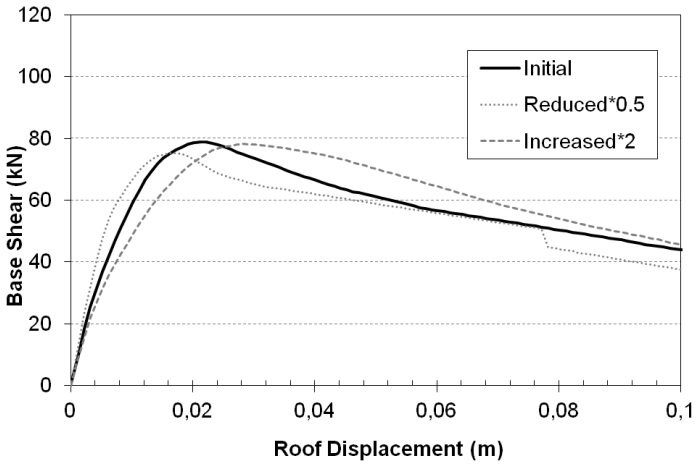


(c)

Figure 6–5 Response of the structure depending on the rate of variation in (a) $a_h$, (b) $a_c$, (c) $u_2$

Finally, in order to simulate the infill wall, the vertical compressive strength of the masonry, in all previous results, was considered as 2.2Mpa and the value for the modulus of elasticity as 1600Mpa. As is well known accurate values for the strength of the wall is difficult to establish because of the many uncertainties. So it is considered the response of the structure for different values which are being proposed in the literature for these material properties. In order to compare the change of results based on these parameters (that of course are linked with the definitions of $F_1$ to $F_3$ factors but these variables are more handy for an engineer) two more solutions produced each one of them changes only one variable.

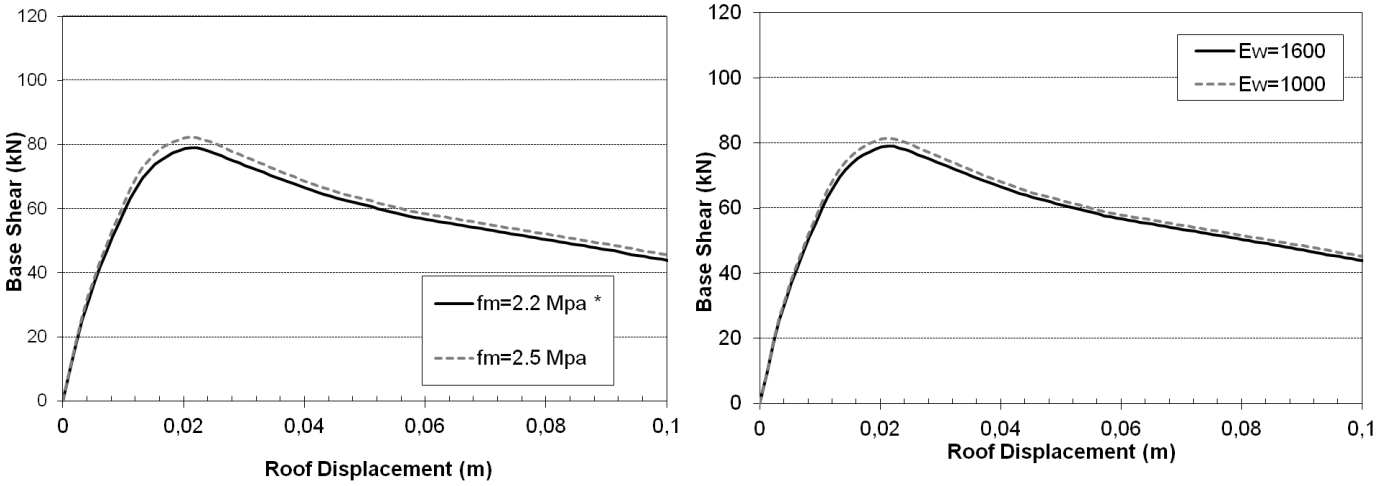


(a) (b)

Figure 6–6 Response of the structure depending on the rate of variation in (a) $f_m$, (b) $E_w$

Figure 6–7 Construction of the infill walls

### 6.2. Alternative infill wall models

As previously mentioned the model of infill walls is almost impossible to be simulated exactly, especially the part after the infill's maximum reaction force, since it is very difficult to estimate it, after the failure. Thus three different wall models developed based on the original but with a diverse form of curve at the part after maximum reaction force.

In the first model is made the assumption that once the maximum strength of vertical wall is developed then it gradually reduced to zero with slope $a_c/a_{el}$. In view of this assumption, the residual strength of the structure is reduced while the maximum base shear remains constant.

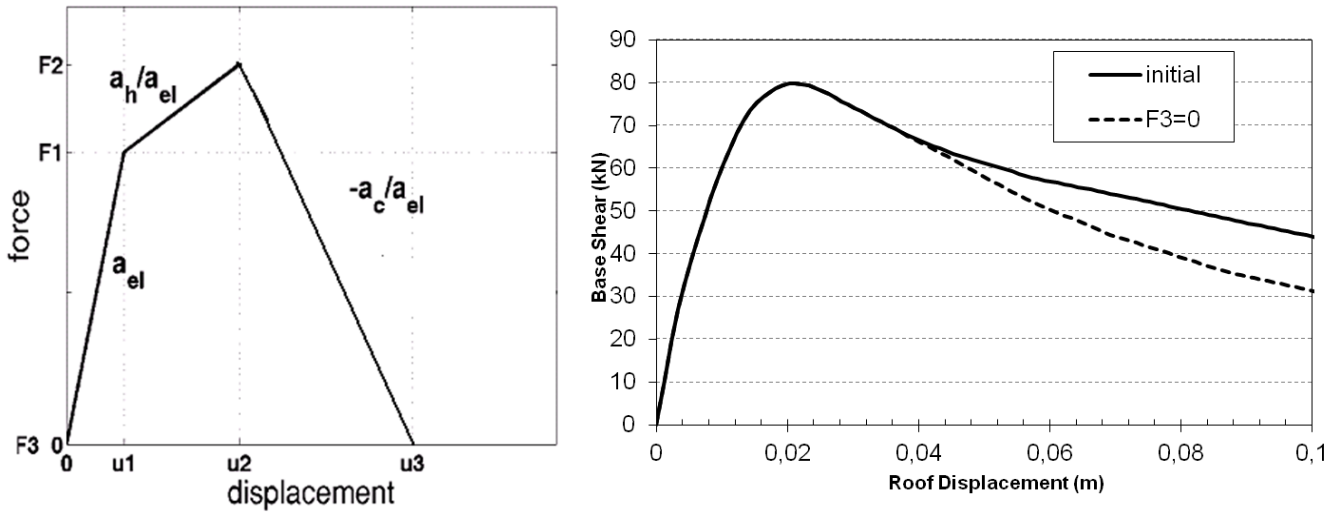


(a) (b)

Figure 6–8 (a) First hypothetical model ($F_3$=0) and (b) the response of the building respectively

## *INCREMENTAL DYNAMIC ANALYSIS*

The next two models it is assumed that after the maximum strength the resistance drops instantaneously up to the finite value of $F_3$ and zero respectively. So for the first model the building's maximum strength capacity is reduced by 5% but the residual strength remains constant. In the second case because the residual strength of the wall is zero, the maximum strength of the structure is reduced by 5% while the residual 25%.

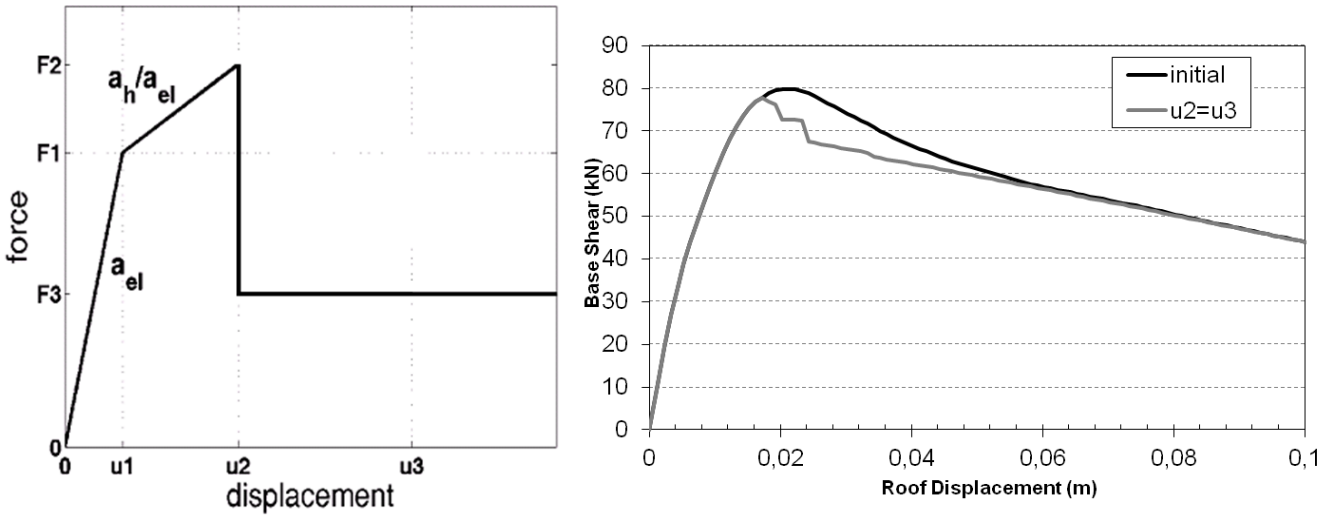


(a) (b)

Figure 6–9 (a) Second hypothetical model ($u_2$= $u_3$) and (b) the response of the building respectively

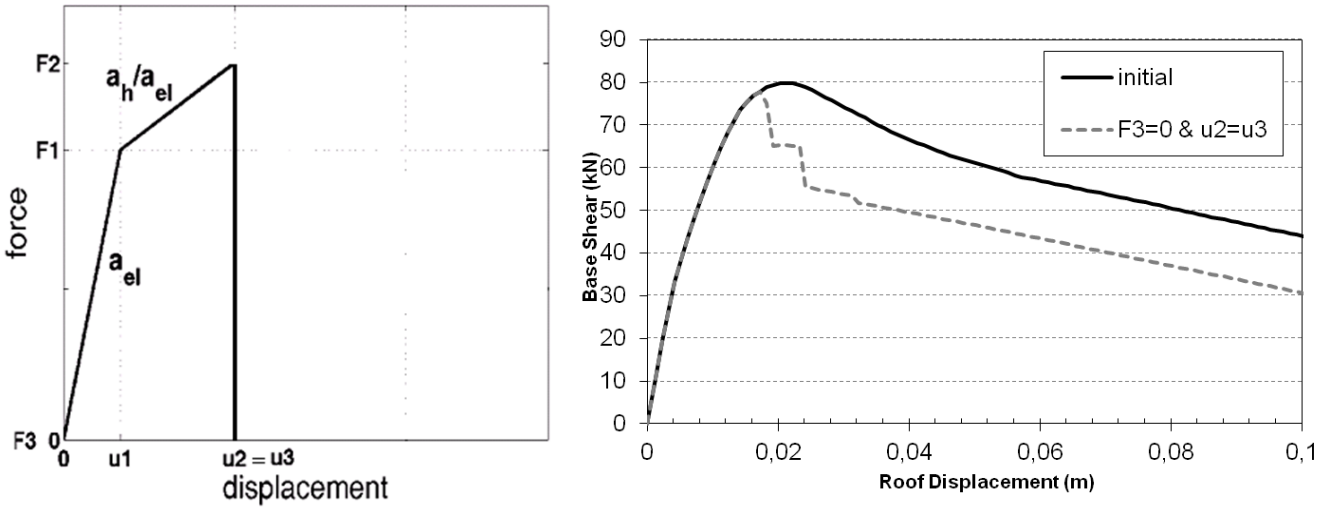


(a) (b)

Figure 6–10 (a) Third hypothetical model ($u_2$= $u_3$ & $F_3$=0) and (b) the response of the building respectively

## *INCREMENTAL DYNAMIC ANALYSIS*

Finally, in the following chart is presented the three responses of the structure of these three previous models in compare with the original. It is now more obvious that changes at the residual part of infill wall could produce reductions in residual strength of structure in the order of 25-30% but even more at the maximum base shear.

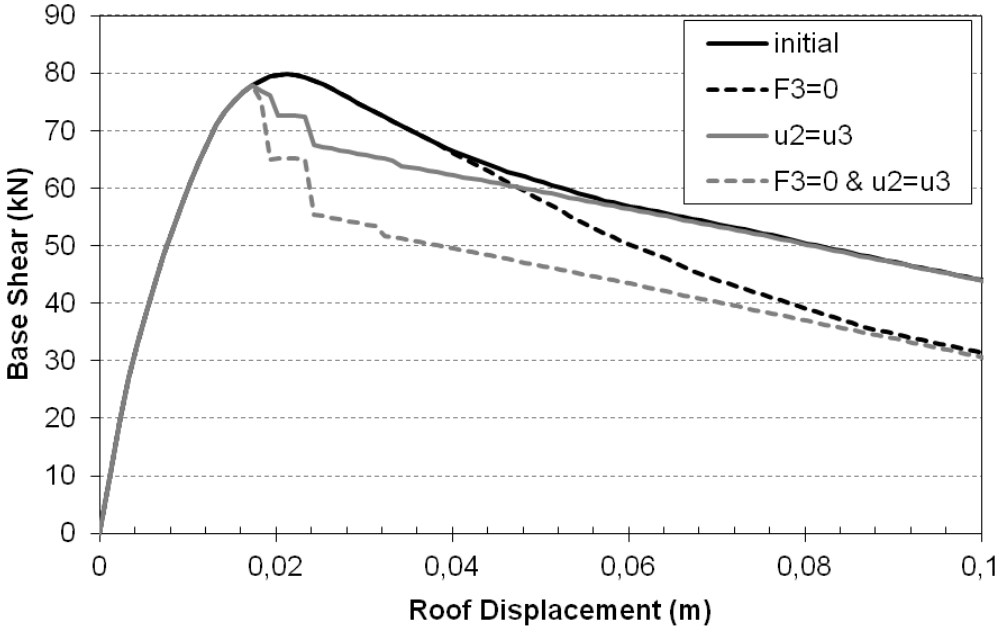


Figure 6–11 Displacement response to the applied hypothetical model of infills wall

# 7. Incremental Dynamic Analysis

## 7.1. Method description

The growth in computer processing power has made possible a continuous drive towards increasingly accurate but at the same time more complex analysis methods. Thus, the state of the art has progressively moved from elastic analysis to dynamic elastic, non-linear static and finally non-linear dynamic analysis. In the last case, the convention has been to run one to several different records thus producing one to several 'single-points' analyses, mostly used for checking the designed structure. On the other hand, methods like non-linear static pushover or the capacity spectrum method offer, by suitable scaling of the static force pattern, a 'continuous' picture as the complete range of structural behavior is investigated, from elasticity to yielding and finally collapse, thus the greatly facilitating our understanding.

In recent years a new concept has been developed by the analogy of passing from a single static analysis to the incremental static pushover, where the seismic 'loading' is scaled. The concept has been mentioned as early as 1977 by Bertero [24], and has been cast in several forms in the work of many researchers. Recently, it has also been adopted by the U.S. Federal Emergency Management Agency (FEMA) guidelines [25,26] as the Incremental Dynamic Analysis (IDA) and established as the state-of-the art method to determine the global collapse capacity.

The IDA study is now a multi-purpose and widely applicable method and its objectives are the:

1. thorough understanding of the range of the response or 'demands' versus the range of potential levels of ground motion record,
2. better understanding of the structural implications of rarer/more severe ground motion levels,
3. study of the changes in the nature of the structural response as the intensity of ground motion increases (e.g. changes in peak deformation patterns with height, onset of stiffness and strength degradation and their patterns and magnitudes),
4. estimation of the dynamic capacity of the global structural system and finally, given a multi-record IDA study,
5. understanding of how stable (or variable) all these items are from one ground motion record to another.

The aim is to provide a basis and terminology to unify the existing formats of the IDA study and set up an essential background to achieve the above-mentioned objectives.

To accomplish the task several important methods have emerged, a promising one being Incremental Dynamic Analysis as proposed by Vamvatsikos and Cornell [23], a computer-intensive procedure that offers thorough (demand and capacity) prediction capability by using a series of nonlinear dynamic analyses under suitably multiply-scaled ground motion records. While it is a simple concept, performing an IDA by this method requires several important steps:

1. Create an appropriate model for the structure under investigation.
2. Select a suite of ground motion records.

3. For each record, incrementally scale it to multiple levels and run a nonlinear dynamic analysis each time. Stop incrementing when numerical non-convergence is first encountered
4. Select a ground motion Intensive Measure IM (e.g., $S_a(T_1,5\%)$, the 5%-damped first-mode spectral acceleration) and a Damage Measure DM (e.g., $\theta_{max}$, the maximum over all stories peak interstory drift ratio) and post process the results of the dynamic analyses:
    i. Interpolate the resulting IM, DM points to generate an IDA curve for each individual record.
    ii. Define limit-states and estimate the corresponding capacities on each IDA curve.
    iii. Summarize the IDA curves and limit-state capacities across all records into 16%,50% and 84% fractiles
    iv. Integrate with results of Probabilistic Seismic Hazard Analysis (PSHA) and calculate MAFs of exceeding each limit-state.
5. Use the IDA data to better understand the behavior of the structure.

In addition it is needed a suite of ground motion records. Previous studies (Shome and Cornell [27]) have shown that for mid-rise buildings, ten to twenty records are usually enough to provide sufficient accuracy in the estimation of seismic demands, assuming a relatively efficient IM, like $S_a(T_1,5\%)$, is used. Consequently, it is selected a set of eight ground motion records, listed in fig. 7-1.

| No | Event | Station | PGA (g) |
|---|---|---|---|
| 1 | Kocaeli, 1999 | Sakaria | 0.54 |
| 2 | Artificial, 1999 | Artificial | 0.44 |
| 3 | Loma Prieta, 1989 | Corralitos | 0.80 |
| 4 | Loma Prieta, 1989 | Emeryville | 0.25 |
| 5 | Friuli, 1976 | Unknown | 0.48 |
| 6 | Hollister, 1974 | City Hall | 0.12 |
| 7 | Chichi, 1999 / Transversal | Unknown | 0.85 |
| 8 | Chichi, 1999 / Longitudinal | Unknown | 0.81 |

Figure 7–1 Ground motion records

Once the model has been formed and the ground motion records have been selected, a fast and automated way is needed to perform the actual dynamic analyses required for IDA. This entails appropriately scaling each record to cover the entire range of structural response, from elasticity, to yielding, and finally global dynamic instability.

Once the desired IM and DM values (in our case $S_a(T_1, 5\%)$ and $\theta_{max}$) are extracted from each of the dynamic analyses, it is left with a set of discrete points for each record that reside in the IM-DM plane and lie on this IDA curve, as in fig. 7-2. By interpolating them, the entire IDA curve can be approximated without performing additional analyses. To do so, it is used a basic piecewise linear approximation, or the superior spline interpolation.

In order to be able to do the performance calculations needed for Performance-Based Earthquake Engineering, it is needed to define limit-states on the IDA curves. For this study, there are chosen three: Immediate Occupancy (IO), Collapse Prevention (CP), both defined in FEMA [25,26], and global dynamic instability (GI). For this older reinforced-concrete frame the IO limit-state appears at $\theta_{max}$=1%. The CP point is defined from FEMA [25] guidelines, which are not exceeded on the IDA curve until the final point where the local tangent reaches 20% of the elastic-slope or $\theta_{max}$=10%, whichever occurs first in IM terms. The main idea is to place the CP limit-state at a point where the IDA curve is softening towards the flatline but at low enough values of $\theta_{max}$ (less than 10%) so that the structural model is still reliable. Finally, GI happens when the flatline is reached and any increase in the IM results in practically infinite DM response.

### 7.2. Evaluation with distributed plasticity elements

In this and the following paragraph, the model was analysed, not as a complete study but more as an indication of how these elements perform in an Incremental Dynamic Analysis. This paragraph focuses on fiber elements and their results, as drawn in figures 7-2 to 7-4, will be discussed.

The smooth IDA curve provided by the interpolation scheme offers much to observe. For Chichi record, depicted in fig. 7-2, the IDA curve is quite simple. It starts as a straight line in the elastic range, then slightly hardens and it starts softening only after $S_a(T_1, 5\%) \approx 0.65g$ where shows the effect of early yielding and local damage by having some slight changes in the local tangent slope but in general it stays on the elastic slope. Thus at any given $S_a(T_1, 5\%)$-level below 0.80g it maintains about the same displacement as an elastic system. Subsequently it hardens having a local slope similar and higher than the elastic, actually the slope of the IDA curve of the building is higher at $S_a(T_1, 5\%)=0.85g$ than it is at $S_a(T_1, 5\%) \approx 1.15g$. Then, at $S_a(T_1, 5\%) \approx 1.15g$ it starts softening, showing ever decreasing tangent slopes until $S_a(T_1, 5\%) \approx 1.25g$ when it hardens again until $S_a(T_1, 5\%)=1.45g$. The IDA starts to soften again as it blends to the flatline. This phenomenon of hardening generates two possible locations where the local slope is 20% of the elastic, as shown in fig 7-2. Obviously, the lower one (in IM-terms) should be rejected, as it does not directly precede a flatline. This indicates that the building is not close to global collapse yet as the CP limit-state definition requires.

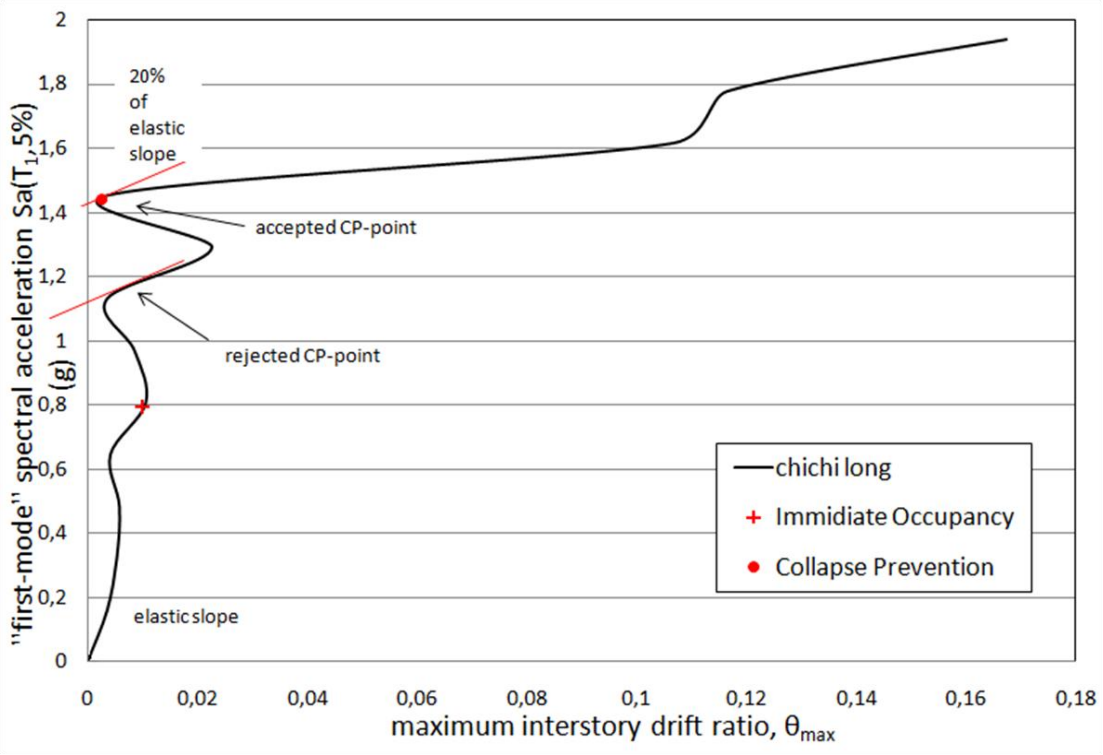


Figure 7–2 The limit-states, as defined on the IDA curve of Chichi record. Note the extreme hardening that causes the appearance of multiple possible CP points, the highest of which (in IM-terms) is the accepted one.

By generating the IDA curve for each record and subsequently defining the limit-state capacities, a large amount of data can be gathered, only part of which is seen in fig. 7-3. There, the IDA curves display a wide range of behavior, showing large record-to-record variability, thus making it essential to summarize such data and quantify the randomness introduced by the records. Thus appropriate summarization techniques are employed that will reduce this data to the distribution of DM given IM and to the probability of exceeding any specific limit-state given the IM level.

The limit-state capacities can be easily summarized into some central value (e.g. the mean or the median) and a measure of dispersion (e.g. the standard deviation, or the difference between two fractiles). Consequently, it is chosen to calculate 16%, 50% and 84% fractile values of DM and IM capacity for each limit-state, as shown in fig. 7-4. There are several methods to summarize the IDA curves, but the cross-sectional fractiles are arguably the most flexible and robust with respect to the infinite DMs introduced by the flatlines (Vamvatsikos and Cornell [23]). Using the spline interpolation stripes of DM-values are generated at arbitrary levels of the IM; each stripe contains ten DM-values, one for each record that may be finite or even when a record has already reached its flatline at a lower IM-level. By summarizing the DM-values for each stripe into their 16%, 50% and 84% percentiles results to fractiles values of DM given IM that are in turn interpolated for each fractile to generate the 16%, 50% and 84% fractile IDA curves shown in fig. 7-4.

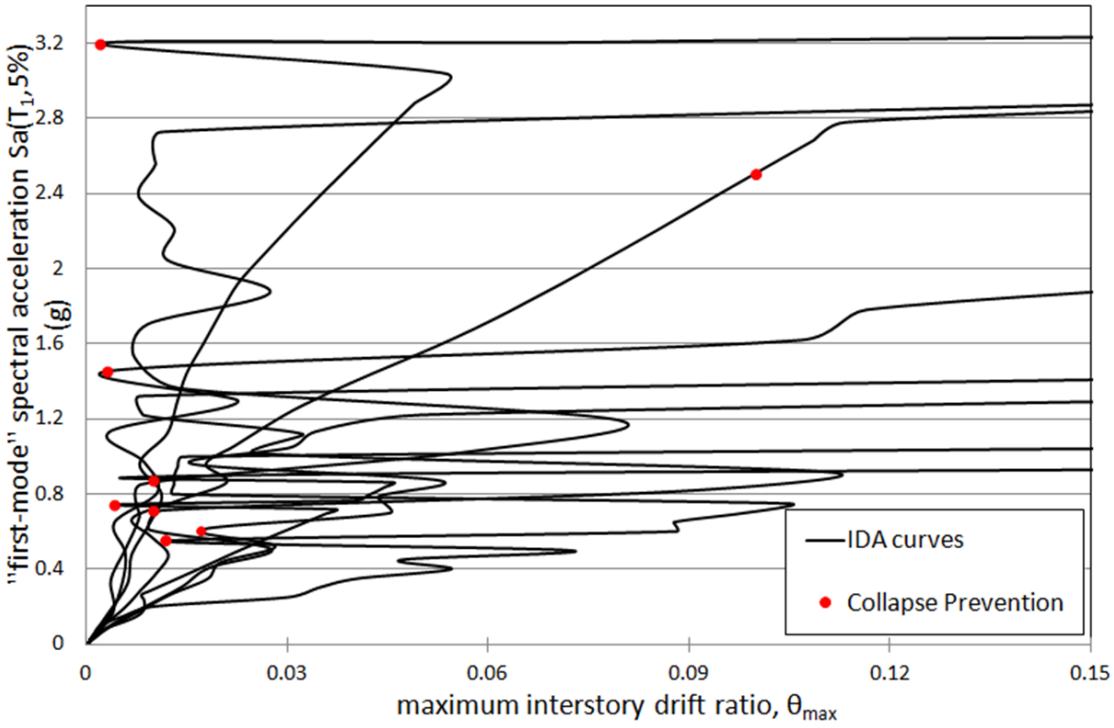


Figure 7–3 All eight IDA curves and the associated limit-state capacities. The IO limit is at the intersection of each IDA with the $\theta_{max}$=1% line, the CP limit is represented by the dots.

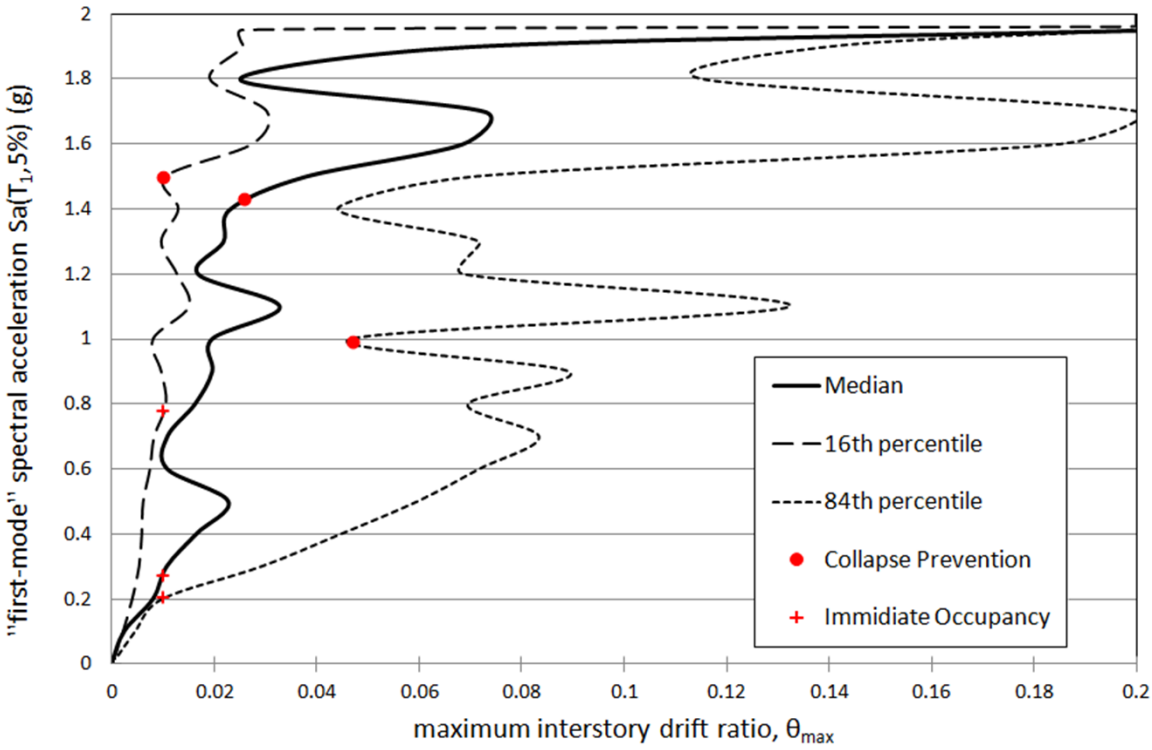


Figure 7–4 The summary of the IDA curves and corresponding limit-state capacities into their 16%, 50% and 84% fractiles.

### 7.3. Evaluation with concentrated plasticity elements

In the following a comparison is made between the simulation of fiber and lumped elements. Until now it was used only the fiber elements and the infill walls weren't taken into account in order to focus only in the elements behaviour. Thus the record of Sakaria is selected (0.51g) in order to achieve the comparison. The curve of fiber elements it starts as a straight line in the elastic range and then shows the effect of early yielding and local damage by having some slight changes in the local tangent slope but in general it stays on the elastic slope. Then, at $S_a(T_1, 5\%) \approx 0.4g$ it starts softening but subsequently it hardens again. Actually the DM-response of the building is higher at $S_a(T_1, 5\%)=0.5g$ than it is at $S_a(T_1, 5\%) \approx 0.7g$. The IDA starts to soften again only after $S_a(T_1, 5\%) \approx 0.75g$ as it blends into the flatline. The curve of fiber lumped elements starts parallel to the fiber-curve until $S_a(T_1, 5\%) \approx 0.4g$ and then shows the effect of early yielding and local damage. Then at $S_a(T_1, 5\%) \approx 0.50g$ it starts softening when a small resurrection happens at $S_a(T_1, 5\%) \approx 1.10g$. Finally the curve decreases showing ever lower tangent slopes, i.e. greater rates of DM accumulation as IM increases, reaching the flatline above $S_a(T_1, 5\%) \approx 1.85g$ where the structure responds with practically ''infinite'' $\theta_{max}$ values and numerical non-convergence has been encountered during the analysis. That is when the building has reached global dynamic instability, when a small increment in the IM-level results in unlimited increase of the DM-response. Finally the curve of elements is the simpler one, it starts parallel with the other two but slightly stiffer and it continues in the elastic region until $S_a(T_1, 5\%) \approx 0.70g$. Then shows the effect of early yielding and local damage by having some slight changes in the local tangent slope but in general it stays on the elastic slope, following the well-known 'equal-displacement' rule for moderate-period structures. Then at $S_a(T_1, 5\%) \approx 1.35g$ it suddenly softens and reaches the flatline quite fast.

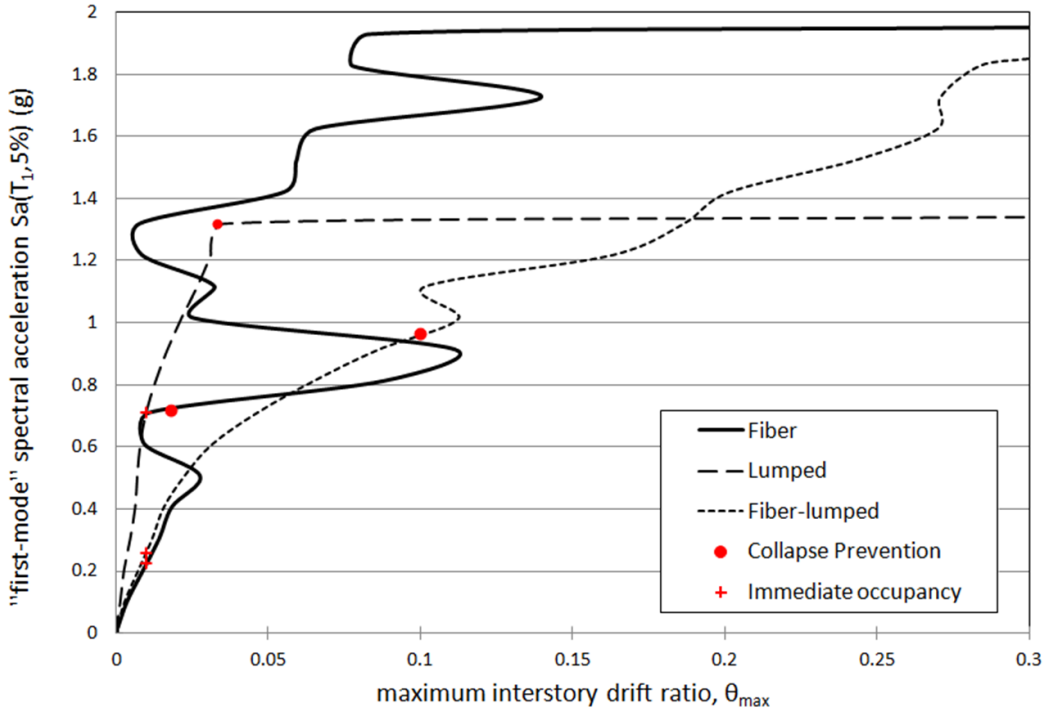


Figure 7–5 IDA curves for the sakaria records, three different elements

## *INCREMENTAL DYNAMIC ANALYSIS*

Finally, a comparison is presented between the median values of distributed and concentrated plasticity elements, as shown in fig. 7-6. The IO points are very close for fiber and fiber lumped elements while the CP points are close for fiber and lumped elements. However, CP points for the median curves of the three simulations are between $S_a(T_1, 5\%) \approx 1.1g$ and $S_a(T_1, 5\%) \approx 1.45g$.

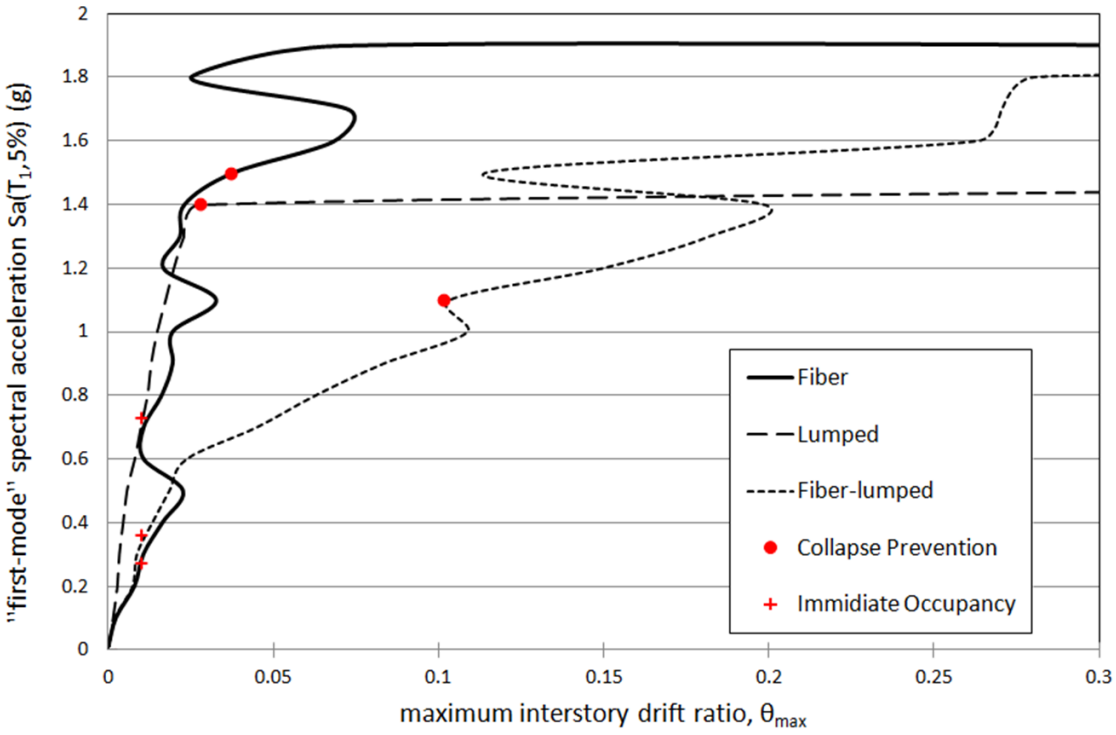


Figure 7–6 Median IDA curves for the three different elements

## 8. Conclusions

This work focuses in the influence of modelling on existing old reinforced concrete buildings. The model of the building consists of force-based beam-column elements either distributed (fiber elements) or, alternatively, concentrated plasticity (lumped &fiber lumped elements). Together with these three types of modeling elements is compared the sensitivity of infill wall modeling.

Push over and dynamic analyses with time histories are considered.

Eigenperiods, roof displacement response, to the base shear, and relevant envelopes of horizontal displacements, as a percentage of the height of each floor, are calculated.

The results of these analyses are compared to the accuracy of the final result, with reference to the computational cost, in respect to the experimental data derived from a RC three-storey building tested dynamically at the TREES lab seismic table. This building designed only for gravity loads, as in those old ones of Southern Europe, and build in 1:2 scale compared to the original.

Finally an IDA (incremental dynamic analysis) study was included, in order to estimate the dynamic capacity of the global structural system.

Result comparisons, of this work, may come to the following conclusions:

- For the eigenperiods:
  Simulations, which do not include the influence of the masonry, proved to be a very good approximation especially for the fiber and lumped elements but good enough for the fiber-lumped. All analytical results produce, however, lower values of eigenperiod than those of the experiment (fig.4-5).
  The simulations that include the influence of the masonry have significantly greater deviation from the experimental results with the additional characteristic that eigenperiods are above than those of the experiment. It seems that the experiment is stiffer than the analytical models. Again the fiber and lumped elements are very close but eigenperiods are now higher than the experimental results compared with the corresponding results for fiber-lumped elements (fig. 4-4).
- For the response charts (there are no experimental data and distributed plasticity elements are used as reference):
  Simulations without infill walls increase the base shear 40% for the lumped elements and reduce 12% for the fiber-lumped. Also the shape of the curve is slightly differentiated (fig. 5-22). The curve of lumped elements shows two abruptly decreasing branches after the maximum base shear and present half of the critical displacement, which is a failure shape quite unlike than the other two elements, having a smoother curve. Simulations with the presence of infill walls have similar characteristics.
  Furthermore, for the push-over analyses, if the non-linearity of geometry (P-Delta) is not taken into account then the resistance of the structure is underestimated and this is more evident in the residual resistance (fig 5-2). Unlike the non-linearity of geometry does not affect the range of displacements at dynamic analyses significantly.

## *CONCLUSIONS*

- For the time histories, displacements of two ground excitations with ground acceleration 0.30g and 0.54g following the accelerograms of Montenegro earthquake are evaluated.

  Fiber and fiber-lumped elements describe satisfactory the response of the building until 60% of the time history, and after that a mistake is slightly apparent on the period and range (fig. 5-16, 5-36). It is possible that the underestimation of the largest ground acceleration it is due to the way of the experiment.

  Lumped elements have larger margins with the experimental results, mostly at the more intense ground acceleration (0.54g) (fig.5-39).
- The quadrilinear peak-oriented model used for modelling the masonry infills is related to 9 factors three of which are linearly dependent. In general the response of the structure is more sensitive to doubling factors than halve them. Seems that the four factors affect more the response of the wall model (see fig. 6-2, 6-5) while the other two do not have an effect to the response of the structure (fig. 6-5).
- Changes at the *residual* part of infill wall model could produce reductions in *residual* strength of structure in the order of 25-30% but even more at the maximum base shear 5% (fig. 6-11).
- IDA offers a complete methodology to handle the abundant data from numerous analyses and calculate the mean annual frequencies of exceeding the specified limit-states. It also offers valuable intuition when used to investigate the seismic behaviour of the structure. It can reveal interesting aspects of structural behaviour, like the large record-to-record variability, the hardening and softening, the flatline and the structural resurrection.

It is also worth noticing that:

- The moment-curvature (M-k) relations, which are chosen for the columns, (consist data for lumped elements) are being related for the initial value of the axial force. This value does not remain constant during the experiment, so the response of the structure is affected (fig 5-31). This sensitivity does not concern fiber and fiber-elements.
- For the concentrated plasticity elements (lumped, fiber-lumped) the length of the plastic hinge is an input data. Changes on this theoretical length influence mostly the results of lumped elements (fig 5-32, 5-33).

# References


1. N. Caterino et al., "Multi-Criteria Decision Making for Seismic Retrofitting of RC Structures", *Journal of Earthquake Engineering*,2008
2. Clough R. Johnston S., "Effect of Stiffness Degradation on Earthquake Ductility Requirements", *Trans. Japan Earthquake Engineering Symposium*, Tokyo (1966)
3. Lai, S., G. Will, S. Otani, "Model for inelastic Biaxial Bending of Concrete Members", *Journal of Earthquake Engineering*, ACSE, 110(ST11), pp. 2563-2584
4. Fardis, M.N. , Panagiotakos, T.B. , "Seismic Response of Infilled RC Frames Structures", *Proceedings of the Eleventh World Conference on Earthquake Engineering*. Paper No.225, 1996.
5. Tassios T. P. "Uncertainties of in structure asessment of concrete strength", *ACI Symposium 4-9/3/84* Phoenix Ariz, 22p (1984)
6. Michael H. Scott and Gregory L. Fenves, "Plastic Hinge Integration Methods for Force-Based Beam-Column Elements", *Journal of Structural Engineering*, February 2006
7. I. Lanese, F.J. Crisafulli, A. Pavese, NEARB-OPCM 3274: "Shake Table Test Of An R.C. Building Designed For Gravity Loads Only, Seismic Response And Frame-Panel Interaction", *International Conference on Computational Methods in Structural Dynamics and Earthquake Engineering,* COMPDYN-2009, 22-24 June 2009, Island of Rhodes, 2009.
8. A. Papachristidis, M. Fragiadakis, M. Papadrakakis, "A shear-deformable fiber beam-column element for seismic analysis of steel structures", *International Conference on Computational Methods in Structural Dynamics and Earthquake Engineering,* COMPDYN-2009, 22-24 June 2009, Island of Rhodes, Greece, 2009.
9. F. Zareian, R. Medina, "A practical method for proper modeling of structural damping in inelastic plane structural systems", *Computers and Structures 88*, 2010
10. M. Dolsek, P. Fajfar, "The effect of masonry infills on the seismic response of a four-storey reinforced concrete frame- a deterministic assessment", *Engineering Structures 03*, 2008
11. M. Kreslin, P. Fajfar, "Seismic evaluation of an existing complex RC building", *Springer Science+Business Media*, 2009
12. M.V. Sivaselvan, A.M. Reinhorn, "Hysteretic models for deteriorating inelastic structures", *Journal of Engineering Mechanics*, 126(6), 633-640, 2000.
13. L. Ibarra, R. Medina, H. Krawinkler, "Hysteretic Models that incorporate strength and stiffness deterioration". *Earthquake Engineering and Structural Dynamics*, 131(4), 1489-1511, 2005.
14. M.N. Fardis, T.B. Panagiotakos, "Seismic design and response of bare and masonry-infilled reinforced concrete buildings. Part II: Infilled structures", *Journal of Earthquake Engineerin*g, 1(3), 475-503, 1997.

## *REFERENCES*


15. G. Magenes, G.M. Calvi, "In-plane seismic response of brick masonry walls", *Earthquake Engineering and Structural Dynamics*, 26(11) 1091-1112, 1997.
16. M. Dolsek, P. Fajfar, "Mathematical modeling of an infilled RC frame structure based on the results of pseudo-dynamic tests", *Earthquake Engineering and Structural Dynamics*, 31(6) 1215-1230, 2002.
17. FEMA 356: "Prestandard and commentary for the seismic rehabilitation of buildings". *Federal Emergency Management Agency*, Washington DC, SAC Joint Venture, 2000.
18. R. Zarnic, S. Gostic, "Masonry infilled frames as an effective structural sub-assemblage". *Seismic Design Methodologies for the Next Generation of Codes*, Fajfar, P., Krawinkler, H. (eds). Balkema Rotterdam, 335-346, 1997
19. A. Madan, A.M. Reinhorn, J.B. Mandar, R.E. Valles, "Modeling of masonry infill panels for structural analysis", *Journal of Structural Engineering*, ASCE, 123(10), 1295-1302
20. R.J. Mainstone, "On the stiffness and strength of infilled frames", *Proceeding of the Institution of Civil Engineers (ICE*), Supplement (IV), Paper No. 7360, 57-90, 1971
21. J. Hall, "Problems encountered from the use (or misuse) of Rayleigh damping", *Earthquake Engineering and Structural Dynamics*, 2006
22. D. Vamvatsikos, M. Fragiadakis, "Incremental dynamic analysis for estimating seismic performance sensitivity and uncertainty", *Earthquake Engineering and Structural Dynamics*, 2009
23. D. Vamvatsikos, C.A. Cornell, "Incremental dynamic analysis", *Earthquake Engineering and Structural Dynamics*, 2002
24. Bertero VV., "Strength and deformation capacities of buildings under extreme environments", *Structural Engineering and Structural Mechanics*, Pister KS (ed.). Prentice-Hall: Englewood Cliffs, NJ 1977; 211-215
25. FEMA, "Recommended seismic design criteria for new steel moment-frame buildings", *Report No. FEMA-350*, SAC Joint Venture, Federal Emergency Management Agency, Washington DC, 2000.
26. FEMA, "Recommended seismic evaluation and upgrade criteria for existing welded steel moment-frame buildings", *Report No. FEMA-351*, SAC Joint Venture, Federal Emergency Management Agency, Washington DC, 2000.
27. Shome N, Cornell CA., "Probabilistic seismic demand analysis of nonlinear structures", *Report No. RMS-35*, RMS Program, Stanford University, Stanford, 1999.
28. PEER, Open System for Earthquake Engineering Simulation (OpenSees). Version 2.0.0. Pacific Earthquake Eng. Research Center, University Of California, Berkeley, 2008. http://opensees.berkley.edu/.
29. Response 2000 A Computer Program for Sectional Analysis, available from URL: http://www.ecf.utoronto.ca/~bentz/home.shtml

# Appendix

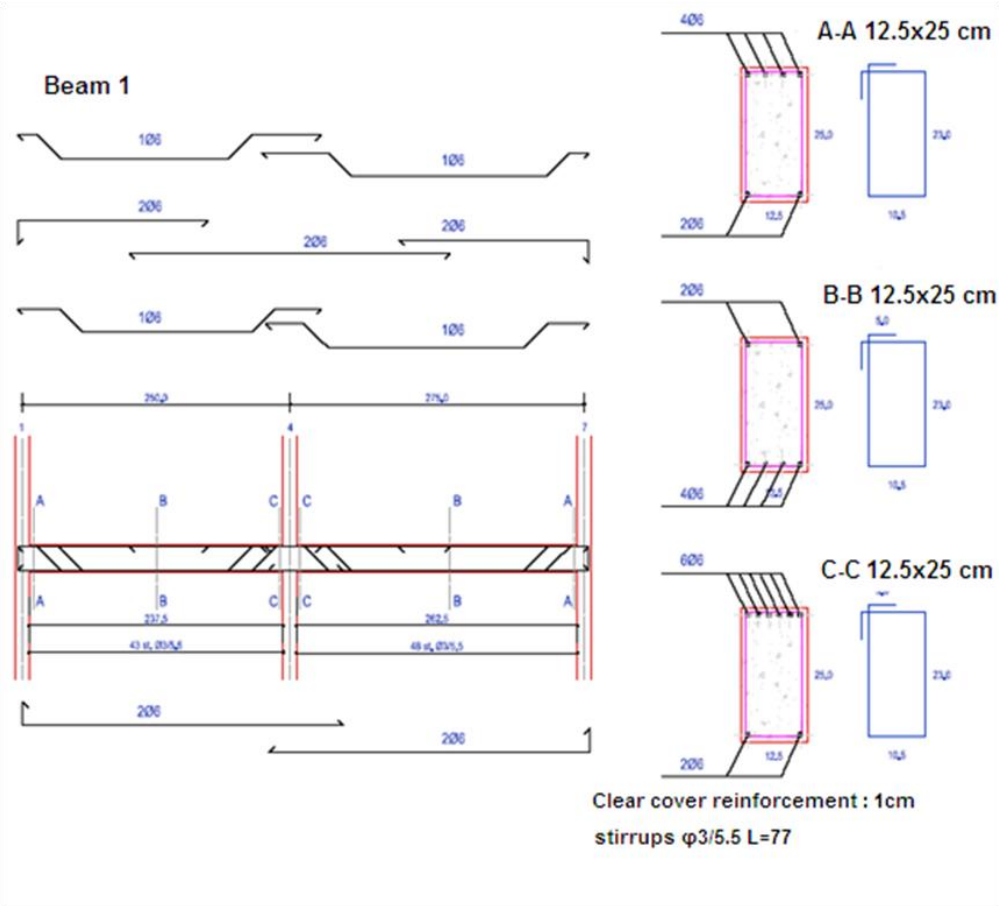


Figure A–1: Typical beam

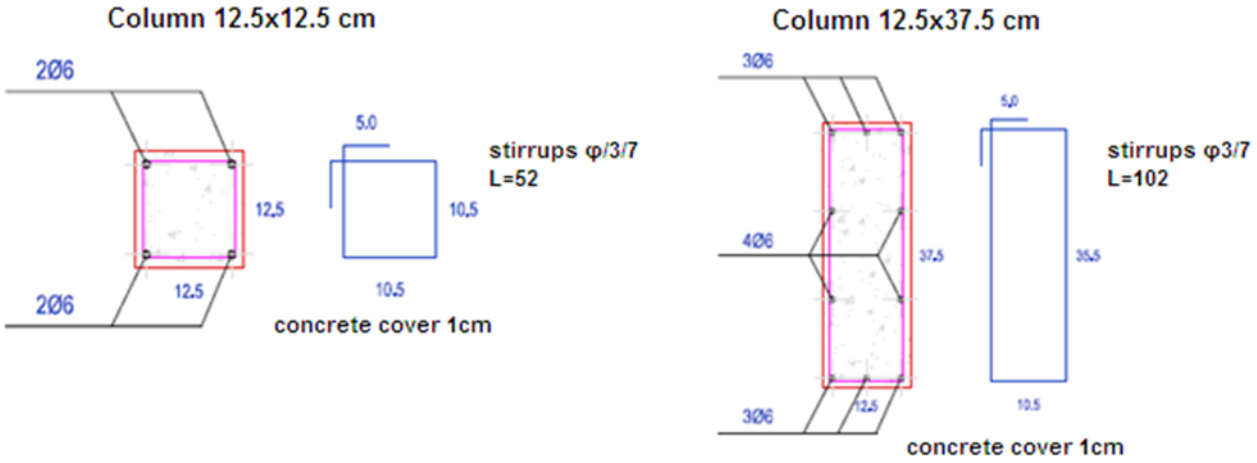


**(a)** **(b)**

Figure A–2: Typical column

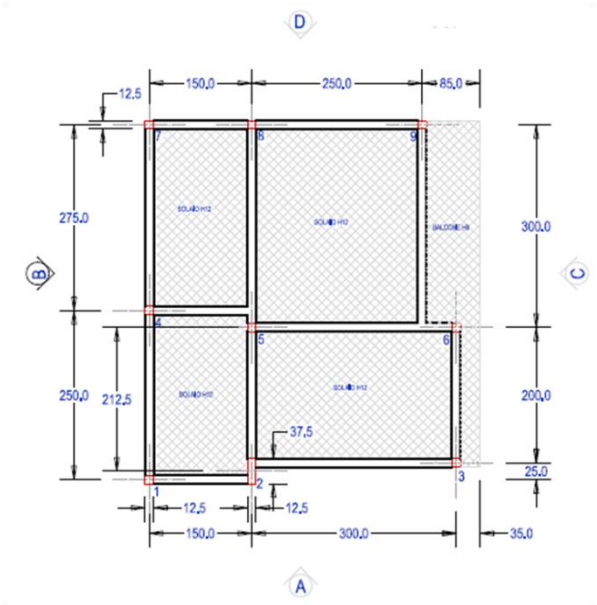


Figure A–3: Typical building floor plan

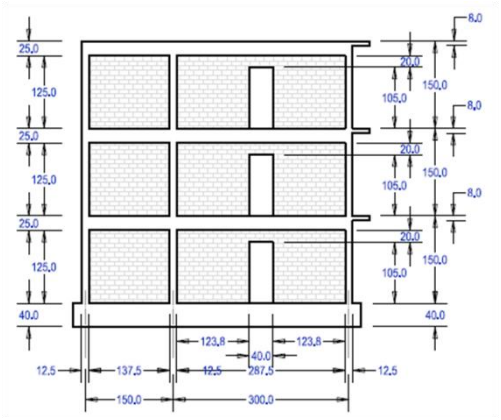

(a)

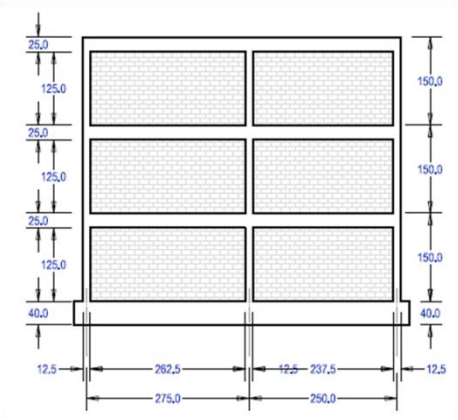

(b)

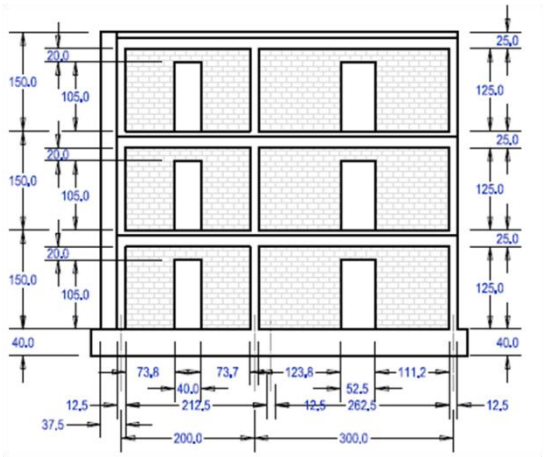

(c)

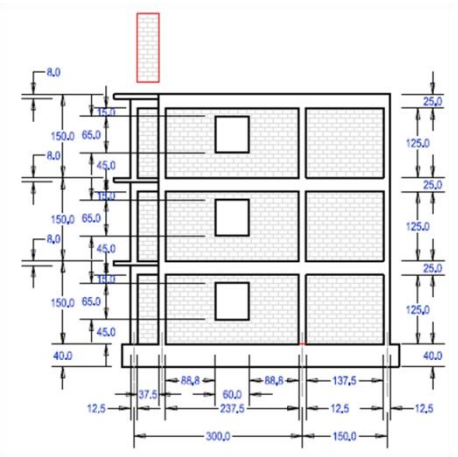

(d)

Figure A–4: Construction of walls (a) A, (b) B, (c) C, (d) D view

(a)

(b)

(c)

(d)

Figure A–5: (a) Detail of the longitudinal reinforcement of beams and columns, no stirrups on the joint as construction practice of the '70s; (b) Detail of slab reinforcement of the first floor; (c) Formwork to the second floor; (d) R.C. frame completed